

Time Reversal Transmission Approach for Ultra Wideband Communications

Von der Fakultät für Elektrotechnik und Informatik

der Gottfried Wilhelm Leibniz Universität Hannover
zur Erlangung des Grades eines

DOKTORS DER INGENIEURWISSENSCHAFTEN

Dr.-Ing.

genehmigte Dissertation
von

M.sc. Trung Kien Nguyen

geboren am 09.09.1980 in Namdinh, Vietnam

2011

Referent: Prof. Dr.-Ing. Thomas Kaiser
Korreferentin: Prof. Dr.-Ing. Maryline H elard, INSA Rennes, France
Korreferent: Prof. Dr.-Ing. Holger Blume
Vorsitzender: Prof. Dr.-Ing. Markus Fidler
Tad der Promotion: 09.09.2011

KURZFASSUNG

Aufgrund der breitbandigen Belegung des Frequenzspektrums wird das UWB-Signal durch den Einfluss der Mehrwegausbreitung extrem verzerrt. Für viele Anwendungen ist der Einsatz von komplexen Empfängerstrukturen, wie z.B. der Rake-Empfänger, unvorteilhaft. Ein Lösungskonzept besteht darin, die Systemkomplexität von der Empfängerseite auf die Senderseite zu verlagern, indem das sogenannte Time reversal (TR) Technologie eingesetzt wird. In Rahmen dieser Arbeit wird die TR-Technologie in verschiedenen UWB-Szenarien bzw. -konfigurationen untersucht.

In einem SISO-UWB-System werden Inter-Frame-Interferenzen und Interferenzen durch Kreuzmodulation anhand einer TR-Vorfilterung unterdrückt. Das weitverbreitete UWB-Modulationsverfahren Time-Hopping Pulse Position Modulation (TH-PPM) ruft solche Interferenzen hervor. Drei TR-Verfahren, bekannt als All-, Partial-, und Selective-TR werden in dieser Arbeit berücksichtigt. Das Selective-TR-Verfahren zeichnet sich durch seine einfache Struktur bzw. hohe Effizienz aus.

Für MIMO-UWB Systeme wird das Konzept des räumlichen Multiplexing untersucht. Eine Kombination aus TR-Vorfilterung und Zero-Forcing (ZF) Vorentzerrung wird verwendet, um vorhandene Intersymbolinterferenz (engl. inter-symbol interference, ISI) bzw. die Multiple-Stream Interferenz (engl. Multiple-stream interference, MSI) zu unterdrückt. Dazu werden die Auswirkungen der räumlichen Korrelationen zwischen den Antennenelementen untersucht. Die Untersuchungsergebnisse zeigen, dass die BER-Performanz eines MIMO-UWB-Systems bei starker räumlicher Korrelation der Antennensignale stark reduziert ist und unter bestimmten Bedingungen schlechter ausfallen kann, als bei einem SISO-System.

Darüber hinaus wird MIMO-UWB für ein Mehr-User (engl. Multiuser, MU) Systemszenario untersucht. In diesem Fall wird das Mehrfachzugriffsverfahren (engl. Multiple-access channel, MAC) auf der Aufwärtsstrecke (Uplink) und der Übertragungskanal (engl. Broadcast Channel, BC) auf der Abwärtsstrecke (Downlink) berücksichtigt. Bei einigen UWB-Anwendungen, bei denen ein leistungsfähiger Zugriffspunkt (Access Point) mit mehreren einfachen Endgeräten kommuniziert, wird die Kombination unterschiedlicher Verfahren vorgezogen. Hierbei wird auf der Senderseite eine Kombination der TR-Vorfilterung und ZF-Vorentzerrung realisiert. Ebenfalls wird für die MAC-Kanäle auf der Empfängerseite eine Kombination der TR-Filterung und einem ZF-Entzerrer realisiert. Hierdurch werden die ISI, MSI, und Multi-User Interferenzen unterdrückt.

Die theoretischen Untersuchungen werden anhand von Simulationen für standardisierte bzw. gemessene UWB-Kanäle verifiziert. Die Messungen im Zeitbereich sind im UWB-Labor des Instituts für Kommunikationstechnik durchgeführt worden.

Schlagwörter: Time Reversal (TR), Ultrabreitband (UWB), Multiple-Input Multiple-Output (MIMO)

ABSTRACT

Due to the extremely large bandwidth property, ultra wideband (UWB) systems suffer from a very long delay spread by the multipath effect. Meanwhile, in many applications, implementing a high complex receiving structure like a Rake receiver to combat the negative effects of fading on the received signal is impractical. Based on the idea of moving the complexity from the receiver to the transmitter, the time reversal (TR) technique is proposed to solve this problem for such a UWB systems. In this work, TR is considered to apply to various scenarios and configurations of UWB systems.

For the single-input-single-output UWB system, the TR pre-filter is proposed to combat the inter-frame interference and the cross-modulation interference. These interferences are relevant to the time-hopping pulse-position modulation scheme which is commonly used in the UWB system. Three TR schemes, namely the all-, partial-, and selective-TR, are investigated. The selective-TR scheme shows the advantage of simplifying the structure while keeping the bit-error-rate (BER) performance good.

For the multiple-input-multiple-output (MIMO) configuration, a spatial multiplexing MIMO-UWB system is studied. A TR pre-filter combined with a zero forcing (ZF) pre-equalizer is adopted to deal with the inter-symbol interference (ISI) and the multiple-stream interference (MSI) problem in such a system. Spatial correlation among antenna elements is also investigated in this work. It is shown that in a high correlation condition, the BER performance of the MIMO-UWB system is greatly degraded and may be even worse than the BER performance of the single-input-multiple-output system.

The case of multiple-user (MU) MIMO-UWB systems is then investigated. For the MU scenario, the multiple-access channel (MAC) on the reverse link and the broadcast channel (BC) on the forward link are considered. Focusing on UWB applications where a powerful access point communicates with number of non-complexity user terminals, the author proposes to implement the combination of the TR pre-filter and the ZF pre-equalizer at the transmitter side on the BC channels and the combination of the TR filter and the ZF equalizer at the receiver side on the MAC channels to mitigate interferences including the ISI, MSI and the multiple-user interference for such a system.

The theoretical studies are validated by simulation with both standard UWB channels and the measured UWB channels. The UWB measurements are performed in the time domain in the UWB laboratory of the Institut für Kommunikationstechnik.

Keywords: Time Reversal (TR), Ultra Wideband (UWB), Multiple-Input Multiple-Output (MIMO)

ACKNOWLEDGEMENTS

I would very much like to express my sincere gratitude to my advisor Prof. Thomas Kaiser for his continual support and guidance both academically and personally over the years. My deeply appreciation is devoted to him for his kindness, encouragements and inspiration from the initial stage until completion of this work.

I am grateful to Dr. Feng Zheng for his insightful comments and remarks on all my publications as well as his kind proof-reading on my dissertation. He has encouraged me try out new ideas and helped me to question them critically during my PhD study. I would like to thank a lot to Dr. Hieu Nguyen for his technical suggestions improving my work considerably.

I would also like to thank to Prof. Maryline H elard from INSA de Rennes, France, Prof. Holger Blume and Prof. Markus Fidler for serving in my dissertation examiner, for sparing their precious time for the reviewing my dissertation and bringing questions.

Special appreciation is devoted to my colleagues at Institute of Communications Technology (IKT): Dr.-Ing. Andreas Wilzeck, M.Sc. Sanam Moghaddamnia, M.Sc. Chung Le, Barbara Adler, Eva-Maria Schr oder, Dipl.-Ing. Rolf Becker, M.Sc. Anggia Anggraini, Dr.-Ing. Amina Ayadi, M.Sc. Zhao Zhao, M.Sc. Qipeng Cai, Dr.-Ing. Claus Kupferschmidt, Dr.-Ing. Bamrung Tau Sieskul, Dr.-Ing. Kiattisak. Maichalernnukul, Dipl. -Ing. Sondos Alaa, Dr.-Ing. Mohamed El-Hadidy, M.Eng. Hanwen Cao for support and the friendship. They have provided an excellent working environment and have been really helpful to me.

I am also thankful to Vietnamese friends of mine in Hannover for the warm friendship. Special thanks would be sent to Duy Cong for his assistance in life. All of them have created a home-atmosphere during my staying here.

My PhD program has been financed by the Government of Vietnam represented by Ministry of Education and Training (MOET). I would like to acknowledge Mr. Nguyen Manh Tan in MOET for his helpful advices and friendly support.

Last but not least, I am much obliged my parents for their constant love and support, without whom none of this work would be possible. I am specially indebted to my dear wife Tra My and our pretty daughter Chich Bong for their understanding during long time I was occupied with my work. They are the very best for all their love and care.

Trung Kien Nguyen
Hannover, September 2011.

*To my family,
my dear wife Tra My
and our pretty daughter Chich Bong*

CONTENTS

1	INTRODUCTION OF DISSERTATION	1
1.1	Fundamentals	1
1.2	Motivation and Research Scope	4
1.3	Organization and Contribution	6
2	TIME REVERSAL FOR SISO-UWB SYSTEMS	9
2.1	Introduction	9
2.2	UWB Channel Model	10
2.3	Principle of Time Reversal	12
2.3.1	Theoretical Basis	12
2.3.2	TR Schemes	18
2.4	TH-PPM-UWB System	20
2.4.1	Signal Model	20
2.4.2	Interferences in TH-PPM-UWB systems	22
2.4.3	Interferences Mitigation with TR	25
2.5	Performance Analyses	26
2.5.1	Performance evaluation of TR schemes	26
2.5.2	Interferences Mitigation with TR	29
2.6	Summary	33
3	TIME REVERSAL FOR SINGLE USER MIMO-UWB SYSTEMS	35
3.1	Introduction	35
3.2	SU-SM-MIMO System	38
3.3	Pre-Filter-Equalizer Design	39
3.3.1	Time Reversal Pre-Filter	39
3.3.2	Pre-Equalizer	40
3.4	Channel Correlation in SM-MIMO systems	44
3.5	BER Performance Analysis	45
3.6	Summary	51
4	TIME REVERSAL FOR MULTI-USER MIMO-UWB SYSTEMS	53
4.1	Introduction	53
4.2	Broadcast MU-MIMO UWB System	56
4.2.1	System Model	56
4.2.2	Interference Mitigation for BC-MU-MIMO System	58
4.2.3	Spatial Correlation	61
4.2.4	Numerical Result	62
4.3	Multiple Access MU-MIMO UWB System	66
4.3.1	System Model	67
4.3.2	Interference Mitigation for MAC-MU-MIMO System	68
4.3.3	Spatial Correlation	70
4.3.4	Numerical Result	70
4.4	Summary	74
5	MEASUREMENTS AND VALIDATIONS	75
5.1	UWB Channel Sounding	75
5.1.1	Time Domain Channel Sounding	77

5.1.2	Frequency Domain Channel Sounding	79
5.2	UWB Channel Measurement in IKT	79
5.2.1	Setup	80
5.2.2	Measurement	81
5.2.3	CIR Extract	84
5.3	BER Performance Evaluation Based on Measured Channels .	89
5.4	Summary	93
6	CONCLUSIONS AND RECOMMENDATIONS	95
6.1	Conclusions	95
6.2	Recommendations for Future Work	96
	BIBLIOGRAPHY	99

LIST OF FIGURES

Figure 1	FCC spectral mask for UWB indoor applications	3
Figure 2	CEPT spectral mask for UWB indoor applications	3
Figure 3	Principle of the Saleh-Valenzuela model.	11
Figure 4	CM ₁ - 100 realizations of CIR.	13
Figure 5	CM ₂ - 100 realizations of CIR.	13
Figure 6	CM ₃ - 100 realizations of CIR.	14
Figure 7	CM ₄ - 100 realizations of CIR.	14
Figure 8	The time reversal concept.	15
Figure 9	Autocorrelation of a CIR, CM ₁ in IEEE 802.15.3a standard	16
Figure 10	TR schemes.	19
Figure 11	A TH-BPPM IR signal where $N_f = 5$, $N_c = 4$, and the TH sequence is $\{2, 1, 3, 2, 0\}$	20
Figure 12	The block diagram of the correlator-based receiver	21
Figure 13	CMI and IFI problem illustration for BPPM-TH: a) bit '0' signal; b) bit '1' signal; c) correlation mask	23
Figure 14	The block diagram of a SISO-TR-UWB system	25
Figure 15	BER vs. SNR for different TR schemes, CM ₁	27
Figure 16	BER vs. SNR for different TR schemes, CM ₂	27
Figure 17	BER vs. SNR for different TR schemes, CM ₃	28
Figure 18	BER vs. SNR for different TR schemes, CM ₄	28
Figure 19	The cumulative density of the SIR for both conventional and proposed PPM-UWB systems with and without TH, both CMI and IFI are taken into account	31
Figure 20	The cumulative density of the SIR for both conventional and proposed PPM-UWB systems when IFI is or is not considered.	31
Figure 21	BER performance of both conventional and proposed PPM-UWB systems with and without TH, both CMI and IFI are taken into account.	32
Figure 22	BER performance of both conventional and proposed PPM-UWB systems when IFI is or is not considered	32
Figure 23	Spatial Multiplexing Encoding Schemes.	36
Figure 24	Block diagram of MIMO-UWB system with pre-Filter and pre-Equalizer.	38
Figure 25	BER versus the length of shortened equivalent channel for the S-TR pre-filter, CM ₄ , $M = N = 2$, SNR = 12 dB, no spatial correlation.	46
Figure 26	BER versus the ratio L_s/L_e for the S-TR pre-filter and the P-TR pre-filter filter, CM ₁₋₄ , $M = N = 2$, SNR = 12 dB, $s = 20$, no spatial correlation.	47

Figure 27	Average BER versus transmit correlation coefficient for the channel CM ₄ , the S-TR pre-filter with $s = 50$, $M = 2$ and SNR = 12 dB.	48
Figure 28	Average BER versus transmit correlation coefficient for the channel CM ₄ , the S-TR pre-filter with $s = 50$, $M = 4$ and SNR = 12 dB.	49
Figure 29	BER performance of 2×2 MIMO and 1×2 SIMO systems for the channel CM ₄ , the S-TR pre-filter with $s = 50$ and SNR = 12 dB.	50
Figure 30	BER performance of 4×4 MIMO and 1×4 SIMO systems for the channel CM ₄ , the S-TR pre-filter with $s = 50$ and SNR = 12 dB.	50
Figure 31	Broadcast and Multipleaccess Channels in a MU-MIMO System	54
Figure 32	Proposed interferences mitigation solution for MU-MIMO UWB systems.	56
Figure 33	The Broadcast MU-MIMO UWB system with a pre-filter and pre-equalizer.	57
Figure 34	Average BER versus the transmit correlation coefficient with $M = 4$, $N = 2$, SNR = 12 dB for the different number of users $K = 1, 2, 3, 4$	63
Figure 35	Average BER versus the transmit correlation coefficient with $M = 4$, $K = 2$, $N = 2$ for the different values of SNR = 10, 12, 15, 20.	63
Figure 36	Average BER versus the transmit correlation coefficient with $K = 2$, $N = 2$, SNR = 12 dB for the different numbers of transmit antenna $M = 1, 2, 3$	64
Figure 37	Average BER versus SNR with $M = 4$, $N = 2$, $\rho_{Tx} = 0.3$ for the different number of users $K = 1, 2, 3$	64
Figure 38	Average BER versus SNR with $K = 2$, $N = 2$, $\rho_{Tx} = 0.3$ for the different numbers of transmit antenna $M = 1, 2, 3, 4$	65
Figure 39	Average BER versus SNR with $M = 4$, $K = 2$, $N = 2$ for the different values of transmit correlation coefficient $\rho_{Tx} = 0, 0.1, 0.3, 0.5, 0.9$	65
Figure 40	The multiple access MU-MIMO UWB system with a filter and equalizer.	67
Figure 41	Average BER versus SNR with $K = 2$, $M = 2$, $\rho_{Rx} = \rho_{Tx} = 0.3$ for the different numbers of transmit antennas per user $N = 1, 2, 3$	72
Figure 42	Average BER versus SNR with $N = 2$, $M = 2$, $\rho_{Rx} = \rho_{Tx} = 0.3$ for the different numbers of users $K = 1, 2, 3$	72
Figure 43	Average BER versus SNR with $K = 2$, $N = 2$, $\rho_{Rx} = \rho_{Tx} = 0.3$ for the different numbers of receive antennas $M = 1, 2, 3, 4$	73

Figure 44	Average BER versus SNR with $K = 2$, $N = 2$, $M = 2$ or 4, $\rho_{Tx} = 0.3$ for the different values of the receive correlation coefficient $\rho_{Rx} = 0, 0.3, 0.9$	73
Figure 45	Time resolution in channel sounding	76
Figure 46	Time domain channel sounding	77
Figure 47	Frequency domain channel sounding	78
Figure 48	Floor plan and measurement configuration	80
Figure 49	A sketch of measurement system	81
Figure 50	Photos of the implementation	82
Figure 51	The probe UWB pulse	83
Figure 52	The measured template used for Clean Algorithm	85
Figure 53	An example of the received signal and the extracted CIR	86
Figure 54	Realizations of CIR measured in LOS environment, 2m of the distance between transmitter and receiver	86
Figure 55	Realizations of CIR measured in NLOS environment, 2m of the distance between transmitter and receiver	87
Figure 56	Realizations of CIR measured in LOS environment, 4m of the distance between transmitter and receiver	87
Figure 57	Realizations of CIR measured in NLOS environment, 4m of the distance between transmitter and receiver	88
Figure 58	An example of the measured (2×2) MIMO channel	88
Figure 59	BER vs. SNR for different TR schemes, measured CIRs in LOS environment	90
Figure 60	BER vs. SNR for different TR schemes, measured CIRs in NLOS environment	90
Figure 61	BER versus the shorten channel ratio (L_s/L_e) for measured channels	91
Figure 62	The BER performance of the 2×2 MIMO-UWB system simulated with measured channels	91
Figure 63	The BER performances of the SISO- and MISO-UWB systems simulated with measured channels	92
Figure 64	BER performance comparison, for standard channels with $\rho_{Tx} = 0.2$ and for measured indoor channels	93

LIST OF TABLES

Table 1	Comparative study of the characteristics of some wireless technologies	2
Table 2	CEPT spectral restrictions for UWB indoor applications	2
Table 3	Key parameters of channel models in IEEE 802.15.3a standard	15
Table 4	Main model characteristics in IEEE 802.15.3a standard	15
Table 5	Power captured by TR pre-filter impulse response . . .	19
Table 6	Simulation parameters	30
Table 7	Power Distribution of Equivalent Channels	41
Table 8	Key Parameters of the Channel Models	41
Table 9	Simulation parameters	62
Table 10	AWG, DPO and probe pulse sequences setting	83

LIST OF ACRONYMS

AP	access point
A-TR	All (full)-Time reversal
AWG	arbitrary waveform generator
BC	broadcast channel
BER	bit-error-rate
BPAM	binary pulse amplitude modulation
BPPM	binary pulse position modulation
CEPT	European Conference of Postal and Telecommunications Administrations
CIR	channel impulse response
CM	channel model
CMI	cross-modulation interference
CSI	channel state information
DPC	dirty paper coding
DPO	digital phosphor oscilloscope
DSO	digital sampling oscilloscope
EIRP	equivalent isotropically radiated power
FCC	Federal Communications Commission
FFT	fast Fourier transform
FH	frequency hopping
HDR	high data rate
IC	inverse channel
IFFT	inverse fast Fourier transform
IFI	inter-frame interference
IKT	Institut fuer Kommunikationstechnik
IR	impulse radio
ISI	inter-symbol interference

LDR	low data rate
LOS	line of sight
LST	layer space-time
MAC	multiple-access channel
MB	multiband
MIMO	multiple-input-multiple-output
MISO	multiple-input-single-output
MSI	multiple-stream interference
MU	multiple-user
MUI	multiple user interference
NLOS	non line of sight
OFDM	orthogonal frequency division multiplexing
PN	pseudo-noise
PPM	pulse position modulation
PSD	power spectral density
P-TR	Partial-Time reversal
RMS	Root Mean Square
SIMO	single-input multiple-output
SINR	interference-plus-noise power ratio
SIR	signal to interference ratio
SISO	single-input-single-output
SM	spatial multiplexing
SNR	signal-to-noise ratio
S-TR	Selective-Time reversal
STTCs	Space Time Trellis Codes
S-V mode	Saleh-Valenzuela model
TH	time hopping
TR	time reversal
UWB	ultra wideband
VAN	vector network analyzer
ZF	zero forcing

INTRODUCTION OF DISSERTATION

Overview of Ultra wideband communications is given in the first section of this chapter. Motivation of this work and research scope are stated in Section 1.2, followed by the last section presenting the contribution of our work and the organization the dissertation as well.

1.1 FUNDAMENTALS

For a few years, the world of telecommunications has faced an increasing demand for wireless numerical applications, in the industrial as well as the home environment. This increasing need for wireless connectivity leads to the development of many standards for wireless and short range communication systems such as Bluetooth, the WiFi standards family (IEEE 802.11 a, b and g), Zigbee (IEEE 802.15.4) and the recent standard 802.15.3. Comparison of these wireless communication technologies is shortly represented in Table 1. Ultra-wideband (UWB) transmission has recently received significant attention in both academia and industry for applications in wireless communications due to numerous benefits, including high data rate, availability of low-cost transceivers, low transmit power, and low interference. Research efforts in recent years have proved that that UWB radio is a promising solution for high-rate short-range and moderate-range wireless communications and ranging. In particular, UWB has found a new application for lower-data-rate moderate-range wireless communications, illustrated by IEEE 802.15.4a. Unlike the indoor environment in 802.15.3a (WPAN), the new environments for sensors, IEEE 802.15.4a will be very different, ranging from dense foliage to dense urban obstructions. The application of UWB to low-cost, low-power sensors has a promise. The centimeter accuracy in ranging and communications provides unique solutions to applications, including logistics, security applications, medical applications, control of home appliances, search-and-rescue, family communications and supervision of children, and military applications.

The transmitted power of UWB devices is controlled by the regulatory agencies such as the Federal Communications Commission (FCC) in the United States or the European Conference of Postal and Telecommunications Administrations (CEPT) in Europe, so that narrowband systems are affected from UWB signals only at a inappreciable level. UWB systems, therefore, are allowed to coexist with other technologies only under stringent power constraints. As defined in [1, 75], any wireless communication technology that produces signals with a 10 dB bandwidth $(f_H - f_L)$ ¹ wider than 500 MHz or a fractional bandwidth $(f_H - f_L)/[(f_H + f_L)/2]$ greater than 0.2 can be considered as ultra wideband. The FCC approved the deployment of

¹ f_H and f_L are the upper and lower edge frequencies, respectively

Table 1: Comparative study of the characteristics of some wireless technologies

Technology	Data rate	Freq. band	EIRP	Spec. (IEEE)
UWB	≥ 100 Mbps	3.1–10.6 GHz	–41.3 dBm/MHz	802.15.3a
	≥ 500 kbps	3.1–10.6 GHz	–41.3 dBm/MHz	802.15.4a
Bluetooth	≥ 700 kbps	ISM 2.4 GHz	type 1: 20 dBm type 2: 0 dBm	802.15.1
WiFi	≥ 54 Mbps	5 GHz	0.2 – 1 W	802.11a
	≥ 11 Mbps	ISM 2.4 GHz	0.2 – 1 W	802.11b
	≥ 54 Mbps	ISM 2.4 GHz	0.1 – 1 W	802.11g

UWB on an unlicensed basis in the 3.1–10.6 GHz band in the USA [1] while in Europe, at least 6.0 to 8.5 GHz band was approved [38]. The 1.6 – 10.6 GHz band can be used in Europe, but a stricter spectral mask is specified than that in the USA. The essence of the rulings is that power spectral density (PSD) of the modulated UWB signal must satisfy the spectral masks specified by spectrum-regulating agencies. The spectral masks for indoor applications specified by the FCC in the United States and the CEPT in the Europe are shown in Figures 1 and 2, respectively. Beside, the CEPT prescribes the maximum peak of equivalent isotropically radiated power (EIRP) emission for the UWB systems as shown in Table 2[34].

Table 2: CEPT spectral restrictions for UWB indoor applications

Freq. range (GHz)	Maximum mean EIRP density (dBm/MHz)	Maximum peak EIRP density (dBm/50 MHz)
Below 1.6	-90.0	-50.0
1.6 to 3.4	-85.0	-45.0
3.4 to 3.8	-85.0	-45.0
3.8 to 4.2	-70.0	-30.0
4.2 to 4.8	-41.3 (until 31/12/10)	0.0 (until 31/12/10)
	-70.0 (beyond 31/12/10)	-30.0 (beyond 31/12/10)
4.8 to 6.0	-70.0	-30.0
6.0 to 8.5	-41.3	0.0
8.5 to 10.6	-65.0	-25.0
Above 10.6	-85.0	-45.0

The main stream papers in the literature deal with two kinds of UWB systems including impulse radio (IR)-based UWB systems and multiband

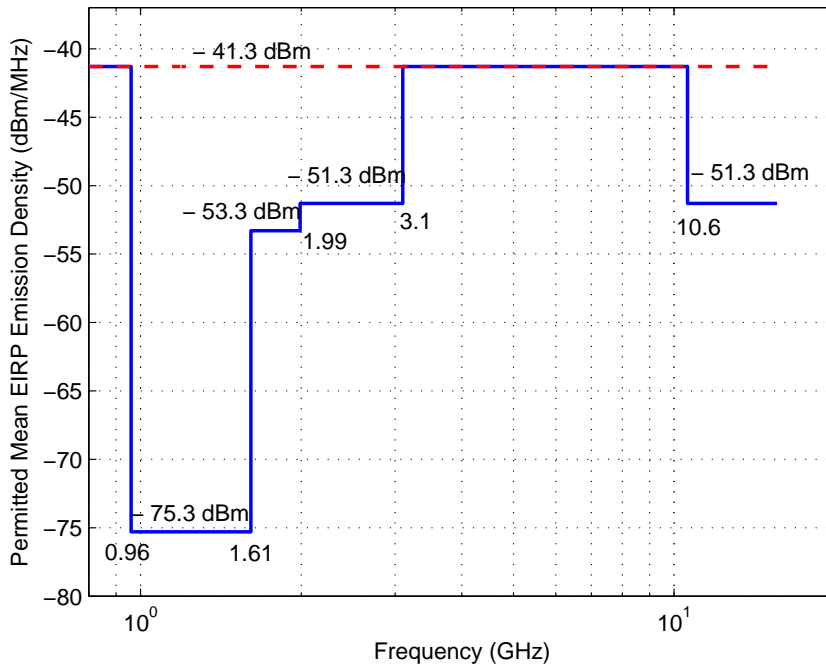


Figure 1: FCC spectral mask for UWB indoor applications

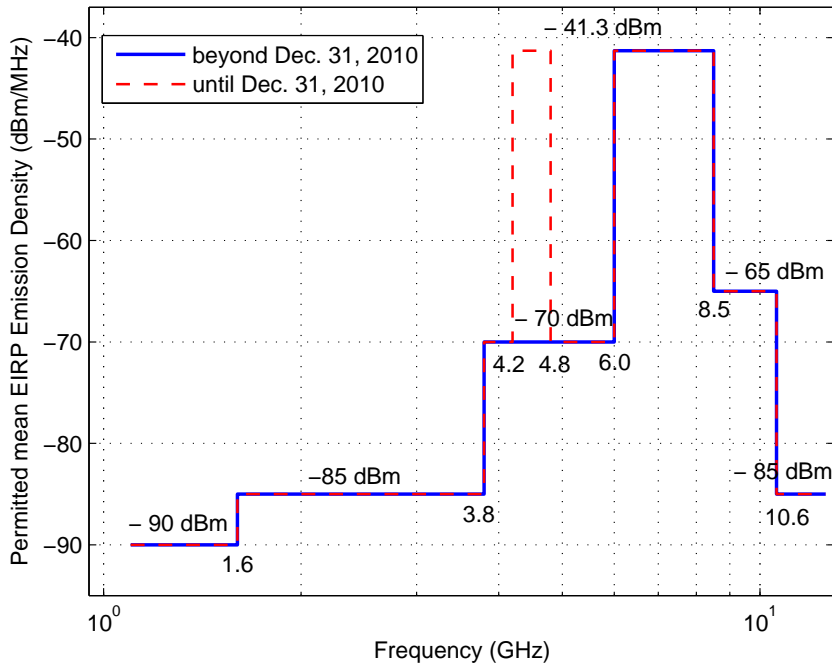


Figure 2: CEPT spectral mask for UWB indoor applications

(MB)-based UWB systems. In the former approach, information data is transmitted by using a sequence of very-short-duration (several tens of picoseconds) pulses. This pulse sequence is directly transmitted through the antenna without any carriers. In the latter approach, MB-based approach, the information data is multiplexed into sub-frequency bands in the entire band or a part of it, with each sub-band having 528MHz bandwidth. In each sub-band, the information data is transmitted by using traditional multi-carrier orthogonal frequency-division multiplexing (OFDM) technology.

The drawback of the IR-based UWB systems is the large number of multipaths, typically on the order of hundreds for a normal office environment. This causes a big challenge for the synchronizer design with reasonably quick acquisition time and the rake receiver implementation with sufficient fingers to capture enough energy. In comparison with the MB-based UWB system, however, the IR-based UWB system has a simple transceiver structure where up- and down-mixers are not needed. The Fourier transform (FFT) and the inverse FFT (IFFT) algorithms at the receiver and transmitter sides respectively are not required in IR-based UWB system. This advantage is one of the most important reasons boosting research interests in UWB systems at the very beginning of UWB-related studies. Furthermore, due to the simplicity in the transceiver structure leading to low-cost devices, the IR-based UWB technology has been a promising candidate for many applications such as indoor wireless localization, location-based sensor networks. The IR-based UWB systems are object that we focus on in our work for reasons above mentioned. From now on, the use of the term "UWB" will imply "IR-UWB" unless stated otherwise.

1.2 MOTIVATION AND RESEARCH SCOPE

Rake receiver brings a ability to resolve individual multipath components of the channel in UWB communications [7, 72, 16]. If the large number of resolvable paths in such a system makes it unrealistic to employ the traditional Rake receiver to capture a significant portion of the energy contained in the received multipath components, a partial or a selective Rake receiver is an alternative solution [15]. One of the major application classes of UWB is low-data-rate (LDR) communications [86]. LDR applications is synonymous with sensor networks for all practical purposes where very low power consumption and low-cost implementation due to the densely distributed nature are often required. In such systems, deploying high complexity receivers like Rake is impractical. Base on the idea of moving the complexity from the receiver to the transmitter, the time reversal (TR) technique, also referred to as the pre-Rake combining, can overcome this problem.

The essence of time reversal is to exploit multiple scattering between the scatters. After the time-reversal operation, the whole multiple-scattering medium behaves, in effect, as a coherent focusing source whose large angular aperture enhances the resolution at the final focus [76]. Owing to the high resolution of a short UWB pulse, rich resolvable multipath makes

the UWB channel act like an underwater acoustical channel. The success of using time reversal for underwater acoustical communications [27, 24] motivates the research UWB radio.

In a time-reversal scheme, the channel impulse response (CIR) is used as a pre-filter at the transmitter. After the encoded information bits pass through the channel, the response of the channel is the autocorrelation of the CIR. A signal is precoded such that it focuses both in time and in space at a particular receiver. Owing to temporal focusing, the received power is concentrated within a few taps and the task of equalizer design becomes much simpler than without focusing. It could be said that TR scheme is used to shift the design complexity from the receiver to the transmitter.

Basically, there are two ways to design a pre-filter upon the domain, time or frequency, that one considers the problem. Considering the problem in the time domain leads to the TR pre-filter and if the problem is considered in the frequency domain, it leads to the inverse channel (IC) pre-filter (maybe referred as zero-forcing pre-filter in the literature). As shown in [39], the TR approach is selected for UWB systems instead of the IC approach because of the following reasons:

- **Output SNR:** The TR pre-filter maximizes the output signal-to-noise ratio (SNR) at a specific time instant over all the constrained weighting filters.
- **Practicality:** Since in the practical UWB channel, which is generally of non-minimum phase, the frequency selectivity of the channel cannot be completely compensated by the IC filter, the TR pre-filter can outperform the IC pre-filter.
- **Robustness:** The CIR estimation errors may affect seriously the performance of the system using the IC pre-filter. Meanwhile the TR approach is quite robust to this problem.
- **Complexity:** Factorizing the channel transfer functions in real time, that is required in the IC pre-filter, leads to computational expense for a moderate scale system. Moreover, the factorization is prohibitive in computation for a multiple antennas system. In contrast, in the TR approach, a computational burden is not required for either a single antenna or multiple antennas system.

A well-studied and the most popularly-adopted modulation scheme in UWB communications is pulse position modulation (PPM) where each pulse is delayed or sent in advance of a regular time scale [33]. Besides, in such systems, randomizing the position in time of the generated pulses is applied to smooth the spectrum of the signal. Time hopping (TH) technique [57, 67] is such a approach. It may say that, PPM modulation combined with TH is basic and common in UWB communication systems. The potential in dealing with the inter-symbol interference (ISI) problems in UWB of TR technique has been verified in numerous papers [78, 26, 44, 45]. In a TH-PPM UWB system, however, not only the ISI, but also inter-frame

interference (IFI) and the cross-modulation interference (CMI) exist. TR technique can also provide a low complexity receiver solution to suppress these interferences [64].

Like in other wireless communications networks, there is more and more demand for data rates in UWB systems. In order to reach the target order of Gbps, advanced techniques should be adopted and UWB technology combined with multiple-input multiple-output (MIMO) technique might provide a solution [38]. To get comprehensive view on applying TR in UWB communications, TR in MIMO-UWB systems and related issues should be studied.

Most past works on the TR UWB scheme focus on the issue of point-to-point or single user transmission [78, 62, 53, 97]. In many applications of UWB communications, however, including high-data-rate (HDR) applications like home entertainment or LDR applications like sensor networks, a host device (named base station) uses several antennas to communicate simultaneously with numerous terminal devices (named users) where each user may be equipped one or more antenna(s). This is scenario of multiple-user (MU) UWB communications. Therefore, investigation in the single user case needs be extended for the MU case.

Theoretically, the performance of the UWB systems in term of bit error rate (BER), throughput or capacity can be improved by having multiple antennas at the transmitter and the receiver somehow. In practice, however, since in many situations, sparse scattering and insufficient spacing between adjacent antennas make the channels between different antennas be often correlated and the multi-antenna gains may not always be obtainable. This problem is named spatial correlation that needs to be considered.

1.3 ORGANIZATION AND CONTRIBUTION

Most of the contents of this dissertation have been presented and published. The outline as well as the major contribution of this work can be succinctly introduced as follow:

- *Chapter 2: Time Reversal for SISO-UWB Communications Systems.* Time reversal technique with three schemes including All-TR, Partial-TR and Selective-TR are investigated for the single user UWB system in which the transmitter and the receiver are equipped with only one antenna. Simulation results based on IEEE 802.15.3a channel models [29] show that with limited number of used multipath components of the CIR, the Selective-TR scheme can provide nearly the same BER performance which is achieved by the All-TR scheme. This also means that we can reduce the complexity of the transmitter by using Selective-TR pre-filter instead of All-TR pre-filter while still keeping intact the system performance. In this chapter, interferences in the TH-PPM-UWB system including the CMI and the IFI are clarified. The TR pre-filter is proposed to deploy at the transmitter to mitigated these interferences. Most of the content of this chapter has been published in [64]:

Trung Kien Nguyen, Thanh Hieu Nguyen, and Thomas Kaiser, "CMI and IFI mitigation for TH-PPM Ultra wideband systems with a low complexity receiver," In *The 2009 International Conference on Advanced Technologies for Communications (ATC'09)*, Oct. 2009.

- *Chapter 3: Time Reversal for Single User MIMO-UWB Communications Systems.* Continuously studying TR applying for single user UWB system, we pay our attention to a spatial multiplexing (SM) MIMO system in this chapter. The combination of the TR pre-filter and the zero-forcing pre-equalizer is adopted to lessen the ISI and the multiple-stream interference (MSI) in such a system. Spatial correlation caused by deploying multiple antennas in both transmitter side and receiver side is investigated. When the TR pre-filter is used in the SM-MIMO system, the number data streams simultaneously transmitted depends on the number of receive antennas. Therefore, one can transmit several data streams at the same time on a single antenna and definition of virtual MIMO is given consequently. It is verified by simulation results that the virtual MIMO system with single transmit antenna can perform better the real one in high correlation condition. The content of this chapter has been published in [66]:

Trung Kien Nguyen, Hieu Nguyen, Feng Zheng, and Thomas Kaiser, "Spatial correlation in SM-MIMO-UWB systems using a pre-equalizer and pre-rake filter," In *The 2010 IEEE International Conference on Ultra-Wideband (ICUWB2010)*, September 20-23 2010.

- *Chapter 4: Time Reversal for Multiple User MIMO-UWB Communications Systems.* The work on the single user SM-MIMO UWB system is extended for multiple user SM-MIMO UWB systems. Similar problems in the former system such as the ISI, the MSI, the correlation are studied in the latter system in this chapter. Multiple user interference (MUI) is also considered thereto. We investigate broadcast channel (BC) and multiple access channel (MAC) in a MU-MIMO-UWB system separately. Based on an idea of keeping the complexity at the access point, we propose to use a zero forcing (ZF) pre-equalizer and a TR pre-filter on the downlink channel (BC) and a ZF equalizer and a TR filter on the uplink channel (MAC) to mitigate interferences in the complete MU-MIMO-UWB system. A part of the content of this chapter has been published in [65]:

Trung Kien Nguyen, Hieu Nguyen, Feng Zheng, and Thomas Kaiser, "Spatial correlation in the Broadcast MU-MIMO-UWB system using a pre-equalizer and time reversal pre-filter," In *The 4th International Conference on Signal Processing and Communication Systems, ICSPCS'2010*, 13-15 December 2010.

- *Chapter 5: Measurements and Validations.* UWB channel sounding techniques in general and our channel measurements performed in the IKT laboratory in detail are presented. Based on measured channels, we evaluate the BER performances of the UWB systems, then compare with results obtained by simulating with the standard channel models.

- *Chapter 6: Conclusions and Recommendations.* The final chapter contains the dissertation conclusions and an outlook on future researches.

The basic format of chapters in the dissertation (except this chapter and the final chapter) is as follows. Each chapter starts with an introductory section, which includes a research background and motivation of the problem, as well as briefly introduction to research state on the topic. The model of the problem being developed including detailed form formulation and appropriate derivations and proposed solutions are represented in the next sections. Following is a section containing the system performance evaluation by simulation results and discussion. The final section in each chapter summarizes the chapter and conclusions as well.

In this chapter, a brief introduction to the UWB channel models that are used in our work is shown in Section 2.2, followed by Principle of Time Reversal in the next Section; SISO-UWB System using the TH-PPM modulation, interference problems and proposed solution using TR are represented in Section 2.4; Performance Analyses are given in Section 2.5, then, the Summary of the Chapter is shown in the final Section.

2.1 INTRODUCTION

Time reversal has been studied extensively to apply in acoustic [27, 43], medical [28] and under water communications [90, 25] applications for two decades. Due to the simplicity in principle and aforementioned advantages, the idea of applying the TR in wireless communication has gained much attention recently [78, 44, 95, 69, 61]. In a TR, the equivalent channel is generated by the convolution of the channel and its time reversed version, which is the impulse response of a pre-filter. Hence, the response of the equivalent channel is the autocorrelation of the CIR. The autocorrelation operation of the matched filter is a process of pulse compression. The longer the train of pulses in a rich multipath channel, the sharper is the autocorrelation of the CIR. This sharpened matched filter response will reduce the inter-symbol interference greatly if the length of the multipath pulse train is large [78, 26]. This exploits the rich multipath, rather than treating it as a nuisance. This simple precoding scheme yields a concentration of power at the receiver at a particular time. Thanks to TR, the received signal is focused on the intended user at some specific position, which is determined by the transmitter using the corresponding channel to pre-filter the intended data signal. This characteristic of the TR is very helpful to mitigate the interference from co-channel users [44, 45]. Exploiting the characteristics of the TR, we can also develop solutions to deal with other interferences, such as cross-modulation interference and inter-frame interference for the TH-PPM-UWB system presented in this chapter.

In spite of all the benefits of the UWB, the extremely wide frequency bands (greater than 500 MHz) and exceptionally narrow pulses (in the range of 10^2 ps) make it difficult to apply conventional narrowband modulation techniques into UWB systems. A well-studied and the most popularly-adopted modulation scheme in UWB communications is pulse position modulation where each pulse is delayed or sent in advance of a regular time scale [33, 9]. In order to smooth the spectrum of the signal, randomizing the position in time of the generated pulses is applied. By this way, the energy spikes are spread all over the spectrum. The main approach to randomizing the pulse train are time hopping techniques [67, 57]. The data modulation

is typically based on PPM using TH as the basis for a UWB communication system.

In TH-PPM systems, a symbol is transmitted by series of pulses which are located within chips per frame according to the TH codes. If the minimum pulse to pulse duration is not long enough, multipaths within a symbol from one frame may leak into the next frame causing inter frame interference (IFI). On the other hand, if the difference in time between two possible hopping positions (due to modulation index) is less than the maximum excess delay of the channel, the multipath propagation causes cross-modulation interference (CMI) for PPM modulated signals. CMI and IFI degrade considerably the performance of the system [17, 76].

The CMI for PPM signaling is identified considering some kinds of receiver in [17, 8]. Instead of fixed modulation index, the variable value is introduced in [8] to reduce the effect of CMI. In [18], a data-aided optimal synchronization algorithm employing the MPE (minimum probability of error) metric that avoids CMI for Rake receivers is presented. The IFI problem in UWB is investigated in [23, 4, 22]. A closed form expression for the inter-symbol/inter-frame interference variance is derived in the context of a TH-UWB system [23]. With the Rake receiver, in [23], or other receiver algorithms, in [4], the IFI effect are eliminated. Efforts have been made to reduce IFI and CMI separately and given solutions, normally, require a complicated structure receiver. In TH-PPM, IFI and CMI can be reduced by increasing the modulation index, or the frame length but at cost of reduced data rate. We propose to use the TR technique to deal with both CMI and IFI problems as a low cost, low power and low complexity receiver solution for TH-PPM-UWB systems [64].

2.2 UWB CHANNEL MODEL

It is a fact that, in any communications system, the channel determines the ultimate (information-theoretic) performance limits, as well as the practical performance limits of various transmission schemes. Understanding the channel is thus a vital prerequisite for designing the systems. This is especially important for researching on the TR techniques. That is a reason for our considering on the UWB channel model represented in this section.

UWB propagation channel research has gathered more interest recently. Research reports on UWB channel modeling are categorized as relating to:

- large-scale path-loss models;
- small-scale amplitude fading models and
- path delay models.

In our work, in order to characterize the UWB channel, we use a model which is widely adopted to model the UWB channel, is proposed by Saleh, A. and Valenzuela, R. [74]. Based on the clustering phenomenon observed from measurements, authors of IEEE 802.15.3a [29] and IEEE 802.15.4 [54] standards also adopt the Saleh-Valenzuela model (S-V model) with a couple

of slight modifications. The UWB channels used in our simulations are extracted from these standard models.

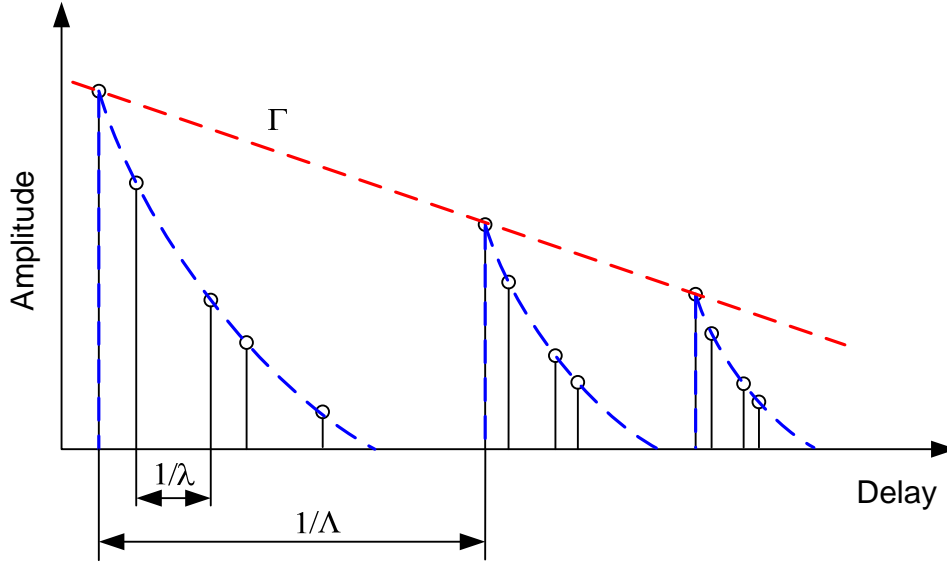


Figure 3: Principle of the Saleh-Valenzuela model.

As shown in Fig. 3, in the S-V model, multipath arrivals are divided into two different categories: a cluster arrival and a ray arrival within a cluster and dependent fading is assumed for each cluster as well as each ray within the cluster. Therefore, the multipath model consists of the following, discrete time impulse response:

$$h(t) = X \sum_{k=1}^K \sum_{l=1}^L \alpha_{k,l} \delta(t - T_k - \tau_{k,l}), \quad (2.1)$$

where X represents the log-normal shadowing, with standard deviation being σ_x , K is the total number of clusters, L the total number of rays within each cluster, $\alpha_{k,l}$ is the multipath gain coefficient of the l -th multipath component in the k -th cluster, T_k is the delay of the k -th cluster, $\tau_{k,l}$ is the delay of the l -th multipath component in the k -th cluster relative to the cluster arrival time T_k .

Let's define Λ , λ , Γ and γ as the cluster arrival rate, the ray arrival rate (i.e., the arrival rate of path within each cluster), the cluster decay factor and the ray decay factor, respectively. Both the cluster and ray arrivals are modeled by Poisson processes, given by

$$p(T_k | T_{k-1}) = \Lambda \exp[-\Lambda(T_k - T_{k-1})], \quad k > 1; \quad (2.2)$$

$$p(\tau_{k,l} | \tau_{k,l-1}) = \lambda \exp[-\lambda(\tau_{k,l} - \tau_{k,l-1})], \quad l > 1. \quad (2.3)$$

By definition, $\tau_{k,0} = 0$ for all k . The channel coefficients are defined as

$$\alpha_{k,l} = p_{k,l} \xi_k \beta_{k,l}, \quad (2.4)$$

where

$$|\xi_k \beta_{k,l}| = 10^{(\mu_{k,l} + n_1 + n_2)/20}, \quad (2.5)$$

$n_1 \propto \text{Normal}(0, \sigma_1^2)$ and $n_2 \propto \text{Normal}(0, \sigma_2^2)$ are independent and correspond to the fading on each cluster and ray, respectively. $p_{k,l}$ is equiprobable $+/- 1$ to account for signal inversion due to reflections. For a given T_k and $\tau_{k,l}$, assumed to be mutually independent, the power delay profile admits the following form:

$$\mathbb{E} \left[|\xi_k \beta_{k,l}|^2 \right] = \Omega_{1,1} \exp \left(-\frac{T_k}{\Gamma} - \frac{\tau_{k,l}}{\gamma} \right), \quad (2.6)$$

where $\Omega_{1,1}$ is the mean energy of the first path of the first cluster. The $\mu_{k,l}$ is given by

$$\mu_{k,l} = \frac{10 \ln \Omega_{1,1} - 10 T_k / \Gamma - 10 \tau_{k,l} / \gamma - (\sigma_1^2 + \sigma_2^2) \ln(10)}{\ln(10)}, \quad (2.7)$$

where σ_1 standard deviation of cluster lognormal fading term and σ_2 standard deviation of ray lognormal fading term. In the above equations, ξ_k reflects the fading associated with the k -th cluster, and $\beta_{k,l}$ corresponds to the fading associated with the l -th ray of the k -th cluster.

These above key parameters of the channel models in IEEE 802.15.3a standard are illustrated in Table 3. The main characteristics of the channel that are used to derive the above model parameters include:

- mean excess delay, τ_m ,
- RMS delay spread, τ_{rms} ,
- number of multipath components, NP.

They are shown in Table 4, where, $\text{NP}_{10\text{dB}}$ is defined as the number of multipath arrivals that are within 10dB of the peak multipath arrival, $\text{NP}_{85\%}$ is the number of multipaths containing 85% power of the channel.

It is noted that in four standard UWB channel models, CM1 and CM2 characterizes a line-of-sight (LOS) and non-line-of-sight (NLOS) scenario, respectively, with a transmission distance (between the transmitter and receiver) less than 4 m, CM3 describes an NLOS scenario with a transmission distance in the range from 4–10 m, and CM4 represents an NLOS scenario with a further longer transmission distance beyond 10 m or RMS of the delay being around 25 ns. One hundred realizations of CMs are represented in Figures 4, 5, 6 and 7.

2.3 PRINCIPLE OF TIME REVERSAL

2.3.1 Theoretical Basis

The time reversal concept is shown graphically in Figure 8. In the TR technique, thus, there are two phases:

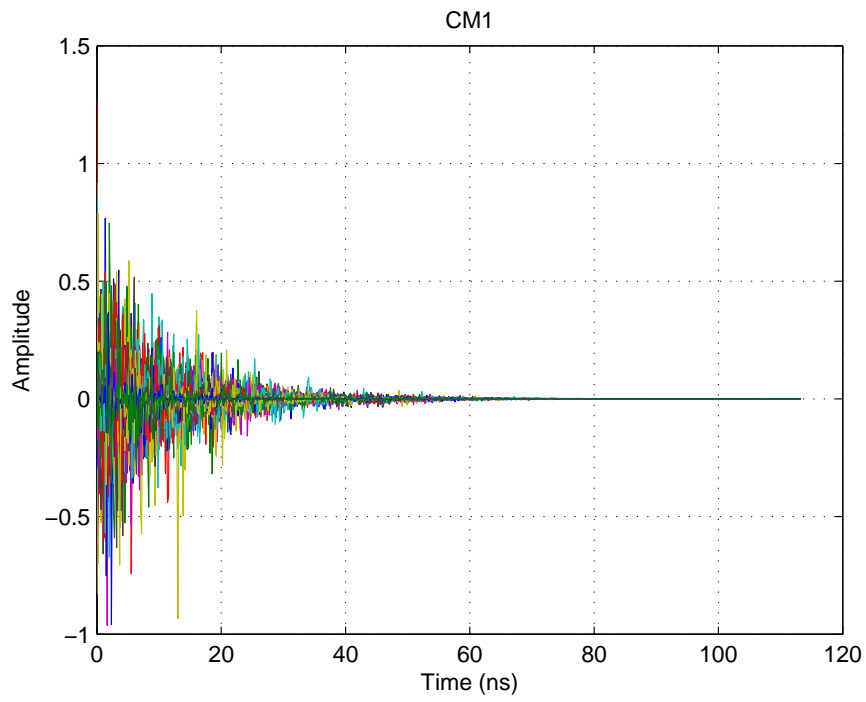


Figure 4: CM1 - 100 realizations of CIR.

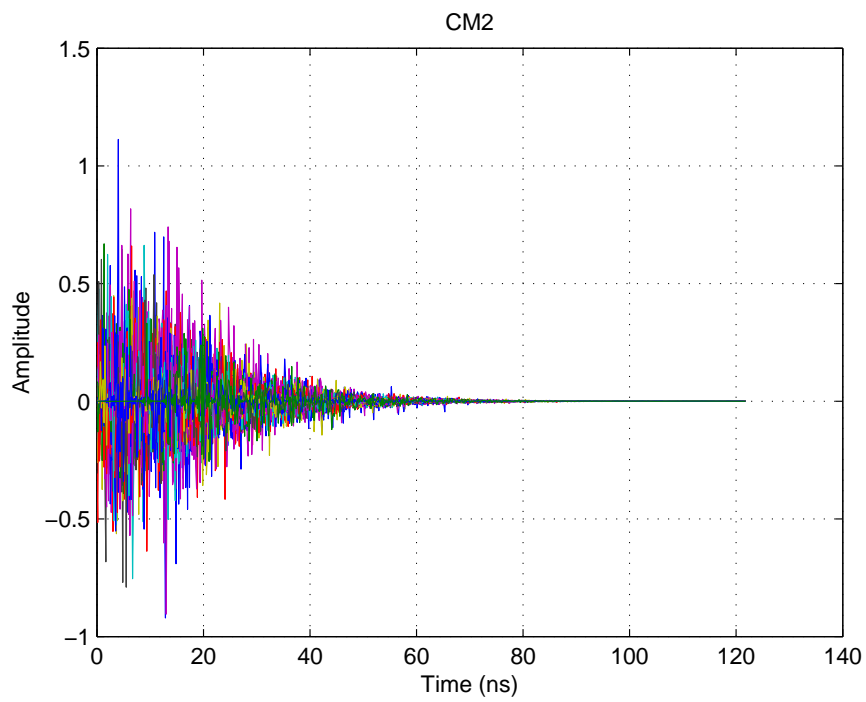


Figure 5: CM2 - 100 realizations of CIR.

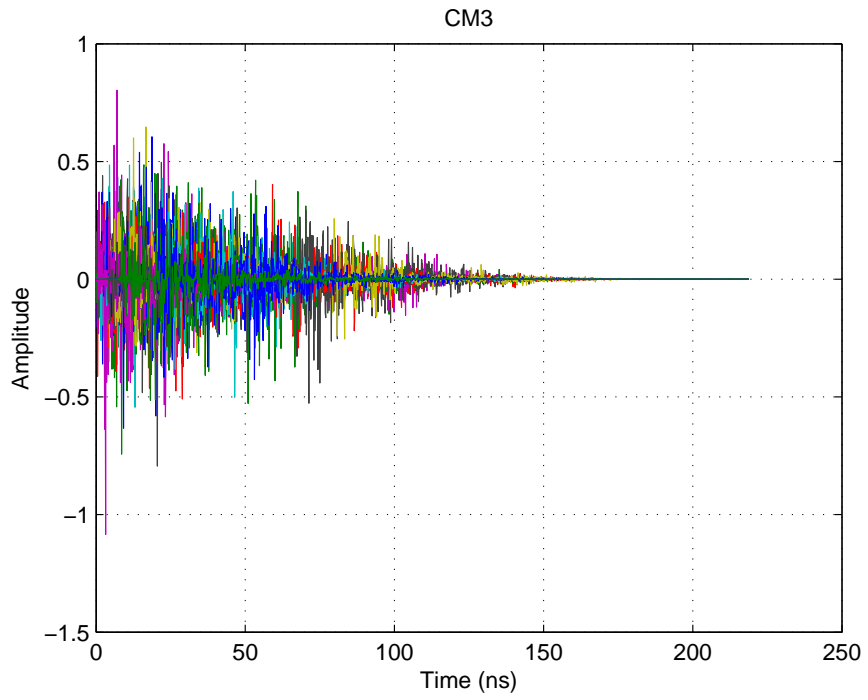


Figure 6: CM₃ - 100 realizations of CIR.

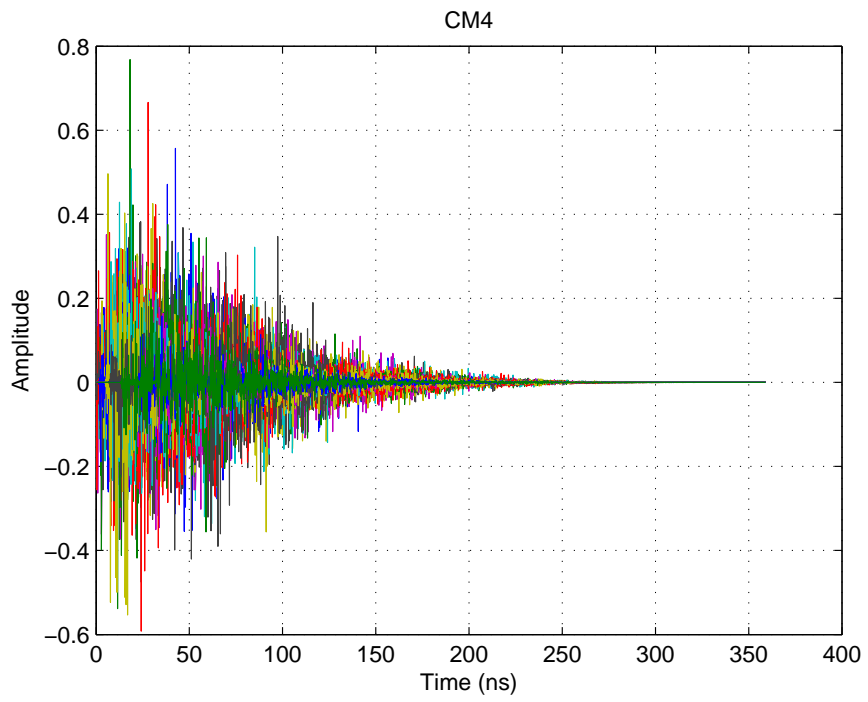


Figure 7: CM₄ - 100 realizations of CIR.

Table 3: Key parameters of channel models in IEEE 802.15.3a standard

Parameters	CM1	CM2	CM3	CM4
Λ (1/nsec)	0.0233	0.4	0.0667	0.0667
λ (1/nsec)	2.5	0.5	2.1	2.1
Γ	7.1	5.5	14	24
γ	4.3	6.7	7.9	12
σ_1 (dB)	3.3941	3.3941	3.3941	3.3941
σ_2 (dB)	3.3941	3.3941	3.3941	3.3941
σ_x (dB)	3	3	3	3

Table 4: Main model characteristics in IEEE 802.15.3a standard

Characteristics	CM1	CM2	CM3	CM4
τ_m (nsec)	4.9	9.4	13.8	26.8
τ_{rms} (nsec)	5	8	14	26
NP _{10dB}	13.3	18.2	25.3	41.4
NP _{85%}	21.4	37.2	62.7	122.8

- Phase 1: the transmitter learns the channel impulse response. A pilot signal can be used to sound the channel.
- Phase 2: the transmitter applies the temporal reverse of the CIR as a pre-filter. Thereby, the desired transmitted signal is convoluted with the complex conjugate of the time reversed version of the CIR.

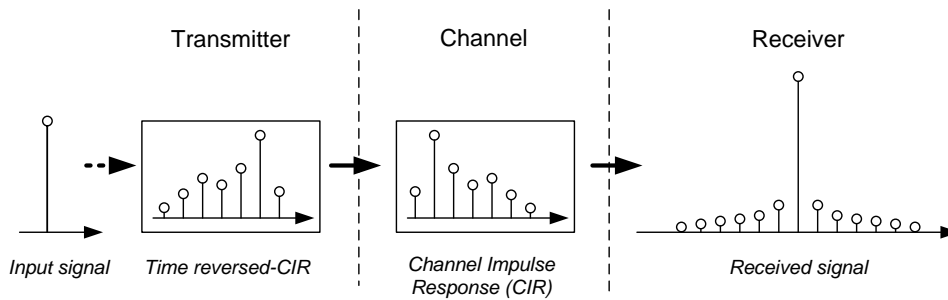


Figure 8: The time reversal concept.

The signal is propagated in the channels after being encoded by the time reverse of the CIR at the transmitter. At the receiver, all the paths add up coherently in the time and spatial domains. Inter symbol interference can be mitigated by temporal compression and multiuser interference is reduced due to spatial focusing.

The mathematical formulation of the received signal of a single-input-single-output (SISO) link using TR in the noise free situation can be represented as

$$y(t) = s(t) \otimes h(-t)^* \otimes h(t) = s(t) \otimes R^{\text{auto}}(t), \quad (2.8)$$

where $h(t)$ is the impulse response (IR) of the channel from the transmit antenna to the intended receive antenna, $s(t)$ is the transmitted signal, \otimes denotes convolution, $(.)^*$ indicates the complex conjugate; $R^{\text{auto}}(t)$ is the autocorrelation of the CIR, $h(t)$. The term *the equivalent CIR*, $h_{\text{eq}}(t)$, is used to denote the autocorrelation $R^{\text{auto}}(t)$, i.e. $h_{\text{eq}}(t) = R^{\text{auto}}(t)$.

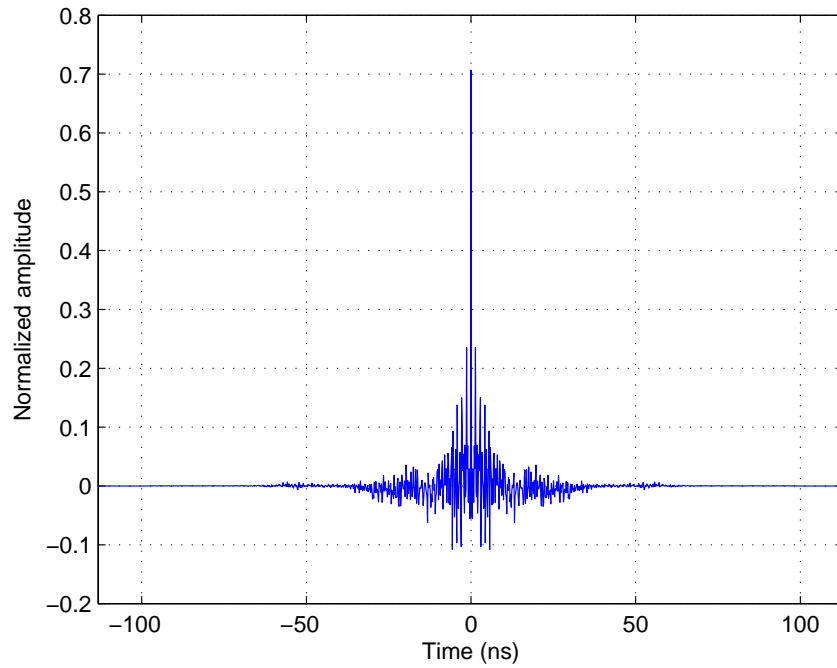


Figure 9: Autocorrelation of a CIR, CM1 in IEEE 802.15.3a standard

It is noted that a sharp peak is usually generated in the equivalent CIR due to the temporal focusing of the TR (see Fig 9). In order to measure the temporal dispersion of the equivalent CIR, we can use the Root Mean Square (RMS) delay spread which is the square root of the second central moment of the power delay profile. Mathematically, RMS delay spread can be represented as

$$\tau_{\text{rms}} = \left[\frac{\int_{-\infty}^{\infty} (t - \tau_m)^2 |h_{\text{eq}}(t)|^2 dt}{\|h_{\text{eq}}(t)\|^2} \right]^{1/2}, \quad (2.9)$$

where

$$\tau_m = \frac{\int_{-\infty}^{\infty} t |h_{\text{eq}}(t)|^2 dt}{\|h_{\text{eq}}(t)\|^2} \quad (2.10)$$

is the mean excess delay spread of the channel. RMS delay spread is one of the most important parameters because it is closely related to the inter-symbol interference.

Another metric that can be used to characterize the temporal focusing is the ratio of the peak energy to the sidelobe energy. In [95], it is defined as the ratio of the energy in the main peak to the rest of the impulse response. This ratio is mathematically expressed as

$$\eta = \frac{\max_t |h_{eq}(t)|^2}{\|h_{eq}(t)\|^2 / dt - \max_t |h_{eq}(t)|^2}. \quad (2.11)$$

As shown in [95], for a SISO-channel, the value of η is approximately 0.5 and it increases sharply when multiple antennas are used. An TR multiple-input-single-output (MISO) provides a higher temporal focusing, e.g. for a 4×1 MISO system, 80% of the energy of the channel is focused in the main peak.

Another important advantage of the TR is spatial focusing. Spatial focusing results in very low co-channel interference in a multicell system, resulting in a very efficient use of bandwidth in the overall network. Let's consider a scenario where M antennas at the transmitter transmit the signal to N receive antennas at the receive side. The signal received at the j -th received antenna is

$$\begin{aligned} y_j(t) &= \underbrace{s_j(t) \otimes \sum_{i=1}^M R_{ij}^{auto}(t)}_{\text{Signal}(j)} \\ &+ \underbrace{\sum_{i=1}^M \sum_{k=1; k \neq j}^N s_k(t) \otimes R_{ikj}^{cross}(t)}_{\text{Interference}(j)} \\ &+ \underbrace{n_j(t)}_{\text{Noise}(j)}, \end{aligned} \quad (2.12)$$

where $s_j(t)$ and $s_k(t)$ are the transmitted signals intended for the j -th and k -th receive antenna, respectively. $R_{ij}^{auto}(t) = h_{ij}(-t)^* \otimes h_{ij}(t)$ is the auto correlation of the CIR $h_{ij}(t)$ and its own time reversed complex conjugated version $h_{ij}(-t)^*$. $R_{ikj}^{cross}(t) = h_{ij}(-t)^* \otimes h_{ik}(t)$ is the cross correlation of the CIR $h_{ik}(t)$ and the time reversed complex conjugated version of the CIR $h_{ij}(-t)^*$.

The spatial focusing characteristics of the TR may be representing by the Signal to Interference ratio (SIR) as in [60]. The instantaneous SIR is calculated as the ratio of the peak power of the interested signal and the corresponding interference power at the same time lag.

$$SIR_j = 10 \log_{10} \left(\frac{|\text{Signal}(j)_{peak}|^2}{|\text{Interference}(j)_{peak}|^2} \right), \quad (2.13)$$

where $|\cdot|$ denotes the absolute value operation.

Three fundamental propagation mechanisms including reflection, diffraction and scattering generally make the propagation channel of each communication link independent and unique. In this case, we expect that the interference part in (2.12) can be suppressed.

Owning the temporal focusing and spatial focusing characteristics, the TR helps to reduce significantly the task of equalization and energy collection. Thereby, we can implement a simple detection scheme at the receiver. The TR also reduces the problem of the per-path pulse distortion since the autocorrelation operation (correlating with its time reversal) yields a much smoother symmetric signal waveform at the receiver.

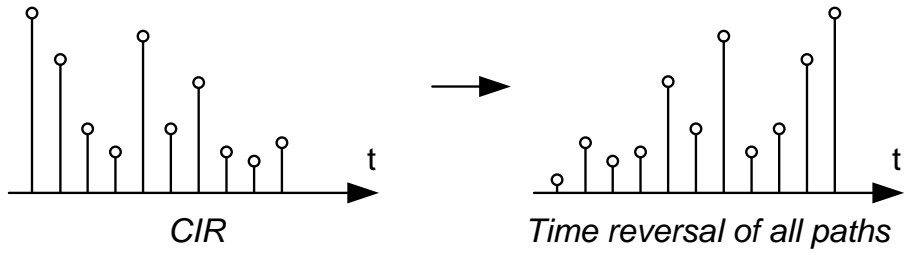
2.3.2 TR Schemes

In literature, the TR scheme is normally referred as the full time reversal [78, 69, 95] where all multipath components of the CIR are time reversed for pre-matched filtering. In the practical implementation of the TR systems, however, we can truncate in time the length of the TR pre-filter, thus reduce the system complexity. Three TR schemes that are studied in [35] and further investigated in our work in [66] include:

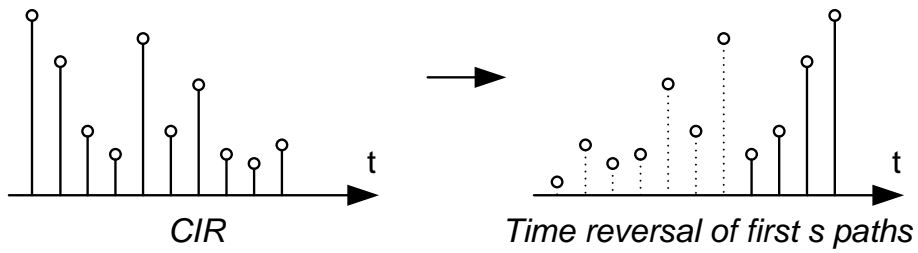
- the All TR, referred as A-TR;
- the Selective TR, referred as S-TR and
- the Partial TR, referred as P-TR.

Concepts of the TR schemes are shown in Figure 10. In the A-TR scheme, the signal is convoluted by the full time reversed CIR (the length is assumed to be L) at the pre-filter before being transmitted through the channel. Whereas, for the P-TR, the transmitted signals are generated by using the information on the s first paths and for the S-TR, the transmitted signals are generated by using the information on the s strongest paths ($s \ll L$). The performance evaluation for these schemes is presented in Section 2.5.1. Table 5 shows the power captured by impulse response of the S-TR and the P-TR pre-filters corresponding with different numbers of paths. It is obtained based on the average of 1000 realizations of the standard UWB channel models CM₁–CM₄ [29], where the sampling interval is chosen to be 0.125 ns.

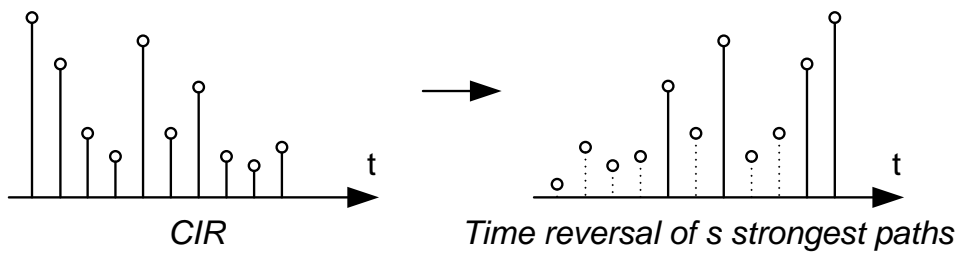
It can be seen in Table 5 that with the same captured power level, the length of the S-TR pre-filter impulse response is much less than the length of the P-TR pre-filter impulse response. For example, in order to capture 95% of total power, the S-TR pre-filter needs 110, 197, 35 and 67 taps for CM₁, CM₂, CM₃ and CM₄, respectively. Meanwhile, for P-TR pre-filter, these values of taps are 2500, 2050, 1470 and 407.



(a) A concept of the A-TR scheme



(b) A concept of the P-TR scheme



(c) A concept of the S-TR scheme

Figure 10: TR schemes.

Table 5: Power captured by TR pre-filter impulse response

	50 %		75 %		95 %		100 %	
	S-TR	P-TR	S-TR	P-TR	S-TR	P-TR	S-TR	P-TR
CM ₁	7	109	23	310	110	2500	3240	
CM ₂	15	184	49	434	197	2050	2522	
CM ₃	4	21	10	174	35	1470	3625	
CM ₄	8	47	23	257	67	407	553	

2.4 TH-PPM-UWB SYSTEM

2.4.1 Signal Model

Let us consider an impulse UWB system using the TH code and Binary Pulse Position Modulation (BPPM), with a reference pulse shape $w_{tx}(t)$. Each data symbol with symbol duration T_s is transmitted by employing N_f

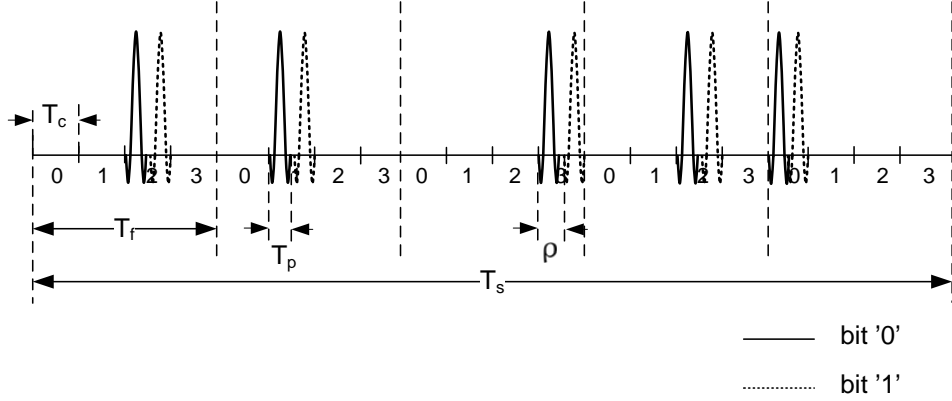


Figure 11: A TH-BPPM IR signal where $N_f = 5$, $N_c = 4$, and the TH sequence is $\{2, 1, 3, 2, 0\}$.

very short pulses, one pulse is transmitted in each frame of time T_f . The unmodulated pulse stream is represented as

$$x(t) = \sum_{n=0}^{N_f-1} w_{tx}(t - nT_f). \quad (2.14)$$

In the PPM modulation, a small shift in the pulse positions $b_n \rho$ is added, where ρ is the modulation index, $b_{\lfloor n/N_f \rfloor} \in \{0, 1\}$ is the n^{th} transmitted pulse, $b_{\lfloor n/N_f \rfloor} \in \{0, 1\}$ for the binary data stream. To avoid spectral lines, a time-shift based on a time-hopping code $c_n T_c$ is added, where the code c_n repeats after a certain interval, T_c is the chip duration. The final TH-PPM signal at the transmitter is then given by [9]

$$x(t) = \sum_{n=0}^{N_f-1} w_{tx}(t - nT_f - b_{\lfloor n/N_f \rfloor} \rho - c_n T_c), \quad (2.15)$$

where $w_{tx}(t)$ is the transmitted pulse with the duration of T_p , $T_p \leq T_c$. An example IR-UWB signal is shown in Figure 11, where five pulses are transmitted for each information symbol ($N_f = 5$) with the TH sequence $\{2, 1, 3, 2, 0\}$.

The pulse shaped signal is transmitted over a multipath channel with its channel impulse response $h(t)$ which is modeled by a tap delay line model with L taps:

$$h(t) = \sum_{l=0}^{L-1} \alpha_l \delta(t - \tau_l), \quad (2.16)$$

where α_l and τ_l are the gain and the delay of each path, respectively. The channel coefficients are normalized as $\sum_{l=0}^{L-1} \alpha_l^2 = 1$. The received signal after transmission over the multipath channel is

$$y(t) = x(t) \otimes h(t) + n(t), \quad (2.17)$$

where $n(t)$ is the white Gaussian noise with zero mean and variance of σ_n^2 and \otimes denotes convolution operation. Equation 2.17 can be written as

$$y(t) = \sum_{n=0}^{N_f-1} \sum_{l=0}^{L-1} \alpha_l^n w_{rx}(t - nT_f - b_{\lfloor n/N_f \rfloor} \rho - c_n T_c - \tau_l^n) + n(t), \quad (2.18)$$

where α_l^n and τ_l^n are the gain and the delay of the l th path for the n th bit, $w_{rx}(t)$ is the received pulse at the output of the receiver antenna. It is usually modeled as the derivative of $w_{tx}(t)$ due to the effects of the antennas [11].

The receiver using a single correlator for BPPM-TH signals is shown in Figure 12, where τ is the integration start point (supposed to be known perfectly) and $m(t)$, correlation mask, is defined later. The receiver imple-

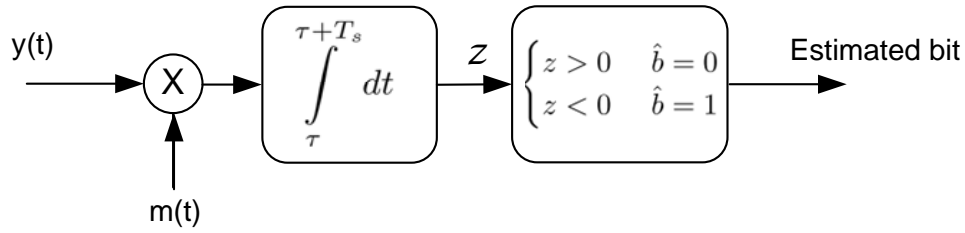


Figure 12: The block diagram of the correlator-based receiver

ments N_f independent decisions over N_f pulses that represent one bit. The final decision is obtained by applying a simple majority criterion. Giving the number of pulses falling over a threshold and comparing this number with the number of pulses falling below the same threshold, the estimated bit corresponds to the highest of these two numbers.

For the case of binary orthogonal PPM with TH coding, two possible signals are generated by the transmitter in the reference frame period $[0, T_f]$:

$$s_m(t) = \begin{cases} w_0(t - nT_f - c_n T_c), & \text{for } b = 0 \\ w_0(t - nT_f - c_n T_c - \rho), & \text{for } b = 1, \end{cases} \quad (2.19)$$

where w_0 is the energy normalized waveform of the received pulse. Let's define $W_0(t) = w_0(t - nT_f - c_n T_c)$ and $W_1(t) = W_0(t - \rho)$, $s_m(t)$ can be represented as linear combination of two orthonormal functions as

$$s_m(t) = s_{m0} W_0(t) + s_{m1} W_1(t), \quad (2.20)$$

where $m = 0, 1$ and

$$\begin{cases} s_{00} = s_{11} = 1, \\ s_{10} = s_{01} = 0. \end{cases}$$

The incoming signal is multiplied by $m(t)$, indicated as the correlation mask [10]. It is defined as follows:

$$m(t) = w_0(t - nT_f - c_n T_c) - w_0(t - nT_f - c_n T_c - \rho), \quad (2.21)$$

The output of the correlator is represented as,

$$z = \alpha_1 s_m + n_0 - n_1, \quad (2.22)$$

where

$$s_m = \begin{cases} s_0 = +1, & \text{for } b = 0, \\ s_1 = -1, & \text{for } b = 1, \end{cases}$$

and n_0, n_1 are two independent and equally distributed Gaussian random variables with zero mean and variance $N_0/2$.

2.4.2 Interferences in TH-PPM-UWB systems

In a binary PPM modulation, the bits are transmitted at two possible positions separated by the modulation index ρ . At the receiver, the decision for estimated bits is made by comparing the energy at two positions. When the modulation index is less than the maximum excess delay of the channel, the multipath component of the bit '0' is likely to appear at the location the opposite bits, '1', and vice versa. Therefore, the undesired energy due to the multipath component will affect the bit decision depending on the relative path energy at the desired and the opposite bit locations. This problem is referred as the cross-modulation interference [64].

Inside different frames of a symbol, pulses are transmitted at different positions based on TH codes when the time hopping technique is used. The distance in time between any two consecutive pulses of two frames within a symbol is denoted as D . When D is less than the channel maximum excess delay, multipath components of the bit in previous frame fall in the pulse position in the next one. This problem is called as inter-frame interference [64].

Figure 13 presents the CMI and IFI problems. For simplicity, a 3-pulse symbol is shown; all of them correspond to the transmission of the pulse that reflects the same bit value. We assume that ρ is greater than the pulse duration, the PPM modulation here is an orthogonal modulation.

In this figure, the solid and dash curves express the desired and interference signals respectively. Figure 13a) presents a bit '0' in which pulses are located in different positions per frame due to the TH codes. Pulses of bit '1' is shifted in comparison with bit '0' with amount in time of ρ as

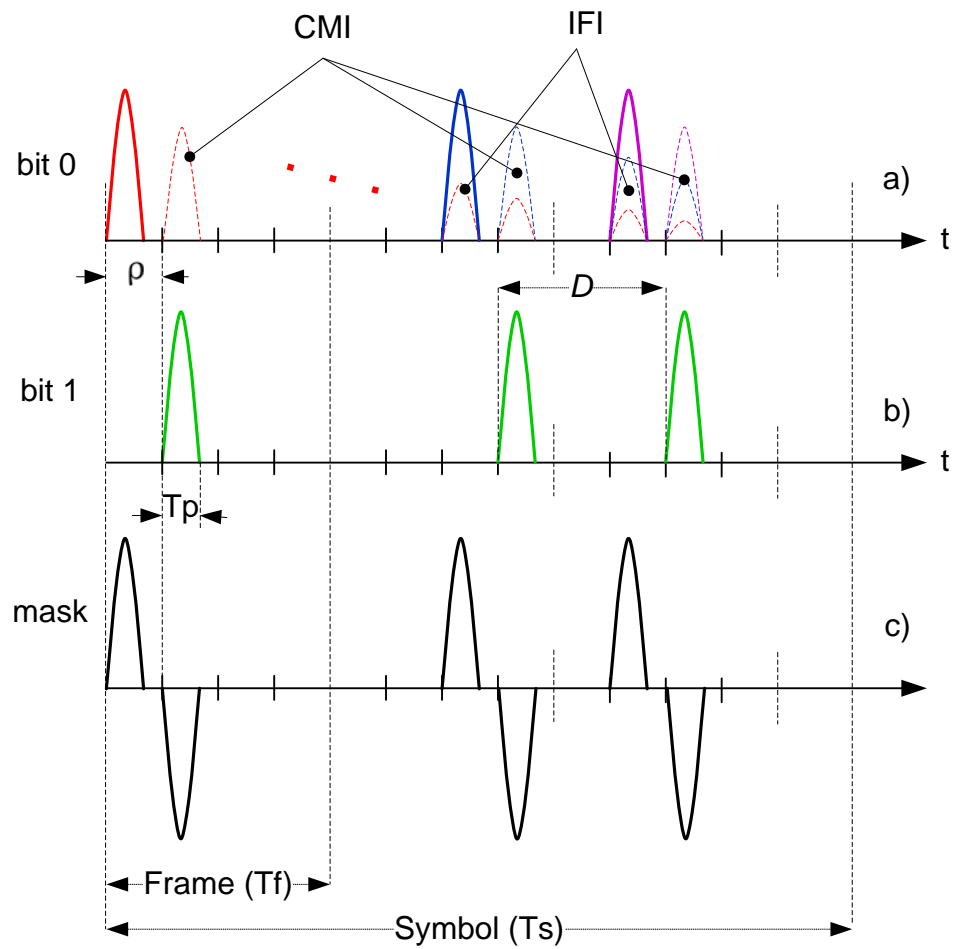


Figure 13: CMI and IFI problem illustration for BPPM-TH: a) bit '0' signal; b) bit '1' signal; c) correlation mask

presented in Figure 13b). Figure 13c) shows the mask that is mentioned above.

It can be seen that the multipath components of bit '0' fall in the pulse position of bit '1'. Consequently, even though bit '1' is not transmitted, due to these multipath components, the interference effect will occur. Within a bit, multipath components of the pulse in one frame also affect pulse(s) in one or more next frame(s) obviously. For example, here the multipath component of the first pulse (red dash curves) falls in the pulse position in the next frame and so on. The former interference is the CMI and the latter one is referred to the IFI.

For the system in which symbols are consequently transmitted, in order to avoid ISI, the $T_s \geq \tau_{\max}$ supposition is not enough, when TH is applied especially. The reason is that, multipath components of the last pulse of this symbol still affect the first pulse or others of the next. In our work, we assume that each symbol has a guard interval with the length in time equal to τ_{\max} .

The correlator receiver for $y(t)$ is composed of a bank of N_f cross-correlator, which output N_f decision variable z corresponding with one symbol given by

$$z = \int_{\tau}^{\tau+T_s} y(t)m(t)dt = \int_{\tau}^{\tau+T_s} r(t)dt. \quad (2.23)$$

For the TH-PPM scheme, when both the CMI and the IFI are taken into account, $r(t)$ is

$$\begin{aligned} r(t) = & \underbrace{\sum_{n=0}^{N_f-1} \alpha_0^n w_0^2(t - nT_f - c_n T_c - b_{\lfloor n/N_f \rfloor} \rho)}_{S\text{-signal}} \\ & + \underbrace{\sum_{n=0}^{N_f-1} \sum_{l=1}^{N_f-1} \alpha_l^n w_0(t - nT_f - c_n T_c - b_{\lfloor n/N_f \rfloor} \rho) w_0(t - nT_f - c_n T_c - b_{\lfloor n/N_f \rfloor} \rho - \tau_l^n)}_{(I_{\text{IFI}} + I_{\text{CMI}})\text{-interference}}, \end{aligned} \quad (2.24)$$

where α_0^n is the gain of the strongest path for the n th pulse. When the TH is not applied, we have

$$\begin{aligned} r(t) = & \underbrace{\sum_{n=0}^{N_f-1} \alpha_0^n w_0^2(t - nT_f - b_{\lfloor n/N_f \rfloor} \rho)}_{S\text{-signal}} \\ & + \underbrace{\sum_{n=0}^{N_f-1} \sum_{l=1}^{N_f-1} \alpha_l^n w_0(t - nT_f - b_{\lfloor n/N_f \rfloor} \rho) w_0(t - nT_f - b_{\lfloor n/N_f \rfloor} \rho - \tau_l^n)}_{(I_{\text{IFI}} + I_{\text{CMI}})\text{-interference}}. \end{aligned} \quad (2.25)$$

If we assumed that the frame length is greater than the maximum channel excess delay and the transmitted pulse normally is located in the first (bit

'o') and the second (bit '1') chip in each frame, the IFI can be avoided. Then, $r(t)$ is presented as

$$r(t) = \underbrace{\sum_{n=0}^{N_f-1} \alpha_0^n w_0^2(t - nT_f - b_{\lfloor n/N_f \rfloor} \rho)}_{S\text{-signal}} + \underbrace{\sum_{n=0}^{N_f-1} \alpha_1^n w_0(t - nT_f - b_{\lfloor n/N_f \rfloor} \rho) w_0(t - nT_f - b_{\lfloor n/N_f \rfloor} \rho - \tau_1^n)}_{I_{\text{CMI-interference}}}, \quad (2.26)$$

where α_1^n and τ_1^n is the gain and the delay of the multipath component nearest the strongest path for the n th pulse.

2.4.3 Interferences Mitigation with TR

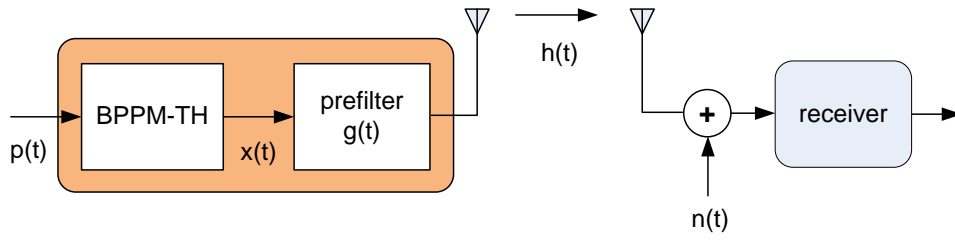


Figure 14: The block diagram of a SISO-TR-UWB system

The time reversal technique is proposed to combat the CMI and IFI problem. We suppose that the A-TR scheme is use and the result can be also extended for other TR schemes. The transmission scheme is shown in Figure 14. The temporal reverse of the CIR $h(-t)$ is deployed at the transmitter side as a pre-matched filter to generate the encoded data $c(t) = g(t) \otimes x(t)$, where $g(t) = \Lambda h(-t)$ is the prefilter response, Λ is the power scaling factor to normalize the transmission power. In order to ensure that the prefilter does not amplify the signal, the value of Λ is set to be

$$\Lambda = \frac{1}{\sqrt{\int_{-\infty}^{+\infty} |h(t)|^2 dt}}, \quad (2.27)$$

The equivalent CIR of the TR-UWB system, thus, can be expressed as

$$\begin{aligned} h_{\text{eq}}(t) &= \Lambda h(-t) \otimes h(t) \\ &= \Lambda \sum_{m=0}^{L-1} \sum_{l=0}^{L-1} \beta_m \alpha_l \delta \left(t - \left(\tau_l - \tau'_m \right) \right), \end{aligned} \quad (2.28)$$

where $\beta_m = \alpha_{L-1-m}$ and $\tau'_m = \tau_{L-1-m}$. Equation 2.28 can be rewritten as

$$h_{eq}(t) = \Lambda \sum_{i=0}^{L-1} (\alpha_i)^2 \delta(t) + \Lambda \sum_{\substack{m=0 \\ m \neq l}}^{L-1} \sum_{l=0}^{L-1} \alpha_m \alpha_l \delta\left(t - (\tau_l - \tau'_m)\right). \quad (2.29)$$

It can be seen from Equation 2.29 that at $t = 0$, all the energies of paths add coherently. However this is not true for $t \neq 0$, as other terms in the second part of 2.29 will add destructively and form interference-like spikes. As mentioned above that the TR can provide a high peak to sidelobe energy ratio. Hence, in the system using the TR, multipath components of each bit are suppressed and affect less the opposite bit located at the opposite position. In the same way, multipath components of the pulse in this frame do not bring about bad effects on pulses of other frames. In other words, the TR can lessen efficiently the CMI and the IFI.

2.5 PERFORMANCE ANALYSES

2.5.1 Performance evaluation of TR schemes

For the A-TR scheme, at the transmitter, the signal is convoluted by the full time reversed CIR. This equivalent to the operation where the transmitted signal is scaled by factors related to the multipath gains of the channel. After passing the TR pre-filter, the transmitted signal is represented as

$$x(t) = \sum_{n=0}^{N_f-1} \sum_{m=0}^{L-1} \Lambda^n \beta_m^n w_{tx}\left(t - nT_f - b_{\lfloor n/N_f \rfloor} \rho - c_n T_c - \tau_m'^n\right), \quad (2.30)$$

where Λ^n , $\beta_m^n = \alpha_{L-1-m}^n$ and $\tau_m'^n = \tau_{L-1-m}^n$ are the normalized power factor, the m th sample amplitude and delay for the n th pulse respectively. The received signal is given by

$$y(t) = \sum_{n=0}^{N_f-1} \sum_{m=0}^{L-1} \sum_{l=0}^{L-1} \Lambda^n \beta_m^n \alpha_l^n w_{rx}\left(t - nT_f - b_{\lfloor n/N_f \rfloor} \rho - c_n T_c - (\tau_m'^n + \tau_l^n)\right) + n(t). \quad (2.31)$$

For the P-TR, the transmitted signals are generated by using the information on the s first paths while for the S-TR, the transmitted signals are generated by using the information on the s strongest paths ($s \ll L$). The S-TR and the P-TR schemes reduce the complexity of the transmitter and the amount of the required channel information to generate the transmitted signals. The concepts of these two schemes with the number of needed paths $s = 4$ are illustrated in Figures 10b and 10b.

The transmitted signal for the P-TR and the S-TR is expressed as

$$x(t) = \sum_{n=0}^{N_f-1} \sum_{m=0}^{s-1} \Lambda_c^n \beta_m^n w_{tx}\left(t - nT_f - b_{\lfloor n/N_f \rfloor} \rho - c_n T_c - \tau_m'^n\right), \quad (2.32)$$

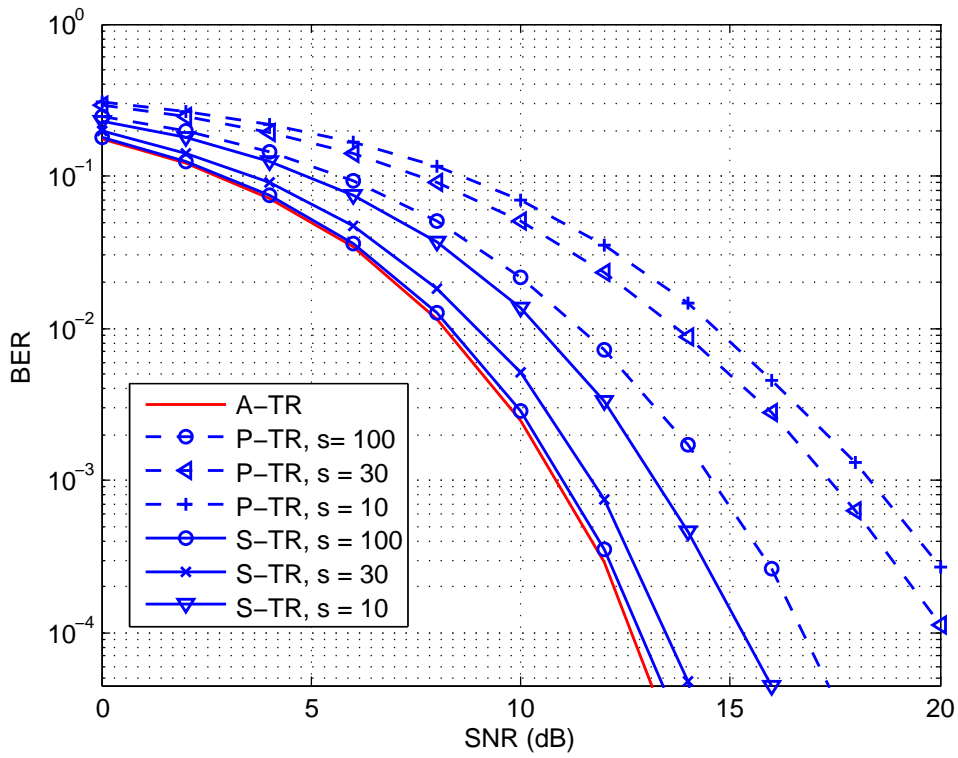


Figure 15: BER vs. SNR for different TR schemes, CM1

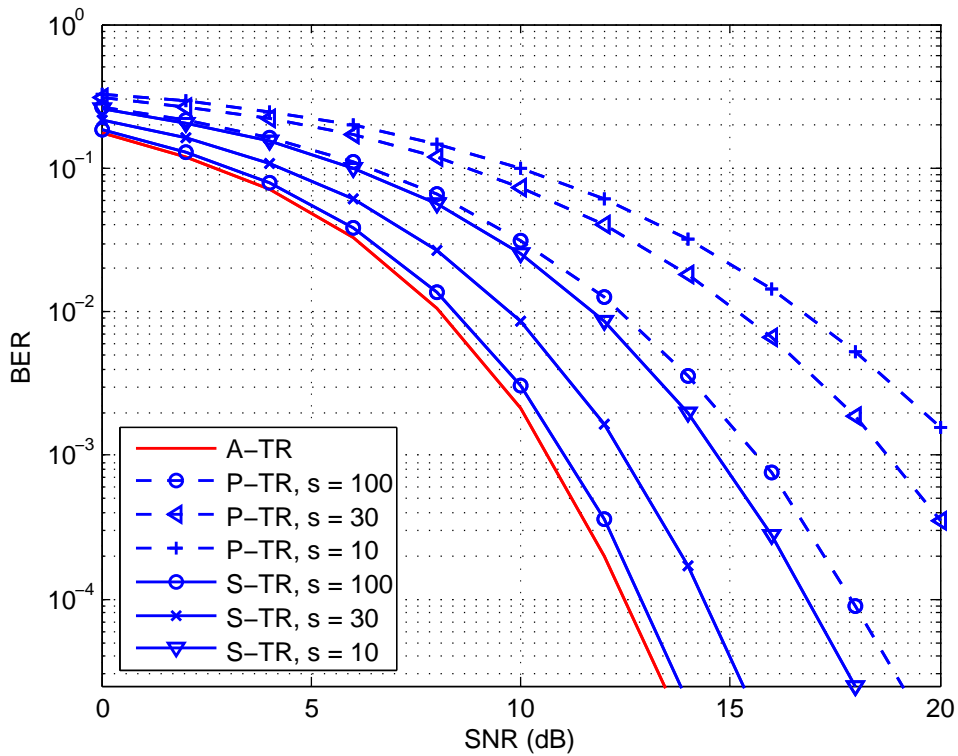


Figure 16: BER vs. SNR for different TR schemes, CM2

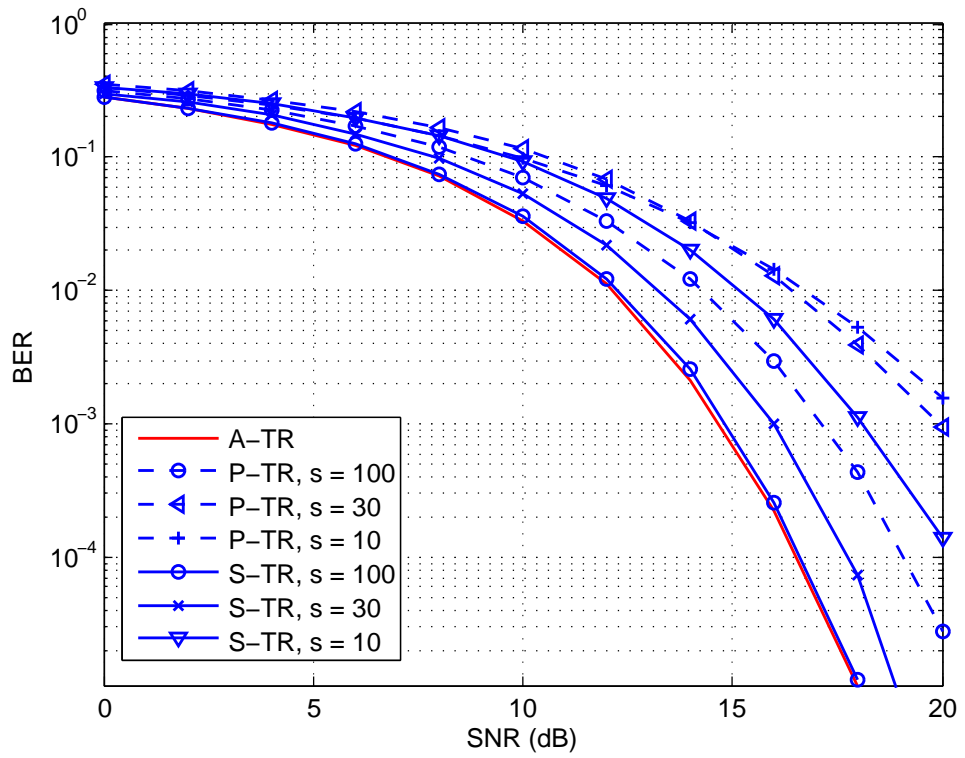


Figure 17: BER vs. SNR for different TR schemes, CM₃

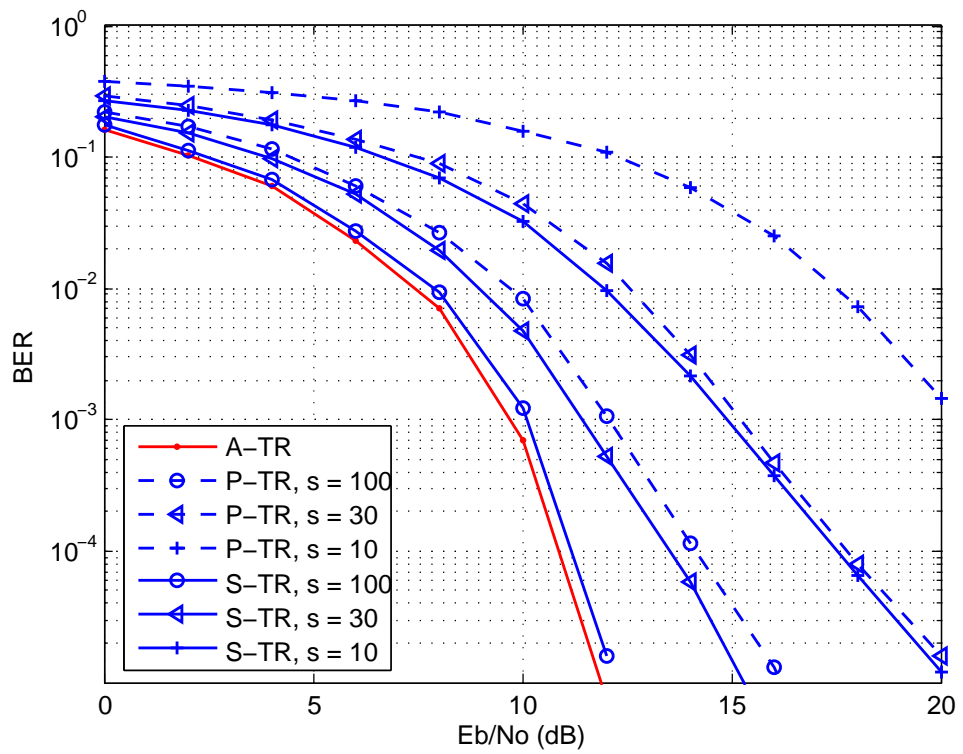


Figure 18: BER vs. SNR for different TR schemes, CM₄

where Λ_c^n , $\beta_m^n = \alpha_{s-1-m}^n$ and $\tau_m'^n = \tau_{s-1-m}^n$ are the normalized power factor, m th sample amplitude and delay for the n th pulse respectively. The received signal is represented as

$$y(t) = \sum_{n=0}^{N_f-1} \sum_{m=0}^{s-1} \sum_{l=0}^{L-1} \Lambda_c^n \beta_m^n \alpha_l^n w_{rx}(t - nT_f - b_{\lfloor n/N_f \rfloor} \rho - c_n T_c - (\tau_m'^n + \tau_m^n)) + n(t). \quad (2.33)$$

Simulation is carried out to evaluate the performances of the systems using above mentioned TR schemes with IEEE 802.15.3a multipath channel models, CM1-CM4 [29].

The BER performance as a function of the SNR of the PPM-UWB systems for CM1, CM2, CM3 and CM4 are shown in Figures 15, 16, 17 and 18, respectively. In these figures, the BER performances are calculated for P-TR and S-TR schemes, the number of paths is $s = 10, 30, 100$. It can be seen that the performance of the system using the A-TR is the best, and for the S-TR and P-TR schemes, when the number of paths increases, the BER performance is mostly improved. However, with $s = 100$, the S-TR scheme can provide nearly the same BER performance that the system using the A-TR scheme can achieve.

2.5.2 Interferences Mitigation with TR

Simulation is conducted to verify the performance improvement of the proposed scheme for TH-PPM-UWB systems in term of the SIR and BER when both the CMI and the IFI or only the CMI are (is) considered. It is assumed that the data is transmitted by sequence of 1st derivative Gaussian pulses. Because of the antennas effect, the received pulse which is the derivative of the transmitted pulse, is as follows:

$$w_0(t) = \left[1 - 4\pi \left(\frac{t - t_c}{w_d} \right)^2 \right] e^{-2\pi \left(\frac{t - t_c}{w_d} \right)^2}, \quad (2.34)$$

where w_d is a parameter corresponding to pulse width (pulse duration T_p), and t_c is a time shifting of the pulse. A guard interval equaling to the maximum channel excess delay is used to exterminate the ISI. The signal is transmitted over UWB channels, perfectly known at the transmitter side. In this chapter, the IEEE 802.15.3a CM4 channel model [29] is used in simulation. The parameters of the simulation are presented in Table 6.

The SIR cumulative distribution of the PPM system with or without TH is shown in Figure 19. It can be seen in this figure that TH does not influence the SIR of the system when we consider both the CMI and the IFI. This can be explained as follows. The energy of the desired signal (S) is the sum of the energy from the direct paths of transmitted pulses and always constant no matter TH is applied or not. Similarly, the energy of the interference caused by the CMI is constant because of being sum of the energy from

Table 6: Simulation parameters

Parameters	Value	Unit
Channel	CM4	-
Center Freq.	4.5	GHz
Sample Freq.	6	GHz
Pulse Shape	Gaus. (second der.)	
Pulse duration	0.83	ns
t_c	0.42	ns
w	0.42	ns
Modulation	BPPM	-
TH code	random	-
No. pulse per bit	5	pulse

the second strongest paths of transmitted pulses. As mentioned above, TH codes are random, it means pulses are located randomly in each frame. Thus, the interference energy that one pulse interfere with the others is contingently and the average value over multiple frames should be the same for the TH and no TH case. The interference energy caused by both the CMI and the IFI is consequently constant in two cases.

Figure 20 illustrates the difference of the SIR density for the PPM system when the IFI is considered or not. We can observe that the IFI is responsible for about 5 dB increase.

For all cases in Figure 19 and 20, the proposed scheme provides a significant improvement in term of the SIR. With the probability at 10^{-2} , this improvement is nearly 15 dB of the SIR. Notice that with the proposed PPM transmitter, the energy of desired signal mostly higher than interference, but with conventional scheme it is not like this, especially if both the CMI and the IFI are considered. The improvement in the SIR will, therefore, affect the BER performance. Figure 21 and 22 show the BER performance comparison of the proposed and conventional PPM transmitters.

Because TH has no effect on the SIR, it almost does not make the difference in the BER performance, presented in Figure 21. Using the TR as a pre-filter at the transmitter side, we can gain the very good performance, i.e at $E_b/N_0 = 14\text{dB}$, $\text{BER} \approx 10^{-3}$ while without TR, the system performance is unacceptable.

Figure 22 presents different BER curves of the PPM system when the IFI is considered or not. If the IFI is ignored, the BER performance of the conventional PPM system is better noticeably. The performance of the proposed scheme is still much better than the conventional, however. For example, at $\text{BER} = 8 \cdot 10^{-2}$, the better is 12dB. In the proposed system, at $\text{BER} = 10^{-3}$, the performance increases approximately 3dB when the IFI is skipped.

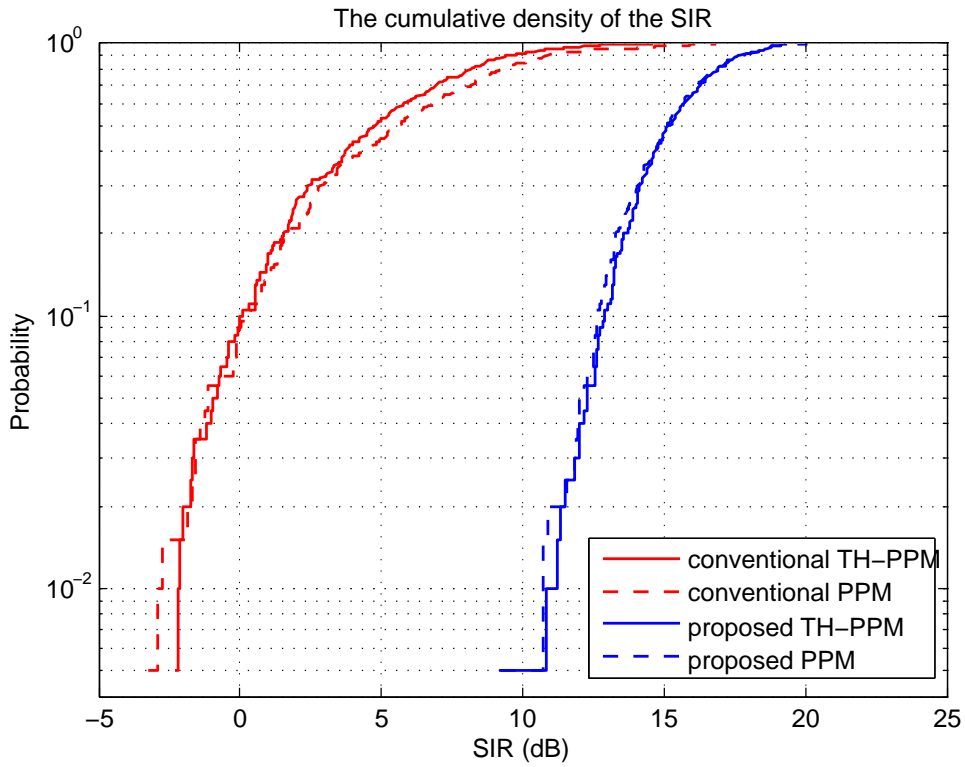


Figure 19: The cumulative density of the SIR for both conventional and proposed PPM-UWB systems with and without TH, both CMI and IFI are taken into account

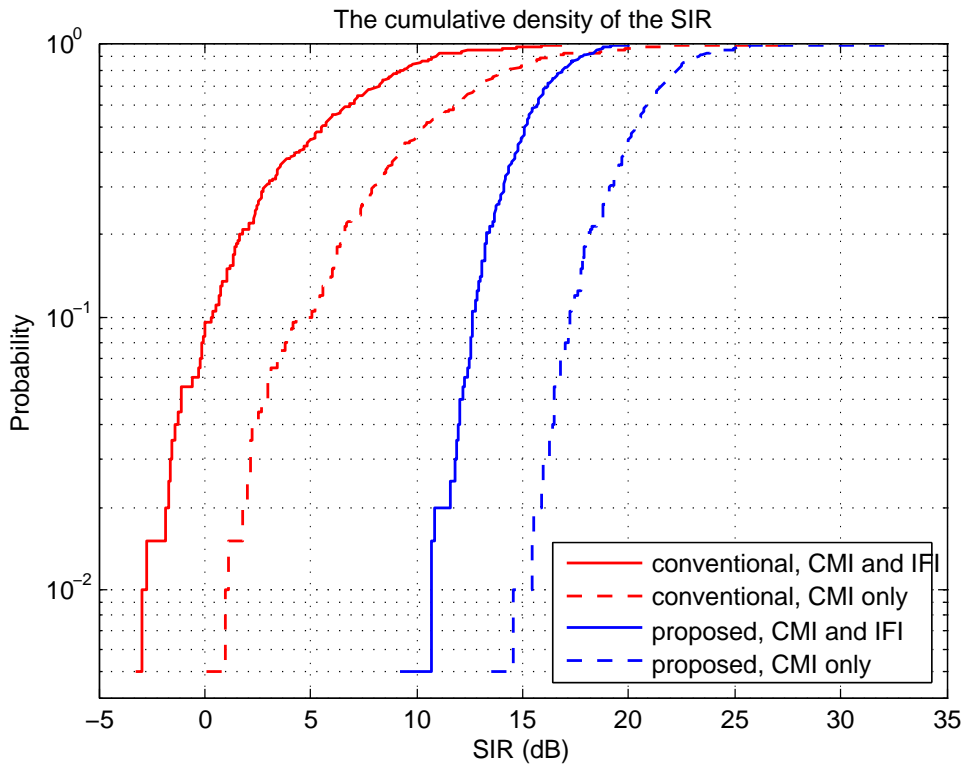


Figure 20: The cumulative density of the SIR for both conventional and proposed PPM-UWB systems when IFI is or is not considered.

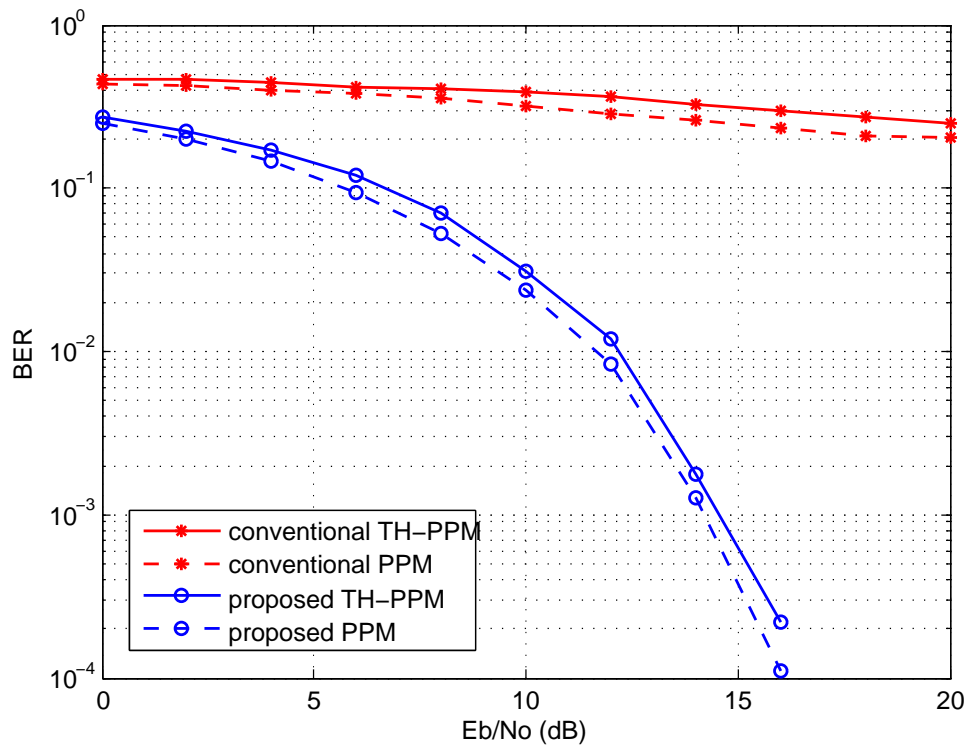


Figure 21: BER performance of both conventional and proposed PPM-UWB systems with and without TH, both CMI and IFI are taken into account.

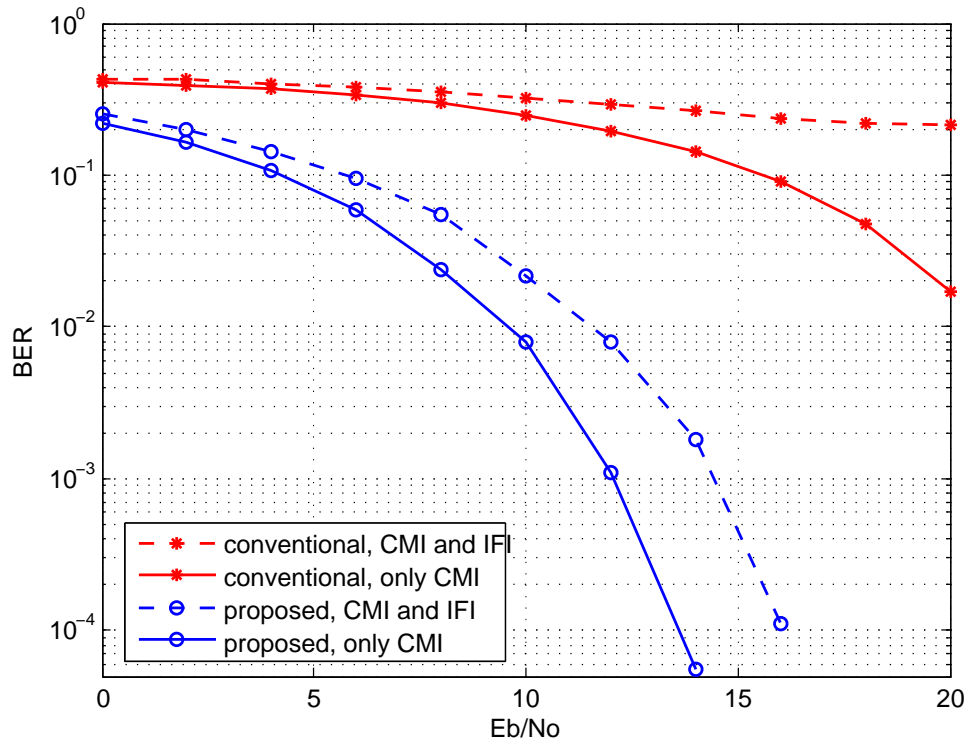


Figure 22: BER performance of both conventional and proposed PPM-UWB systems when IFI is or is not considered

2.6 SUMMARY

The beginning sections of this chapter are spent for briefly introducing the UWB channel models that are applied and used in simulation in our whole work and the theoretical basis of the time reversal technique.

In this chapter, we focus on the TR technique applying for the SISO-UWB system. Three schemes of TR including the A-TR, the P-TR and the S-TR are presented. We evaluate the performance of the TR schemes for SISO-UWB systems in IEEE 802.15.3a UWB multipath channel model by computer simulation. From the simulation results, we show that the S-TR scheme is effective to achieve the good BER performance with less amount of the channel information.

The CMI and the IFI problem in the TH-PPM SISO-UWB system are investigated in this chapter. In order to suppress these interferences we propose to use the TR pre-matched filter at transmitter. Base on a idea of shifting the design complexity from the receiver to the transmitter, the TR technique has been applied for UWB applications. Due to a unique feature of space-time domain focusing of the TR pre-filtering, the ISI in the UWB system is combated without complicated Rake receivers. In the same way, the CMI and the IFI can be also mitigated.

The amount of the CMI and the IFI is evaluated by the SIR. As being presented in simulation results for both the PPM and the TH-PPM scheme, the efficiency of the proposed scheme is expressed by increasing the SIR greatly, and improving the BER performance of the system correspondingly. The proposed approach can be extended for multi-user cases when different TH codes are allocated for various users.

TIME REVERSAL FOR SINGLE USER MIMO-UWB SYSTEMS

Application of the time reversal technique in the single user UWB system is further studied in this chapter for MIMO configuration with the spatial multiplexing scheme. Contents of this chapter are organized as follow: a succinct introduction of the chapter is provided in the first Section, followed by system descriptions in Section 3.2; Section 3.3 presents the TR-based pre-filter as well as pre-equalizer designing for an SM-MIMO-UWB system; the channel correlation problem is addressed in the Section 3.4; Two last sections, Section 3.5 and 3.6, are BER Performance Analysis and Summary respectively.

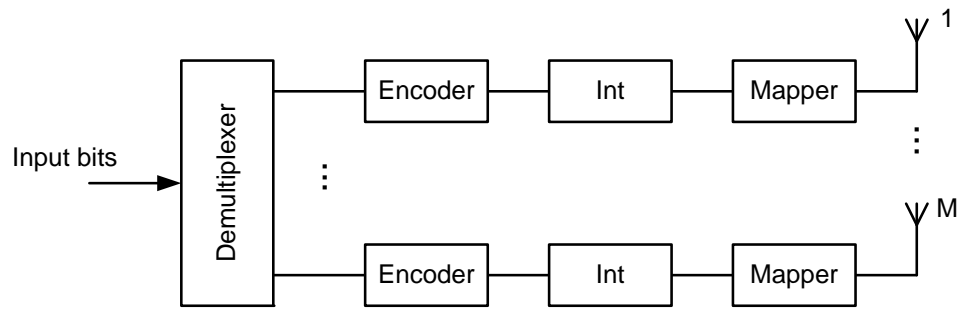
3.1 INTRODUCTION

MIMO technique is mainly based on the theoretical work developed by Teleatar [83] and Foschini [30]. The core of this idea is use multiple antennas both for transmission and reception in order to provide a large increase in capacity compared to traditional single antenna systems. Capacity is expressed as the maximum achievable data rate for an arbitrarily low probability of error. Many coding techniques has been introduced and developed to improve link-level performance or capacity [82, 5, 31].

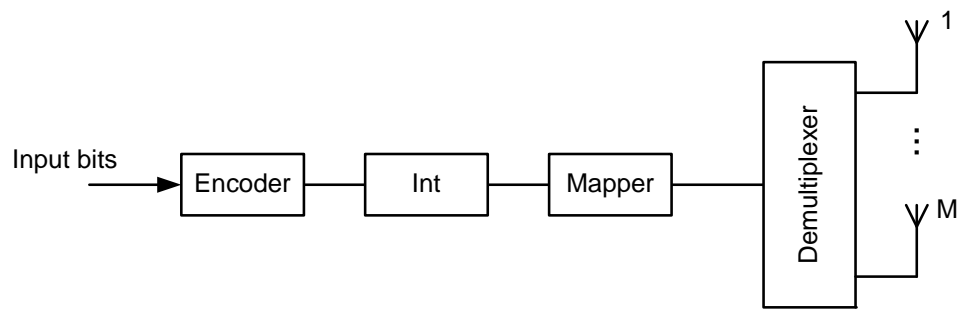
Spatial multiplexing (SM), also called the layer space-time (LST), techniques have a different orientation than the coding methods [31, 6, 30]. The general operation behind SM processing is to break the sequence of information bits into a certain set of sub-streams through a demultiplexer and these sub-streams will be treated differently. The demultiplexing operation can be applied to bits or symbols.

The demultiplexing of the data information stream can be realized in three different ways according to the demultiplexer position in the transmitter chain and the directions of the layers. The encoding processes are known as horizontal, vertical and diagonal SM and are schematically drawn from top to bottom in Figure 23. In the horizontal encoding case, the data bits are demultiplexed into M_T sub-streams that are independently encoded, interleaved and modulated. In vertical encoding SM, the data stream is at first coded, interleaved and modulated and the resulting symbols are then demultiplexed into M_T substreams. Diagonal SM encoding is similar to horizontal encoding with the only difference that, after the final stage, the frames of symbols undergo a stream interleaver, which rotates the transmitted frames by padding with zero some antennas.

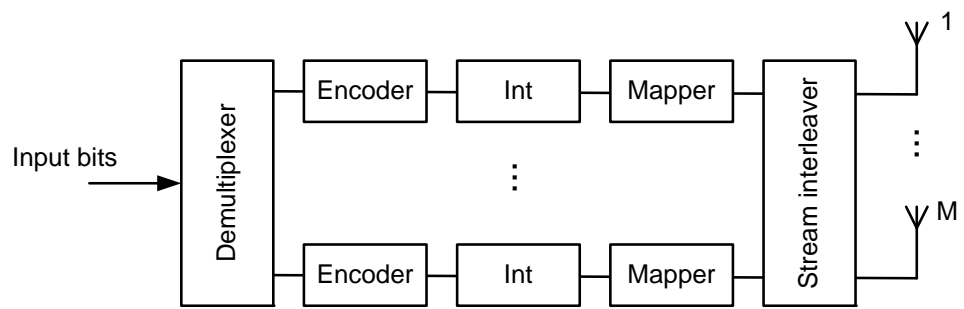
In SM, M_T independent symbols are transmitted from M_T transmitting antennas. Therefore, there are two main advantages of SM techniques. First, these techniques can reach a closer bound to the available capacity of MIMO systems, since the spatial rate is equal to the number of transmit antennas



(a) Horizontal Spatial Multiplexing



(b) Vertical Spatial Multiplexing



(c) Diagonal Spatial Multiplexing

Figure 23: Spatial Multiplexing Encoding Schemes.

M_T . On the other hand, the complexity requirement, while heavy, remains constant and independent of the modulation in use, which is not the case of Space Time Trellis Codes (STTCs). In general, in order to perform SM, the number of receive antennas must be equal to or greater than the number of transmit antennas.

Theoretically, the performance of wireless communication systems can be improved by having multiple antennas at the transmitter and the receiver. In practice, since in many situations sparse scattering and insufficient spacing between adjacent antennas make the channels between different antennas be often correlated, however, and therefore the multi-antenna gains may not always be obtainable. The spatial correlation in the multipath channel is a critical factor in the performance of a MIMO system and it prevents a MIMO system from offering any performance enhancement [46]. High correlation between multiple signal streams can reduce the channel matrix rank. The spatial correlation needs to be taken into account, consequently. There have been numerous correlated channel models applicable for narrowband transmission reported in the literature [41, 52]. For the UWB communication, a comprehensive analysis of spatial correlation is undertaken based on channel measurements in [49] and a constant spatial correlation model for MIMO systems with linear array structures is proposed in [3].

The potential of a MIMO UWB system using spatial multiplexing scheme is considered in [84], where the matching filter plays the role of a time reversal filter and the Maximum Likelihood detector is used to deal with the multi-streams interference but ignores the ISI. The combination of time reversal with UWB-MIMO has been studied recently. The theory of TR applying for the impulse MIMO-UWB is given in [70], where the proposed system paradigm uses TR with non-coherent detection as an alternative to coherent reception. Authors in [96] analyze the performance of the UWB-MIMO-TR system with a simple one-correlator receiver based on UWB channels measured in an office environment.

The SM-MIMO-UWB system using TR is introduced in [59] with the capability of transmit antenna selection. The TR technique and pre-equalizer are proposed in [59] and [58] for the virtual MIMO UWB system. As shown in [58], with the help of the TR pre-filter and a properly designed pre-equalizer, the system with only one transmit antenna can deliver several independent data streams at the same time. However, the spatial correlation among the transmit and receive antennas is not considered in [58].

It is learned from [58, 39] that in the SM-MIMO-UWB system, the MSI increases proportionally with the number of data streams and also with the number of the transmit antennas through the different channels. The signal to interference-plus-noise power ratio (SINR) of the full system will be saturated when the transmit power is very high. The SINR depends only on the numbers of transmit and receive antennas, the power of the channels, and the cross-correlation coefficients of the CIRs of the channels, but it is not affected by the transmitted power. Thus, a BER floor of the system will be produced at the high SNR range. In our work, a pre-filter

and a pre-equalizer are adopted to combat with both the MSI and the ISI in a SM-MIMO system [66].

As shown in Chapter 2, for the SISO configuration, using a limited number of taps of the channel impulse response, the S-TR pre-filter can provide the same performance in term of BER as the A-TR pre-filter does. For this reason, in this chapter, we continue to investigate and compare the efficiency of three kinds of the TR pre-filter (called as pre-Rake in [64]) including the full-TR (A-TR) pre-filter, the partial-TR (P-TR) pre-filter and the selective-TR (S-TR) pre-filter applied for the SM-MIMO system. The appearance of the TR pre-filter makes the equivalent CIR be time focused and we can shorten it efficiently when designing the pre-equalizer. By so doing, the complexity of the transmitter so can be reduced significantly.

Furthermore, the impact of the spatial correlation among the transmit and receive antennas in the SM-MIMO-UWB system is also investigated in this chapter. The MIMO-UWB system can achieve transmit diversity [58], but it suffers from penalty caused by both transmit and receive antenna correlations. The single-input multiple-output UWB (SIMO-UWB) or virtual MIMO-UWB does not face the transmit antenna correlation problem because it has only one transmit antenna. It will be shown that under high spatial correlation conditions, the virtual MIMO outperforms the true MIMO system in term of the BER performance.

3.2 SU-SM-MIMO SYSTEM

In the SM-MIMO system, several streams of data are transmitted over several transmit antennas at the same time. The channel capacity can be increased proportionally to the number of antennas. Let us consider an SM-MIMO-UWB system with M transmit and N receive antennas as shown in Fig. 24.

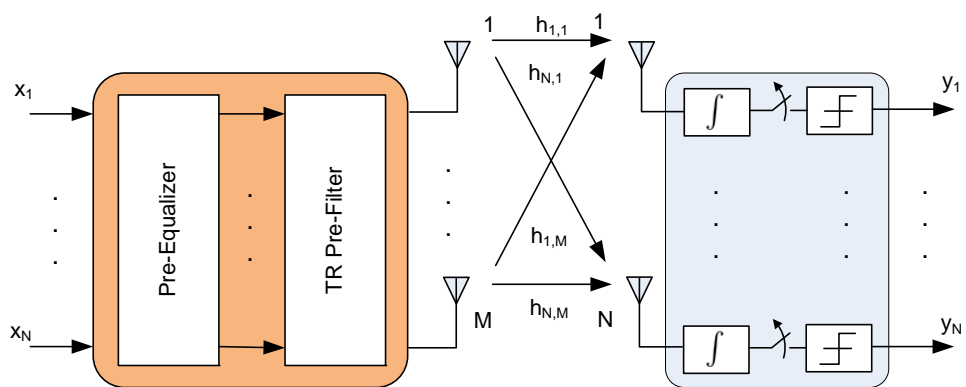


Figure 24: Block diagram of MIMO-UWB system with pre-Filter and pre-Equalizer.

We assume that the binary pulse amplitude modulation (BPAM) with a proper UWB monopulse is used and the transmitted signal for every input of the MIMO system is represented as

$$x(t) = \sqrt{E_b} \sum_{k=-\infty}^{+\infty} d_k p(t - kT), \quad (3.1)$$

where $d_k = \pm 1$ is the transmit data, E_b is the bit energy, $p(t)$ is the desired pulse shape, and T denotes the symbol duration.

After passing through a pre-equalizer and a pre-filter (investigated in the next section), the signal is transmitted over multipath channels which are modeled by a tap delay line model. We assume that the maximum length of each of the $M \times N$ multipath channel realizations between transmit and receiver sides is L . The channel impulse response between the j -th transmit antenna and the i -th receive antenna is

$$h_{i,j}(t) = \sum_{l=0}^{L-1} \alpha_l^{i,j} \delta(t - \tau_l^{i,j}), \quad i = 1 \dots N, j = 1 \dots M, \quad (3.2)$$

where $\alpha_l^{i,j}$ and $\tau_l^{i,j}$ is the amplitude and the delay of the l -th tap.

We can arrange these channels in a matrix form as below

$$\mathbf{H}(t) = \begin{pmatrix} h_{1,1}(t) & h_{1,2}(t) & \dots & h_{1,M}(t) \\ h_{2,1}(t) & h_{2,2}(t) & \dots & h_{2,M}(t) \\ \vdots & \vdots & \ddots & \vdots \\ h_{N,1}(t) & h_{N,2}(t) & \dots & h_{N,M}(t) \end{pmatrix}. \quad (3.3)$$

The receiver for every data stream is a simple integrate-and-dump (I&D) receiver with the sampling rate is $1/T$.

3.3 PRE-FILTER-EQUALIZER DESIGN

3.3.1 Time Reversal Pre-Filter

Owning the temporal focusing property, the TR technique has shown great potential in reducing the ISI caused by the multipath channel in UWB systems [38, 69, 62]. Combining with the pre-equalizer, the TR pre-filter helps to mitigate both the ISI and MSI in the MIMO-UWB system as shown in [59, 58, 66].

As presented in the previous chapter, in the TR system, the temporal reverse of the CIR is deployed at the transmitter side as a pre-matched filter to efficiently shorten the overall CIRs. The transmitted signal $x(t)$ is convoluted with the time reversed CIR $h(-t)$ to generate the encoded data $c(t) = h(-t) \otimes x(t)$. Thereby, we have the equivalent channel $\hat{h}(t) = h(t) \otimes h(-t)$ which is the autocorrelation of the impulse response of the multipath channel. The power of the equivalent channel $\hat{h}(t)$ is focused within a very narrow time duration and the received signal can achieve high focusing gain.

In Chapter 2, simulation results show that in the SISO TR-UWB system, despite using the information on the limited number of strongest paths, the S-TR pre-filter can provide the good performance as the full-TR pre-filter does. In this chapter, we continue to consider three TR schemes and compare their efficiency when they are applied for the SM-MIMO system.

Let $\bar{h}_{i,j}(-t)$ denote the time reversal of the full (for the A-TR scheme) or a path (for the S-TR and the P-TR schemes) of CIR of the channel between the i -th receive antenna and the j -th transmit antenna $h_{i,j}(t)$. The response matrix of the TR pre-filter of the MIMO system thus is given by

$$\bar{\mathbf{H}}(t) = \begin{pmatrix} \bar{h}_{1,1}(-t) & \bar{h}_{2,1}(-t) & \dots & \bar{h}_{N,1}(-t) \\ \bar{h}_{1,2}(-t) & \bar{h}_{2,2}(-t) & \dots & \bar{h}_{N,2}(-t) \\ \vdots & \vdots & \ddots & \vdots \\ \bar{h}_{1,M}(-t) & \bar{h}_{2,M}(-t) & \dots & \bar{h}_{N,M}(-t) \end{pmatrix}, \quad (3.4)$$

which is based on the original CIR matrix transposed in space. The CIR matrix of the equivalent channel is then represented as

$$\hat{\mathbf{H}}(t) = \begin{pmatrix} \hat{h}_{1,1}(t) & \hat{h}_{1,2}(t) & \dots & \hat{h}_{1,N}(t) \\ \hat{h}_{2,1}(t) & \hat{h}_{2,2}(t) & \dots & \hat{h}_{2,N}(t) \\ \vdots & \vdots & \ddots & \vdots \\ \hat{h}_{N,1}(t) & \hat{h}_{N,2}(t) & \dots & \hat{h}_{N,N}(t) \end{pmatrix}, \quad (3.5)$$

where each component of the equivalent channel is calculated by

$$\hat{h}_{i,j}(t) = \sum_{k=1}^M h_{i,k}(t) \otimes \bar{h}_{j,k}(-t), \quad i, j = 1, \dots, N. \quad (3.6)$$

Some remarks can be drawn from the matrix of the equivalent channel. First, the maximum number of independent data streams the system can achieve is N , which is the number of receive instead of transmit antennas. Second, the matrix of the equivalent channel is a square matrix with the entries in the main diagonal being the summation of the auto-correlation of the original CIRs and other entries being the summation of the cross-correlation of the original CIRs between the transmit and receive antennas. Third, the TR technique in the MIMO-UWB system can exploit M order transmit diversity, and the diversity gain depends on the number of transmit antennas.

3.3.2 Pre-Equalizer

The TR pre-filter works in time domain to raise the SNR, but simultaneously leads to a BER performance floor caused by the MSI in the MIMO-SM system. In other words, TR is not enough to mitigate MSI, especially in the high speed UWB system. Combining the TR pre-filter and the linear pre-equalizer is a practical and efficient approach [59, 61].

Due to the high compression in the time domain of the equivalent CIR, we do not need to use the full channel state information (CSI) of the equivalent channel $\hat{\mathbf{H}}(t)$ to design the pre-equalizer. The power of the equivalent channel distributing across the channel taps is shown in Table 7. It is calculated based on the average of 20 realizations of the standard UWB channel models CM1, CM2, CM3 and CM4 [29]. The parameters of the channel models used in the simulations are stated in Table 3.

Table 7: Power Distribution of Equivalent Channels

Percent of power	CM1	CM2	CM3	CM4
50%	1	3	1	1
75%	71	106	15	41
90%	230	356	44	98
95%	363	569	69	140
100%	6407	5043	7249	1105

Table 8: Key Parameters of the Channel Models

Parameter	CM1	CM2	CM3	CM4	Unit
Λ	0.0223	0.4000	0.0667	0.0667	1/ns
λ	2.5	0.5	2.1	2.1	1/ns
Γ	22.61	26.27	14.60	19.80	-
γ	4.3	6.7	7.9	12.0	-
σ_1	3.3941	3.3941	3.3941	3.3941	dB
σ_2	3.3941	3.3941	3.3941	3.3941	dB
σ_x	3	3	3	3	dB
LOS/NLOS	LOS	NLOS	LOS	NLOS	-

It can be seen from the Table 7 that the most energy of the equivalent channel falls into taps nearby the peak instant of the autocorrelation. We can observe the equivalent channels for the cases CM1, CM3 and CM4, respectively 50% of energy falls into one tap (the peak tap of the equivalent CIR). For the equivalent channel of CM2, the same amount of energy is occupied by 3 taps. Additionally, it is also observed that the channel CM3 has the best compression property.

Suppose that the maximum length of the equivalent channel is L_e , giving a threshold of the collected energy level in percentage, we can choose L_s taps ($L_s \ll L_e$) of the equivalent channel and compute the linear pre-equalizer. The new CIR of the equivalent channel is called the shortened

CIR, denoted as $\hat{\mathbf{H}}_s$. Considering the discrete time form of the shortened equivalent channels, we re-index it in the time domain as follow

$$\hat{\mathbf{h}}_{i,j} = [\hat{h}_{i,j}[0], \hat{h}_{i,j}[1], \dots, \hat{h}_{i,j}[L_s - 1]], \quad i, j = 1, \dots, N. \quad (3.7)$$

We assume that channels do not change when a block of $K + L_s - 1$ data symbols are transmitted. The new equivalent channel matrix can be represented by a block Toeplitz matrix as

$$\hat{\mathbf{H}}_s = \begin{pmatrix} \hat{\mathbf{H}}[L_s - 1] & \dots & \hat{\mathbf{H}}[0] & 0 & \dots & 0 \\ 0 & \hat{\mathbf{H}}[L_s - 1] & \dots & \hat{\mathbf{H}}[0] & \dots & 0 \\ \vdots & \ddots & \ddots & \ddots & \ddots & \vdots \\ 0 & \dots & 0 & \hat{\mathbf{H}}[L_s - 1] & \dots & \hat{\mathbf{H}}[0] \end{pmatrix}, \quad (3.8)$$

where each block matrix is

$$\hat{\mathbf{H}}[k] = \begin{pmatrix} \hat{\mathbf{h}}_{1,1}[k] & \hat{\mathbf{h}}_{1,2}[k] & \dots & \hat{\mathbf{h}}_{1,N}[k] \\ \hat{\mathbf{h}}_{2,1}[k] & \hat{\mathbf{h}}_{2,2}[k] & \dots & \hat{\mathbf{h}}_{2,N}[k] \\ \vdots & \vdots & \ddots & \vdots \\ \hat{\mathbf{h}}_{N,1}[k] & \hat{\mathbf{h}}_{N,2}[k] & \dots & \hat{\mathbf{h}}_{N,N}[k] \end{pmatrix}. \quad (3.9)$$

The entire data vector can be formulated as

$$\mathbf{x} = \frac{1}{\sqrt{M}} [\mathbf{x}^T[k - L_s + 1], \mathbf{x}^T[k - L_s + 2], \dots, \mathbf{x}^T[k + K - 1]]^T, \quad (3.10)$$

where each element of vector $\mathbf{x}[k] = [x_1[k], x_2[k], \dots, x_N[k]]^T$ is the input data on the streams at time k . The scale factor $\frac{1}{\sqrt{M}}$ keeps the total transmit power the same as that in the SISO case for fair comparison.

Similarly, we can represent the additive Gaussian noise vector and receive signal as

$$\mathbf{n} = [\mathbf{n}^T[k], \mathbf{n}^T[k + 1], \dots, \mathbf{n}^T[k + K - 1]]^T, \quad (3.11)$$

$$\mathbf{y} = [\mathbf{y}^T[k], \mathbf{y}^T[k + 1], \dots, \mathbf{y}^T[k + K - 1]]^T, \quad (3.12)$$

where $\mathbf{n}[k] = [n_1[k], n_2[k], \dots, n_N[k]]^T$ and $\mathbf{y}[k] = [y_1[k], y_2[k], \dots, y_N[k]]^T$, respectively. The received signal can be represented by

$$\mathbf{y} = \hat{\mathbf{H}}_s \mathbf{x} + \mathbf{n}. \quad (3.13)$$

The pre-equalizer is added before the TR pre-filter as shown in Figure 24. The pre-equalizer matrix, denoted by \mathbf{G} , has dimension of $N(K + L_s - 1) \times NK$. The system model can be rewritten as

$$\tilde{\mathbf{y}} = \hat{\mathbf{H}}_s \mathbf{G} \tilde{\mathbf{x}} + \mathbf{n}, \quad (3.14)$$

where $\tilde{\mathbf{x}} = [\mathbf{x}^\top[k], \mathbf{x}^\top[k+1], \dots, \mathbf{x}^\top[k+K-1]]^\top$ and the estimate of the received signal is $\tilde{\mathbf{y}} = [\tilde{\mathbf{y}}^\top[k], \tilde{\mathbf{y}}^\top[k+1], \dots, \tilde{\mathbf{y}}^\top[k+K-1]]^\top$. The covariance matrix of transmitted signal, received signal and noise are defined by

$$\begin{aligned} E[\tilde{\mathbf{x}}\tilde{\mathbf{x}}^\top] &= \sigma_x^2 \mathbf{I}_{NK}, \\ E[\tilde{\mathbf{y}}\tilde{\mathbf{y}}^\top] &= \sigma_y^2 \mathbf{I}_{NK}, \\ \text{and } E[\mathbf{nn}^\top] &= \sigma_n^2 \mathbf{I}_{NK}, \end{aligned} \quad (3.15)$$

where \mathbf{I}_{NK} is an $NK \times NK$ identity matrix.

Let us investigate a simple pre-equalizer, zero-forcing (ZF). The pre-equalization with zero-forcing criterion guarantees the receive data being identical to transmit data. The value of equalizer matrix derived from the inverse of the channel is large and in some cases makes the transmit power amplifier inefficient. The power constraint for the transmit signal (after pre-equalizer and TR pre-filter) is introduced for the optimization problem as stated below. It is easy to find that the pre-equalizer matrix \mathbf{G}_{ZF} is the inverse of the shortened equivalent channel matrix as

$$\mathbf{G}_{ZF} = \alpha \hat{\mathbf{H}}_s^\dagger = \alpha (\hat{\mathbf{H}}_s^H \hat{\mathbf{H}}_s)^{-1} \hat{\mathbf{H}}_s^H, \quad (3.16)$$

where \dagger and $(\bullet)^H$ denote the Moore-Penrose pseudo-inverse and the conjugate and transpose of a matrix, respectively. The coefficient α is introduced for the power constraint of the transmit signal, which is calculated by [61]

$$\alpha = \sqrt{\frac{E_{tx}}{\sigma_x^2} \frac{1}{\text{tr} \left((\hat{\mathbf{H}}_s^\dagger)^H \hat{\mathbf{H}}^H \hat{\mathbf{H}} \hat{\mathbf{H}}_s^\dagger \right)}}, \quad (3.17)$$

where $\text{tr}(\bullet)$ is the trace of a matrix, σ_x^2 is the variance of the transmit signal and $\hat{\mathbf{H}}$ is the TR pre-filter matrix, which is an $MK \times N(K + L_s - 1)$ block Toeplitz matrix represented by

$$\hat{\mathbf{H}} = \begin{pmatrix} \hat{\mathbf{H}}[0] & \dots & \hat{\mathbf{H}}[L_s - 1] & 0 & \dots & 0 \\ 0 & \hat{\mathbf{H}}[0] & \dots & \hat{\mathbf{H}}[L_s - 1] & \dots & 0 \\ \vdots & \ddots & \ddots & \ddots & \ddots & \vdots \\ 0 & \dots & 0 & \hat{\mathbf{H}}[0] & \dots & \hat{\mathbf{H}}[L_s - 1] \end{pmatrix}, \quad (3.18)$$

where each block matrix is

$$\hat{\mathbf{H}}[k] = \begin{pmatrix} \bar{\mathbf{h}}_{1,1}[k] & \bar{\mathbf{h}}_{2,1}[k] & \dots & \bar{\mathbf{h}}_{N,1}[k] \\ \bar{\mathbf{h}}_{1,2}[k] & \bar{\mathbf{h}}_{2,2}[k] & \dots & \bar{\mathbf{h}}_{N,2}[k] \\ \vdots & \vdots & \ddots & \vdots \\ \bar{\mathbf{h}}_{1,M}[k] & \bar{\mathbf{h}}_{2,M}[k] & \dots & \bar{\mathbf{h}}_{N,M}[k] \end{pmatrix}. \quad (3.19)$$

and $\bar{\mathbf{h}}_{i,j}$ with $i = 1, \dots, M$, $j = 1, \dots, N$ is discrete time reversed of $h_{i,j}(t)$.

3.4 CHANNEL CORRELATION IN SM-MIMO SYSTEMS

Generally, the entries of the MIMO channel matrix \mathbf{H} are assumed to be independent of each other. In the real world, however, the spatial correlation among antennas (transmit or/and receive antennas) exists. In other words, the individual channels of \mathbf{H} are correlated [37, 49].

The degree of correlation between the individual $M \times N$ channel realizations comprising the MIMO channel is a complicated function of the scattering in the environment and antenna spacing at the transmitter and the receiver. Consider an extreme condition were all antenna elements at the transmitter are collocated and likewise at the receiver. In this case, all the elements of \mathbf{H} will be fully correlated (in fact identical) and the spatial diversity order of the channel is one. The correlation is caused by a variety of reasons such as inadequate antenna spacing or rich scattering in the environment.

Correlated channels imply that elements of \mathbf{H} are correlated and may be modeled by [68]

$$\text{vec}(\mathbf{H}) = \mathbf{R}^{1/2} \text{vec}(\mathbf{H}_w), \quad (3.20)$$

where \mathbf{H}_w is the spatially white $M \times N$ MIMO channel with its properties being described as

$$\varepsilon\{[\mathbf{H}_w]_{i,j}\} = 0, \quad (3.21)$$

$$\varepsilon\{[|\mathbf{H}_w]_{i,j}|^2\} = 1, \quad (3.22)$$

$$\varepsilon\{[\mathbf{H}_w]_{i,j}[\mathbf{H}_w]_{m,n}^*\} = 0 \text{ if } i \neq m \text{ or } j \neq n. \quad (3.23)$$

\mathbf{R} is the $MN \times MN$ covariance matrix defined as

$$\mathbf{R} = \varepsilon\{\text{vec}(\mathbf{H})\text{vec}(\mathbf{H})^H\}. \quad (3.24)$$

\mathbf{R} is a positive semi-definite Hermitian matrix. If $\mathbf{R} = \mathbf{I}_{MN}$, then $\mathbf{H} = \mathbf{H}_w$.

Although the model described above is capable of capturing any correlation effects between the elements of \mathbf{H} , a simpler and less generalized model is often adequate and is given by

$$\mathbf{H} = \mathbf{R}_{\text{Rx}}^{1/2} \mathbf{H}_w \mathbf{R}_{\text{Tx}}^{1/2}, \quad (3.25)$$

where \mathbf{R}_{Tx} and \mathbf{R}_{Rx} are the $M \times M$ transmit covariance matrix and $N \times N$ receive covariance matrix, respectively. Both \mathbf{R}_{Tx} and \mathbf{R}_{Rx} are positive semi-definite Hermitian matrices. This model has fewer degree of freedom than Equation (3.20). Equation (3.25) implies that receive antenna correlation \mathbf{R}_{Tx} is equal to the covariance of the $N \times 1$ receive vector channel when excited by any transmit antennas, and is therefore the same for all transmit antennas. The model can occur when the angle spectra of the scatterers at the receive array for signals arriving from any transmit antenna are identical. This condition arises if all the transmit antennas are closely located and have identical radiation patterns. These remarks also carry over to the transmit antenna correlation \mathbf{R}_{Tx} .

Note also that \mathbf{H}_w is a full rank matrix with probability 1. In the presence of receive or transmit correlation, the rank of \mathbf{H} is constrained by $\min(r(\mathbf{R}_{\text{Rx}}), r(\mathbf{R}_{\text{Tx}}))$, where $r(\mathbf{A})$ denotes the rank of \mathbf{A} .

For a uniform linear array of antennas, the correlation matrices are typically described by [68]

$$\mathbf{R}_{\text{Tx}} = \begin{pmatrix} 1 & \rho_{\text{Tx}} & \rho_{\text{Tx}}^2 & \cdots & \rho_{\text{Tx}}^{M-1} \\ \rho_{\text{Tx}} & 1 & \rho_{\text{Tx}} & \cdots & \rho_{\text{Tx}}^{M-2} \\ \vdots & \vdots & \vdots & \ddots & \vdots \\ \rho_{\text{Tx}}^{M-1} & \rho_{\text{Tx}}^{M-2} & \rho_{\text{Tx}}^{M-3} & \cdots & 1 \end{pmatrix}, \quad (3.26)$$

and

$$\mathbf{R}_{\text{Rx}} = \begin{pmatrix} 1 & \rho_{\text{Rx}} & \rho_{\text{Rx}}^2 & \cdots & \rho_{\text{Rx}}^{N-1} \\ \rho_{\text{Rx}} & 1 & \rho_{\text{Rx}} & \cdots & \rho_{\text{Rx}}^{N-2} \\ \vdots & \vdots & \vdots & \ddots & \vdots \\ \rho_{\text{Rx}}^{N-1} & \rho_{\text{Rx}}^{N-2} & \rho_{\text{Rx}}^{N-3} & \cdots & 1 \end{pmatrix}, \quad (3.27)$$

where ρ_{Tx} and ρ_{Rx} are the correlation coefficient of transmit and receive antennas, respectively. The similar model is used in [3], where the BER performances of the MIMO system based on the simulated channel and based on the measured channel are similar for the appropriate correlation coefficients.

In the MIMO-UWB system where multiple antennas are deployed in transmitter and receiver sides, the spatial correlation thus appears in both ends and doubly degrades the performance of system. As mentioned, from Equation (3.5) we can see that the maximum number of independent data streams a TR-MIMO-UWB system can achieve is N , number of receive antennas. It also means that the equivalent CIR is still a square $N \times N$ matrix if only one transmit antenna is used. In this case, several data streams are multiplexed to transmit over one antenna. The system can be, thus, named the virtual MIMO-UWB. Due to only one antenna being used at the transmitter, the correlation appears only at the receiver side. Therefore, the virtual MIMO can mitigate the impact of the transmit correlation, but cannot achieve the transmit diversity gain as the true one.

3.5 BER PERFORMANCE ANALYSIS

Simulation is conducted to verify the performance of the SM-MIMO-UWB system when the pre-equalizer and the TR pre-filter are deployed and evaluate the impact of the transmit spatial correlation on the system performance as well. Let us consider the system where the binary data is modulated to the binary phase-amplitude modulation format. The UWB monocycle waveform is

$$p(t) = \left[1 - 4\pi \left(\frac{t - t_c}{w} \right)^2 \right] e^{-2\pi \left(\frac{t - t_c}{w} \right)^2}, \quad (3.28)$$

where w is a parameter corresponding to pulse width, and t_c is a time shifting of the pulse. In our simulation, $w=1\text{ns}$, and $t_c = w/2$. The symbol duration T is 2ns corresponding to a data rate 500 Mbps per data stream. We assume that the signal is transmitted over UWB channels and perfectly synchronized at the receiver. The IEEE 802.15.3a CM4 channel model [29] is used for each channel in simulation.

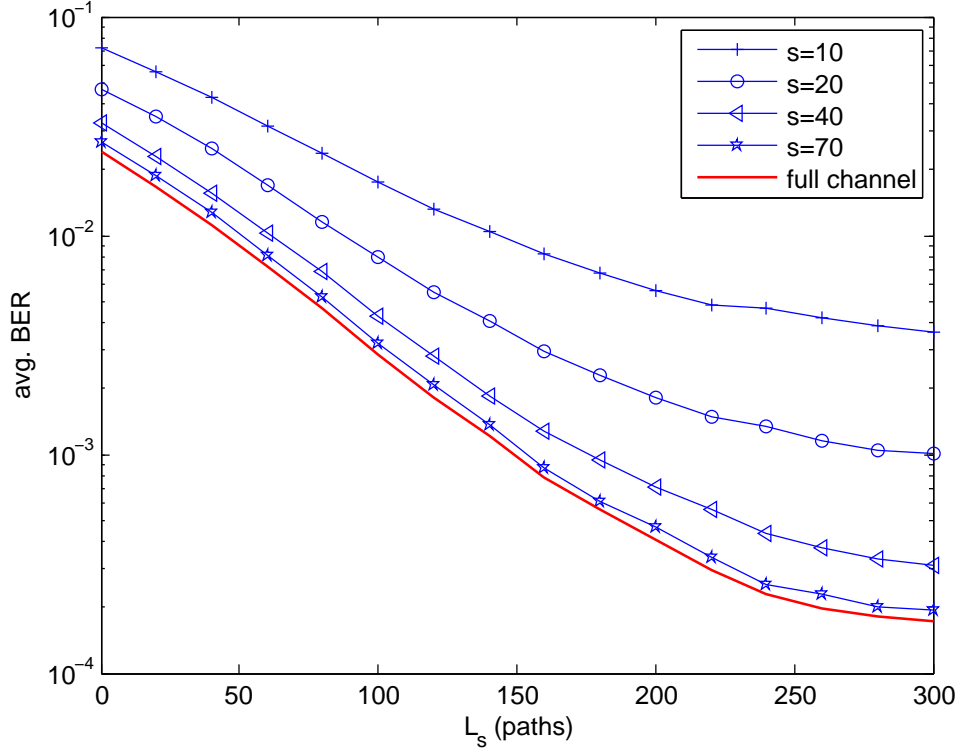


Figure 25: BER versus the length of shortened equivalent channel for the S-TR pre-filter, CM4, $M = N = 2$, $\text{SNR} = 12\text{ dB}$, no spatial correlation.

The average BER as a function of the length of the shortened equivalent channel used for pre-equalizer calculation is shown in Figure 25 for the S-TR pre-filter with different numbers of fingers s . From this figure, we can evaluate the efficiency of the TR pre-filter in shortening the equivalent channel as well as the ability S-TR in comparison with A-TR. With the same 2×2 MIMO configuration, at the same $\text{SNR} = 12\text{ dB}$, when the length of the equivalent channel L_s increases, the average BER is greatly ameliorated. However, when the equivalent channel is long enough, this improvement is negligible. It can be observed that the BER almost does not change with L_s when $L_s \geq 250$. The BER performance can be bettered by increasing not only the equivalent CIR's length but also the number of multipath components of the TR pre-filter, but the increasing rate is almost saturated when $s \geq 70$. It can be seen that with $s = 70$, the BER performance is nearly as good as the case when the A-TR pre-filter is used.

In the Figure 26, we investigate the average BER of the system versus the length of shortened equivalent CIRs when the S-TR pre-filter or the P-TR pre-filter is used for different channel models. For the fair comparison, the

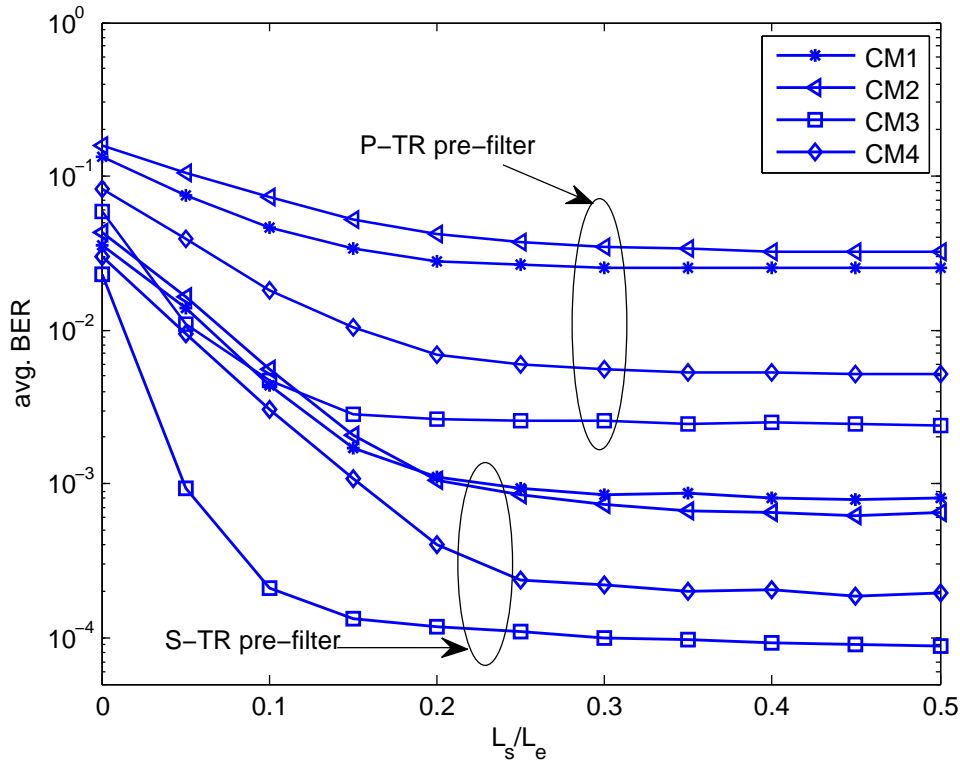


Figure 26: BER versus the ratio L_s/L_e for the S-TR pre-filter and the P-TR pre-filter filter, CM1-4, $M = N = 2$, SNR = 12 dB, $s = 20$, no spatial correlation.

BER performances are considered as a function of the ratio between the length of shortened equivalent channel L_s and the full equivalent channel length L_e , and the number of taps is 20 for both S-TR and P-TR pre-filters. As shown in this figure, with the same number of taps, the S-TR pre-filter provides better performance than the P-TR pre-filter for all channel models. Simulation results show that the equivalent channel CM3 possesses best compression property among the four channel models for both S-TR and P-TR pre-filters. When the ratio L_s/L_e increases, the BER performance decreases drastically first and then approaches to saturation points.

How the transmit spatial correlation affects the performance in term of BER is presented in Figures 27, 28, 29 and 30. The correlation models for the transmitter and receiver in Equation 3.26 and 3.27 are used for simulation. The correlation of receive antennas affects in the same way on SIMO and MIMO-TR-UWB systems. The receive correlation coefficient is fixed at $\rho_{RX} = 0.5$ and the S-TR pre-filter with number of taps $s = 50$ is used.

In Figure 27, two data streams are transmitted over $M = 1, 2$, and 4 transmit antennas, respectively with SNR = 12dB. We can see from that figure that when the transmit correlation coefficient ρ_{TX} increases, the average BER of the SIMO or the virtual MIMO-TR-UWB system keeps unchanged while it increases in the true MIMO case. The BER performance of the MIMO system is worse than the SIMO system if the transmit correlation coefficient is greater than a critical value. For example, the performance of the 2×2

MIMO system is worse than the 1×2 SIMO system if $\rho_{Tx} \geq 0.4$, and the performance of the 4×2 MIMO system is worse than the 1×2 SIMO system if $\rho_{Tx} \geq 0.35$.

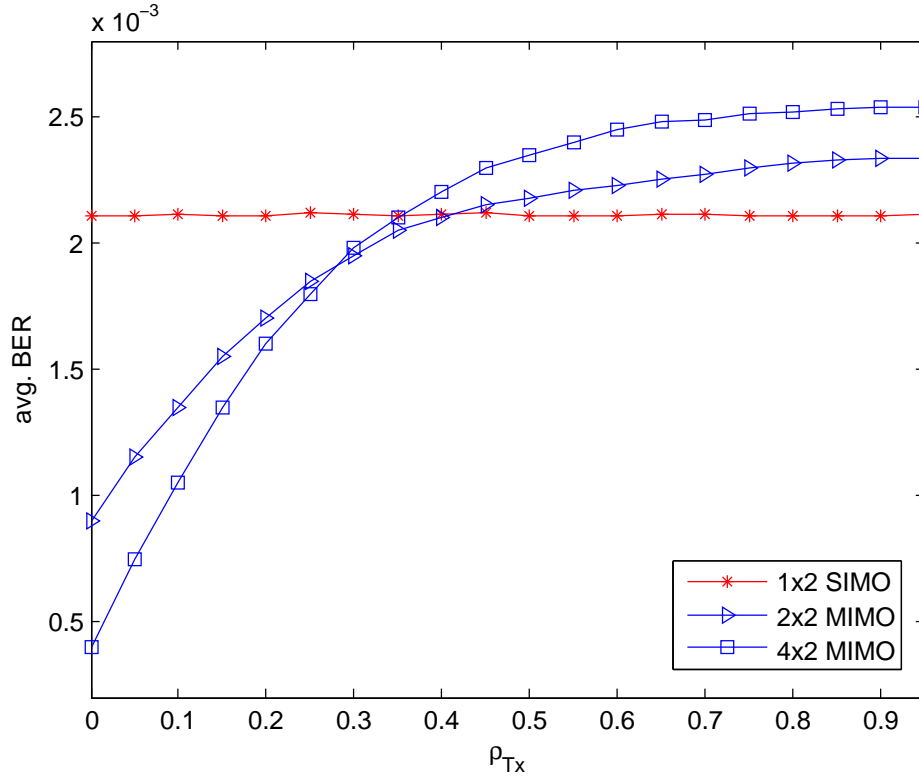


Figure 27: Average BER versus transmit correlation coefficient for the channel CM4, the S-TR pre-filter with $s = 50$, $M = 2$ and $SNR = 12$ dB.

At the low transmit correlation regime, the more transmit antennas the system has, the better BER performance the system can achieve. This is the advantage of the transmit diversity possessed by the MIMO-TR-UWB system. However, if the correlation is strong, more transmit antennas will rapidly degrade the performance of MIMO systems. As shown in Figure 27, when the transmit correlation coefficient ρ_{Tx} is greater than 0.3, the performance of the 2×2 MIMO system outperforms the performance of the 4×2 MIMO system.

The effect of transmit correlation is also illustrated in Figure 28 for 1×4 SIMO and 4×4 MIMO systems. The 4×4 MIMO system outperforms the 1×4 SIMO system at low correlation and the critical value of transmit correlation coefficient is about 0.65.

Figure 29 depicts the BER performance of 1×2 SIMO and 2×2 MIMO systems with some values of ρ_{Tx} and Figure 30 shows the BER performance of 1×4 SIMO and 4×4 MIMO systems. As can be seen from both figures, if there is no transmit correlation, the MIMO-TR-UWB system achieves good BER performance. However, if the transmit correlation appears, the average BER declines sharply. Consequently, the performance of the MIMO system is even worse than the SIMO system in the high transmit correlation condition.

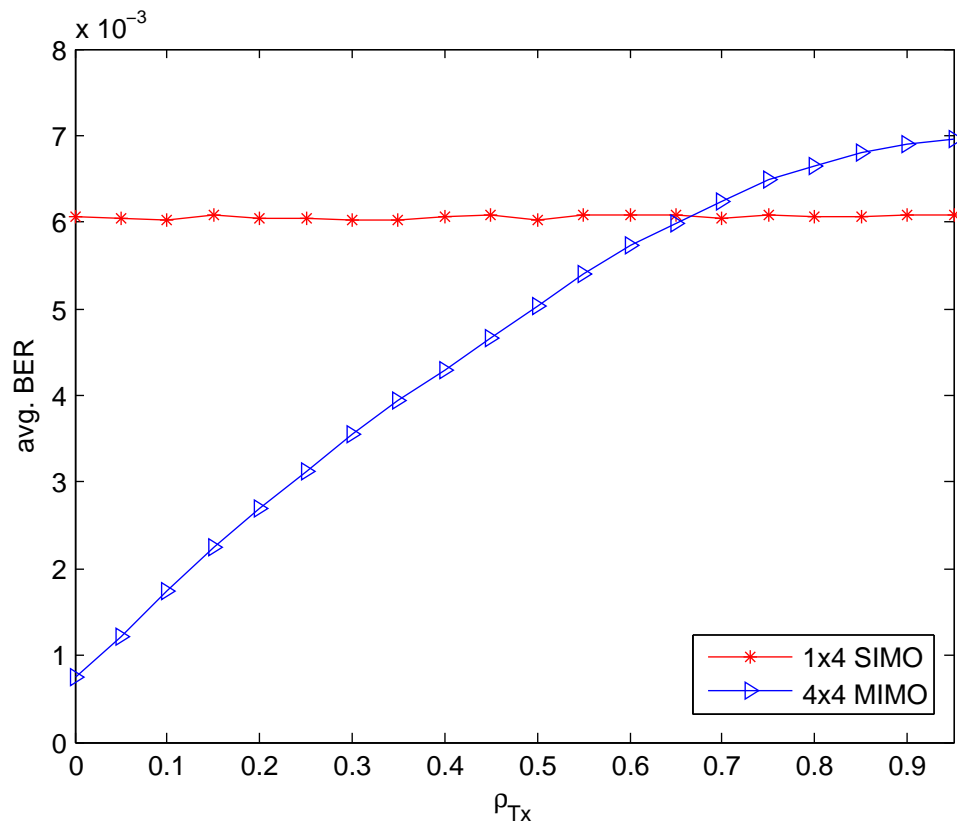


Figure 28: Average BER versus transmit correlation coefficient for the channel CM₄, the S-TR pre-filter with $s = 50$, $M = 4$ and SNR = 12 dB.

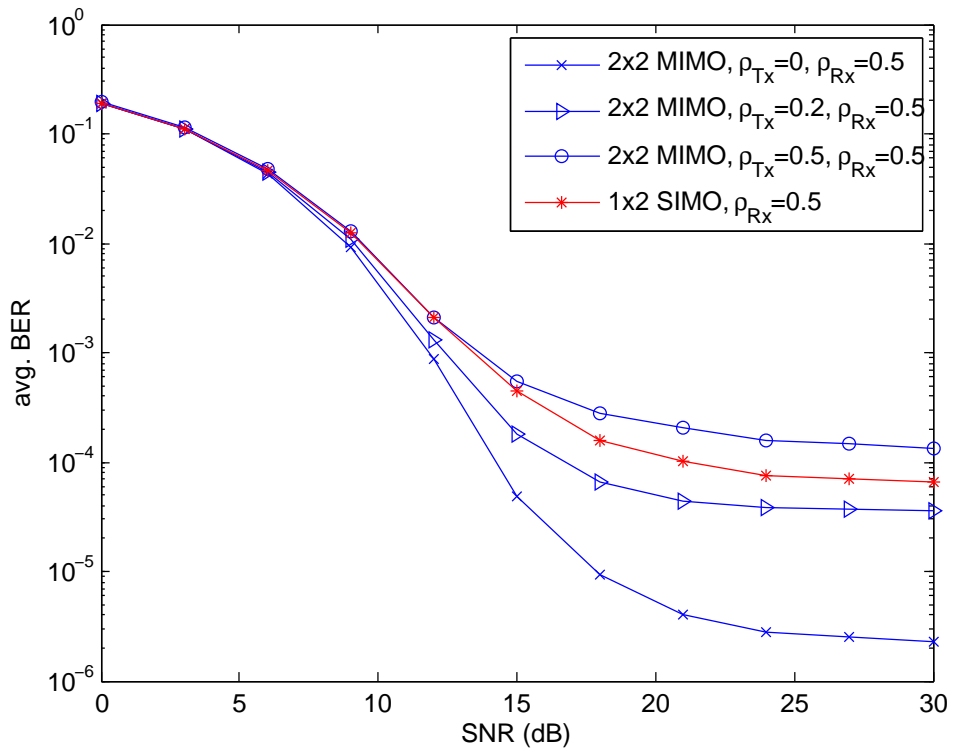


Figure 29: BER performance of 2×2 MIMO and 1×2 SIMO systems for the channel CM₄, the S-TR pre-filter with $s = 50$ and SNR = 12 dB.

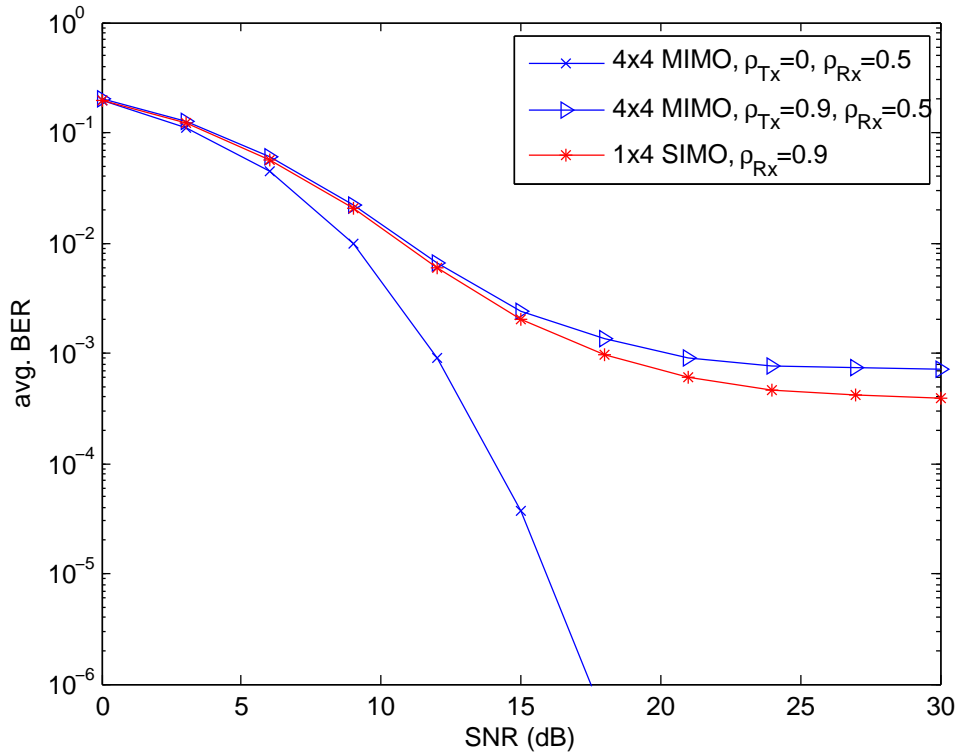


Figure 30: BER performance of 4×4 MIMO and 1×4 SIMO systems for the channel CM₄, the S-TR pre-filter with $s = 50$ and SNR = 12 dB.

3.6 SUMMARY

In the SM-MIMO UWB system, we can transmit at the same time several data streams and the capacity is increased as a result. This leads to the fact that the SM-MIMO UWB system faces not only the ISI but also the MSI problems. In order to solve these problems, implementing the TR pre-filter and the ZF pre-equalizer at the transmitter of the SM-MIMO system is considered in this chapter. We also propose to use the S-TR pre-filter instead of the A-TR pre-filter since simulation results show that with limited number of multipath components, the S-TR pre-filter can provide almost the same BER performance as the A-TR pre-filter does. Thanks to the TR pre-filter, the equivalent channel is compressed in the time domain and the pre-equalizer can be designed based on the shortened equivalent channels. These contribute to reduce considerably the complexity of the transmitter for the MIMO-UWB system.

Furthermore, we have also investigated the impact of the spatial correlation caused by multiple antennas on the performance of SM-MIMO UWB systems. When the TR pre-filter is deployed at the transmitter, several data streams are multiplexed to transmit over one antenna and the system is thus named the virtual MIMO. The virtual MIMO (or SIMO) UWB system can avoid the impact of the transmit correlation, but can not achieve the transmit diversity of course. As observed from simulation results, at the low transmit correlation regime, the MIMO-TR-UWB systems outperform the SIMO-TR-UWB systems in the BER performance. However, when the transmit correlation is high, the performance of the MIMO systems is worse than that of the SIMO systems.

TIME REVERSAL FOR MULTI-USER MIMO-UWB SYSTEMS

Both multiple access and broadcast channels of a multiple user SM-MIMO-UWB system which is different from the system of single user as studied in earlier chapter are investigated. A Time Reversal (pre-)filter combined with a Zero Forcing (pre-)equalizer are adopted to mitigate the interference problems in such a system. Sections in this chapter are ordered as follow: the first Section is Introduction; Then, the main contents of the chapter are presented in turn in Sections 4.2 and 4.3, entitled Broadcast MU-MIMO UWB System and Multiple Access MU-MIMO UWB System, respectively; The final Section is Summary of the chapter.

4.1 INTRODUCTION

The transition of MIMO communication from a theoretical concept to a practical technique for enhancing performance of wireless networks has been witnessed for the recent decade. Point-to-point (single user) MIMO promises large gains for both channel capacity and reliability, essentially via the use of space-time codes combined with stream multiplexed transmission. The extra spatial degrees of freedom brought by the use of multiple antennas can be advantageously exploited to enhance the system capacity when multiple streams are scheduled to share the spatial channel simultaneously. This fundamental paradigm shifts from single user to multiple users (MU) communications that can experience substantial benefit from channel state information at the transmitter and, at the same time, require more complex scheduling strategies and transceiver methodologies.

Multiple users MIMO communications can be generalized into two categories: MIMO broadcast channels (MIMO BC) and MIMO multiple access channels (MIMO MAC) for downlink and uplink situations, respectively. The MIMO BC consists of one multiple-antenna transmitter (access point) sending the signal to many multiple-antenna receivers (users) and the MIMO MAC consists of many multiple-antenna transmitters (users) sending the signal to a single multiple-antenna receiver (access point). The uplink and downlink channels are illustrated in Figure 31.

On the uplink channel, the development of MU-MIMO techniques appears as a generalization of known SU-MIMO concepts to the multiuser case. As usual in information theory, the downlink or BC channel case is by far the most challenging case. Information theory reveals that the optimum transmit strategy for the MU-MIMO broadcast channel involves a theoretical pre-interference cancellation technique known as dirty paper coding (DPC) combined with an implicit user scheduling and power loading algorithm [14].

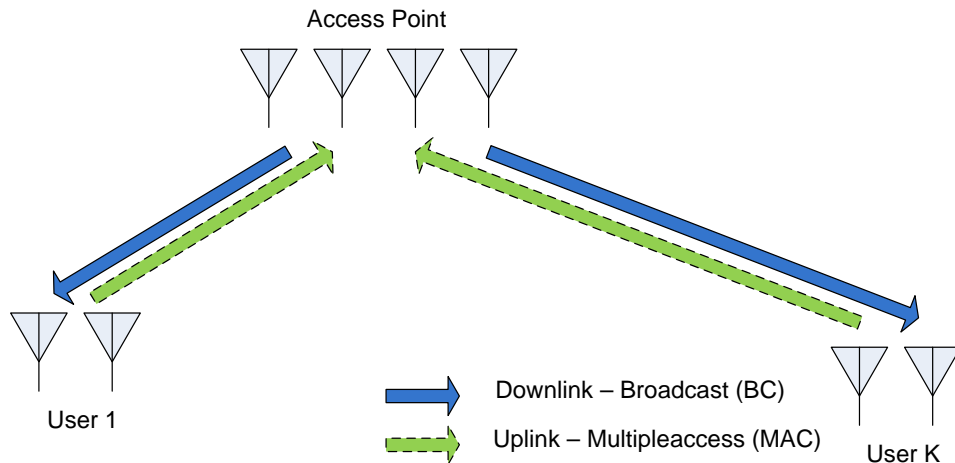


Figure 31: Broadcast and Multiplexing Channels in a MU-MIMO System

Multuser MIMO techniques and performance have been intensely investigated due to several key advantages over single user MIMO communications [32]

- MU-MIMO schemes allow for a direct gain in multiple access capacity (proportional to the number of access point antennas) thanks to so-called multiuser multiplexing schemes.
- MU-MIMO appears more immune to most of propagation limitations plaguing single user MIMO communications such as channel rank loss or antenna correlation. Although increased correlation still affects per-user diversity, this may not be a major issue if multiuser diversity can be extracted by the scheduler instead. Additionally, line of sight propagation, which causes severe degradation in single user spatial multiplexing schemes, is no longer a problem in multiuser setting.
- MU-MIMO allows the spatial multiplexing gain at the base station to be obtained without the need for multiple antenna terminals, thereby allowing the development of small and cheap terminals while intelligence and cost is kept on the infrastructure side.

It is a fact that MU-MIMO requires (although benefits from) channel knowledge at the transmitter to properly serve the spatially multiplexed users. Normally, however, users are separately located, obtaining complete channel state information at the transmitters is more complicated than that for the single user case. This raises the complexity of the transmitter and the price as a result.

From several other points of view, MU-MIMO and SU-MIMO also pose some distinct problems:

- SU-MIMO is a point-to-point link that has a defined link capacity. Whereas, the link (a multiple access channel on the reverse link or a broadcast channel on the forward link) rates are characterized in term of a capacity region [20, 21].

- In MU-MIMO, each user link has a specific data rate and BER performance, that are generally equal for all users. Conversely, in SU-MIMO, all streams are delivered to the same user, only the sum rate performance of the overall link matters.
- In MU-MIMO, path loss from each user to the access point (AP) is significantly different while not all of these differences can be compensated by power control due to peak power constraints and power control errors. Thus, there may be large differences in SINR in the links. This problem does not exist in SU-MIMO case.
- In MU-MIMO, users can co-operate in encoding on the forward link and in decoding on the reverse link at the AP, but cannot co-operate in decoding on the forward link or encoding on the reverse link. The limitation on co-operation may come from the difference in power and rate. Meanwhile, in SU-MIMO, encoding at the transmitter and decoding at the receiver can be done with co-operation between co-located antennas.
- In SU-MIMO, if the channel is known in both the transmitter and receiver, for the same transmit power, the capacity on the forward link and on the reverse link is exactly equal. In contrast, the relationship between the multiple access and broadcast capacity regions is still a subject of research.

MIMO in UWB communications has been also a topic of interest of many researchers. Topics that researchers normally focus on include channel measurement and characterizations [40, 50, 49], channel capacity [93, 92, 51, 71, 94], STC [89, 2, 81, 80]. However, these studies generally investigate the SU-MIMO UWB systems.

Compared with the volumes of literature in SU-MIMO IR-UWB research, there are only a few studies of MU-MIMO IR-UWB. TH spreading code are normally a plausible choice to separate different users in such systems [85, 77, 56, 73, 42, 19, 79]. Besides, Frequency hopping (FH) scheme [88] or joint TH-FH scheme [55, 12] are also used to avoid multiple user interference in MU-UWB systems.

Time reversal technique whose efficiency has been verified in the single user UWB system may provide an efficient solution for the MU-MIMO UWB system. Unfortunately, most past works on the TR UWB scheme focus on the issue of single user transmission and detection and there have been few contributions on the topic of a multiuser TR UWB scheme. The topic of multiuser TR UWB scheme has been analyzed in [63] in which a shifted time-reversed transmission scheme has been proposed to enable several users to transmit simultaneously data to one receiver in an MISO system. In [87], with different approach, the author has employed orthogonal codes for different users. While above works have considered MISO-MAC UWB systems, multiple-antenna time reversal downlink (or broadcast) transmission has been studied in [36]. In [36], a UWB beamformer focusing on the

intended user while minimizing its interference on unintended users and eavesdropping access points has been designed.

TR scheme in the single user MIMO-UWB system has been investigated in our work in [64, 66] and in the previous chapter. We now shift our examination to the case comprising multiple users, each with one or more antennas interacting with a multiple antenna array at the AP.

It is a fact that due to limitation of the supply power, the affordable cost, and the dimension, a complicated processing mechanism is not suitable for an user terminal. The complexity, therefore, is generally located at the AP in the real communication system. For this reason, in our investigated MU-MIMO UWB system, we implement the combination of the pre-filter and pre-equalizer at the transmitter in the BC channel and the combination of the filter and equalizer is proposed to use at the receiver in the MAC channel. The sketch of the whole system is shown in Fig. 32.

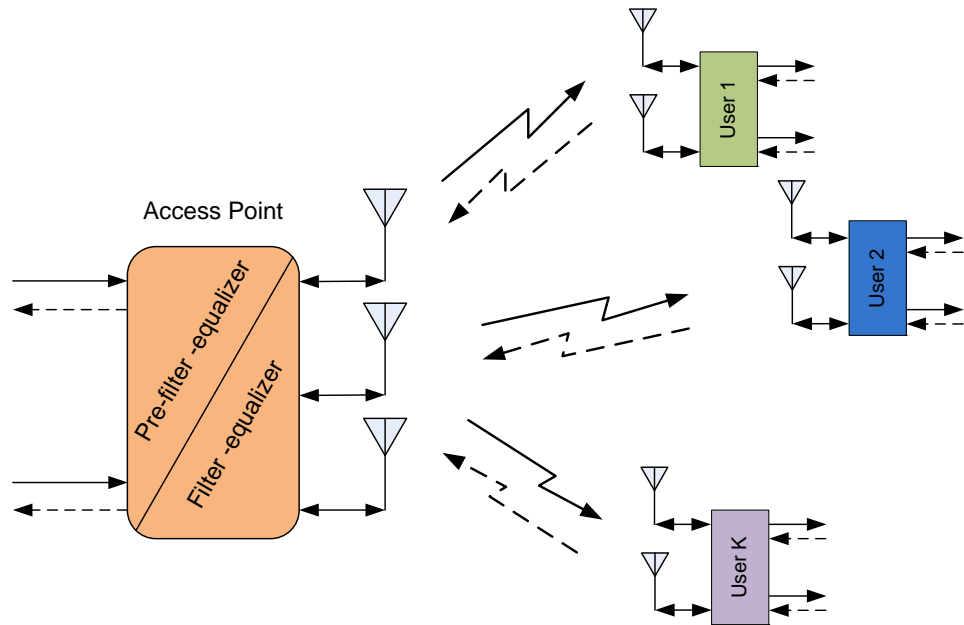


Figure 32: Proposed interferences mitigation solution for MU-MIMO UWB systems.

4.2 BROADCAST MU-MIMO UWB SYSTEM

4.2.1 System Model

In the investigated system, a single transmitter (AP) is equipped with M antennas transmitting at the same time several data streams to K decentralized users. Each user is equipped with more than one receiving antennas. For simplicity we shall assume that all users have the same number of antennas N and the total number of receiving antennas is $N_R = NK$. The block diagram of the Broadcast MU-MIMO UWB system is shown in Fig. 33.

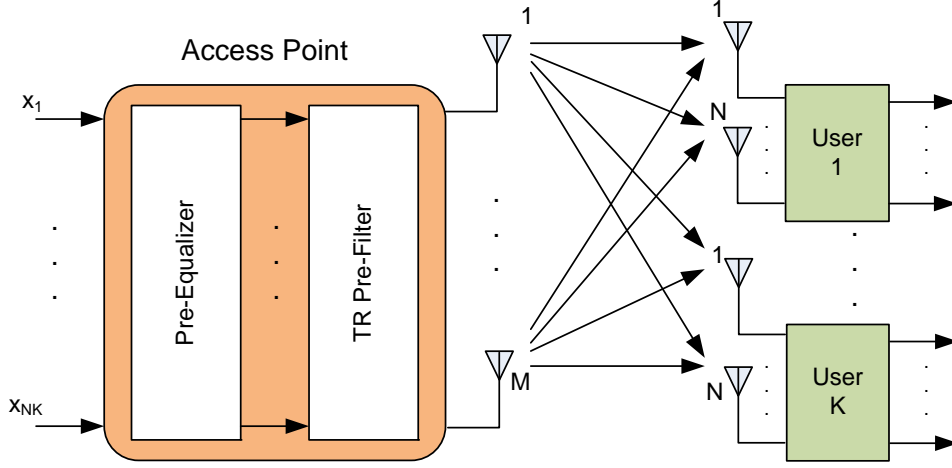


Figure 33: The Broadcast MU-MIMO UWB system with a pre-filter and pre-equalizer.

In this figure, the Pre-Equalizer and Pre-Filter blocks which are deployed to suppress the MUI, the MSI and the ISI are stated in the Section 4.2.2. Let $\mathbf{x} \in \mathbb{C}^{M \times 1}$ denote the transmitted vector signal and let $\mathbf{y}^{(k)} \in \mathbb{C}^{N \times 1}$ be the received signal at the k -th user. The noise at the k -th user is represented by $\mathbf{n}^{(k)} \in \mathbb{C}^{N \times 1}$ and is assumed to be circularly symmetric complex Gaussian ($\mathbf{n}^{(k)} \sim \tilde{\mathcal{N}}(0, \mathbf{I}_M)$). The transmit covariance matrix of the input signal is $\Sigma_x \triangleq E[\mathbf{x}\mathbf{x}^*]$. The transmitter is subject to an average power constraint P , which implies $\text{tr}(\Sigma_x) \leq P$. The signal is transmitted over the UWB multipath channel whose impulse response is assumed to be modeled by a tap delay line model with L taps. The CIR between the j -th transmit antenna and the i -th receive antenna of the k -th user is thus represented as

$$\mathbf{h}_{ij}^{(k)}(t) = \sum_{l=0}^{L-1} \alpha_l^{ij,k} \delta(t - \tau_l^{ij,k}), \quad i = 1, \dots, N, \quad j = 1, \dots, M, \quad (4.1)$$

where $\alpha_l^{ij,k}$ and $\tau_l^{ij,k}$ are the amplitude and the delay of the l -th tap respectively. The discrete time form of $\mathbf{h}_{ij}^{(k)}(t)$ is expressed as

$$\mathbf{h}_{ij}^{(k)} = \left[\mathbf{h}_{ij}^{(k)}[0], \mathbf{h}_{ij}^{(k)}[1], \dots, \mathbf{h}_{ij}^{(k)}[L-1] \right], \quad (4.2)$$

$$k = 1, \dots, K, \quad i = 1, \dots, N, \quad j = 1, \dots, M.$$

The entire channel between the transmitter and the k -th user is

$$\mathbf{H}^{(k)} = \begin{pmatrix} \mathbf{h}_{11}^{(k)} & \mathbf{h}_{12}^{(k)} & \dots & \mathbf{h}_{1M}^{(k)} \\ \mathbf{h}_{21}^{(k)} & \mathbf{h}_{22}^{(k)} & \dots & \mathbf{h}_{2M}^{(k)} \\ \vdots & \vdots & \ddots & \vdots \\ \mathbf{h}_{N1}^{(k)} & \mathbf{h}_{N2}^{(k)} & \dots & \mathbf{h}_{NM}^{(k)} \end{pmatrix}, \quad (4.3)$$

with the dimension $N \times ML$. Let us consider a block $V + L$ symbols of transmit data at the j -th antenna. We assume that channel does not change

within this block. This block of data can be represented by an $L \times V$ Hankel matrix as following

$$\mathbf{x}_j = \begin{pmatrix} \mathbf{x}_j [v-L+1] & \mathbf{x}_j [v-L+2] & \cdots & \mathbf{x}_j [v-L+V] \\ \vdots & \vdots & \ddots & \vdots \\ \mathbf{x}_j [v-1] & \mathbf{x}_j [v] & \cdots & \mathbf{x}_j [v+V-2] \\ \mathbf{x}_j [v] & \mathbf{x}_j [v+1] & \cdots & \mathbf{x}_j [v+V-1] \end{pmatrix}. \quad (4.4)$$

The entire transmit signal matrix is

$$\mathbf{x} = \frac{1}{\sqrt{M}} [\mathbf{x}_1, \mathbf{x}_2, \dots, \mathbf{x}_M]^T, \quad (4.5)$$

with dimension $ML \times V$. The scale factor $1/\sqrt{M}$ keeps the total transmit power of signal as the same as it in the SISO case.

The additive Gaussian noise at the i -th receive antenna of the k -th user is a $V \times 1$ vector

$$\mathbf{n}_i^{(k)} = [\mathbf{n}_i^{(k)} [v], \mathbf{n}_i^{(k)} [v+1], \dots, \mathbf{n}_i^{(k)} [v+V-1]], \quad (4.6)$$

and the entire noise matrix is an $N \times V$ matrix

$$\mathbf{n}^{(k)} = [\mathbf{n}_1^{(k)}, \mathbf{n}_2^{(k)}, \dots, \mathbf{n}_N^{(k)}]^T. \quad (4.7)$$

The received signal at the k -th user is then equal to

$$\mathbf{y}^{(k)} = \mathbf{H}^{(k)} \mathbf{x} + \mathbf{n}^{(k)}, \quad (4.8)$$

where

$$\mathbf{y}^{(k)} = [\mathbf{y}_1^{(k)}, \mathbf{y}_2^{(k)}, \dots, \mathbf{y}_N^{(k)}]^T. \quad (4.9)$$

and

$$\mathbf{y}_i^{(k)} = [\mathbf{y}_i^{(k)} [v], \mathbf{y}_i^{(k)} [v+1], \dots, \mathbf{y}_i^{(k)} [v+V-1]], \quad (4.10)$$

The global channel matrix of the whole system can be represented as

$$\mathbf{H} = [\mathbf{H}^{(1)T} \ \mathbf{H}^{(2)T} \ \dots \ \mathbf{H}^{(K)T}]^T, \quad (4.11)$$

and the input-output relation for the system is thus given by

$$\mathbf{y} = \mathbf{H} \mathbf{x} + \mathbf{n}, \quad (4.12)$$

where $\mathbf{y} = [\mathbf{y}^{(1)} \ \mathbf{y}^{(2)} \ \dots \ \mathbf{y}^{(K)}]^T$ and $\mathbf{n} = [\mathbf{n}^{(1)} \ \mathbf{n}^{(2)} \ \dots \ \mathbf{n}^{(K)}]^T$.

4.2.2 Interference Mitigation for BC-MU-MIMO System

Since the AP transmits simultaneously several data streams to different users, there are not only the ISI and the MSI like in the SU-MIMO system, but also the MUI. The combination of a TR pre-filter and a ZF pre-equalizer is now considered to deploy in the MU-MIMO system to mitigate such interferences.

4.2.2.1 Time Reversal Pre-Filter

As shown in Fig. 33, the TR pre-filter is inserted at the transmitter side in order to efficiently shorten the overall CIRs [66]. By doing so, the signal is convoluted with the time reversed CIR which is the TR pre-filter before transmitted over the multipath channel.

According to the number of multipath components of CIR being used for the pre-filtering, three types of the TR pre-filter are classified as mentioned in the previous chapters. They are the All-TR (A-TR) pre-filter, the Selective-TR (S-TR) pre-filter and the Partial-TR (P-TR) pre-filter. Simulation results in [66] have shown that the S-TR pre-filter with limited number of paths can provide similar performance in comparison with the A-TR pre-filter. In this chapter, therefore, the S-TR pre-filter will be considered for the MU-MIMO UWB system.

Let \mathbf{G} denote the pre-filter matrix, which is expressed as

$$\mathbf{G} = [\mathbf{G}^{(1)} \ \mathbf{G}^{(2)} \ \dots \ \mathbf{G}^{(K)}], \quad (4.13)$$

where matrix $\mathbf{G}^{(k)}$ is based on matrix $\mathbf{H}^{(k)}$ transposed in space and each element $\mathbf{g}_{ij}^{(k)}$ is the time reversal of s -strongest paths (for the S-TR pre-filters) of a element $\mathbf{h}_{ji}^{(k)}$ (denoted as $\mathbf{h}_{ji}^{(k)*}$) of $\mathbf{H}^{(k)}$. $\mathbf{G}^{(k)}$ can be then written as

$$\mathbf{G}^{(k)} = \begin{pmatrix} \mathbf{h}_{11}^{(k)*} & \mathbf{h}_{21}^{(k)*} & \dots & \mathbf{h}_{N1}^{(k)*} \\ \mathbf{h}_{12}^{(k)*} & \mathbf{h}_{22}^{(k)*} & \dots & \mathbf{h}_{N2}^{(k)*} \\ \vdots & \vdots & \ddots & \vdots \\ \mathbf{h}_{1M}^{(k)*} & \mathbf{h}_{2M}^{(k)*} & \dots & \mathbf{h}_{NM}^{(k)*} \end{pmatrix} \quad (4.14)$$

If \mathbb{H} is denoted as the equivalent channel matrix, which is represented as

$$\mathbb{H} = \begin{pmatrix} \hat{\mathbf{H}}_{11} & \hat{\mathbf{H}}_{12} & \dots & \hat{\mathbf{H}}_{1K} \\ \hat{\mathbf{H}}_{21} & \hat{\mathbf{H}}_{22} & \dots & \hat{\mathbf{H}}_{2K} \\ \vdots & \vdots & \ddots & \vdots \\ \hat{\mathbf{H}}_{K1} & \hat{\mathbf{H}}_{K2} & \dots & \hat{\mathbf{H}}_{KK} \end{pmatrix}, \quad (4.15)$$

where $\hat{\mathbf{H}}_{pq} = \mathbf{H}^{(p)}\mathbf{G}^{(q)}$, with $p, q = 1, \dots, K$, is an $N \times N$ matrix and the components of $\hat{\mathbf{H}}_{pq}$ are calculated by

$$\hat{\mathbf{h}}_{ij}^{(pq)} = \sum_{m=1}^M \mathbf{h}_{im}^{(p)} \mathbf{h}_{jm}^{(q)*}, \quad i, j = 1, \dots, N, \quad (4.16)$$

$$p, q = 1, \dots, K.$$

Equation (4.12), i.e., the received signal with the TR prefilter, becomes

$$\mathbf{y} = \mathbb{H}\mathbf{x} + \mathbf{n} \quad (4.17)$$

4.2.2.2 Zero Forcing Pre-Equalizer

The MUI in the SM MU-MIMO UWB system causes a BER performance floor in similar way that the MSI does in the SM SU-MIMO UWB system. The appearance of a ZF pre-equalizer together with the TR pre-filter at the transmitter of the AP will deal with this problem [65].

Due to the high compression in the time domain of the equivalent CIR, in order to design the pre-equalizer we shorten it by giving a threshold of the collected energy level in percentage and choose a limited number of taps L_s in total length of the equivalent channel L_e ($L_s \ll L_e$).

The CIR for the shortened equivalent channel is re-indexed in the time domain as follows:

$$\hat{\mathbf{h}}_{ij}^{(pq)} = [h_{ij}^{pq}[0], h_{ij}^{pq}[1], \dots, h_{ij}^{pq}[L_s - 1]], \quad (4.18)$$

$i, j = 1, \dots, N$, and $p, q = 1, \dots, K$.

We assume that channels do not change when a block of $K + L_s - 1$ data symbols are transmitted. The new equivalent channel matrix can be represented by a block Toeplitz matrix as

$$\mathbf{H}_s = \begin{pmatrix} \mathbf{H}[L_s - 1] & \dots & \mathbf{H}[0] & 0 & \dots & 0 \\ 0 & \mathbf{H}[L_s - 1] & \dots & \mathbf{H}[0] & \dots & 0 \\ \vdots & \ddots & \ddots & \ddots & \ddots & \vdots \\ 0 & \dots & 0 & \mathbf{H}[L_s - 1] & \dots & \mathbf{H}[0] \end{pmatrix}, \quad (4.19)$$

where each block matrix is

$$\mathbf{H}[k] = \begin{pmatrix} \hat{\mathbf{H}}_{11}[k] & \hat{\mathbf{H}}_{12}[k] & \dots & \hat{\mathbf{H}}_{1K}[k] \\ \hat{\mathbf{H}}_{21}[k] & \hat{\mathbf{H}}_{22}[k] & \dots & \hat{\mathbf{H}}_{2K}[k] \\ \vdots & \vdots & \ddots & \vdots \\ \hat{\mathbf{H}}_{K1}[k] & \hat{\mathbf{H}}_{K2}[k] & \dots & \hat{\mathbf{H}}_{KK}[k] \end{pmatrix}, \quad (4.20)$$

and $\hat{\mathbf{H}}_{pq}[k]$ is calculated by

$$\hat{\mathbf{H}}_{pq}[k] = \begin{pmatrix} \hat{\mathbf{h}}_{11}^{pq}[k] & \hat{\mathbf{h}}_{12}^{pq}[k] & \dots & \hat{\mathbf{h}}_{1N}^{pq}[k] \\ \hat{\mathbf{h}}_{21}^{pq}[k] & \hat{\mathbf{h}}_{22}^{pq}[k] & \dots & \hat{\mathbf{h}}_{2N}^{pq}[k] \\ \vdots & \vdots & \ddots & \vdots \\ \hat{\mathbf{h}}_{N1}^{pq}[k] & \hat{\mathbf{h}}_{N2}^{pq}[k] & \dots & \hat{\mathbf{h}}_{NN}^{pq}[k] \end{pmatrix}, \quad (4.21)$$

$p, q = 1, \dots, K$.

The pre-equalizer matrix \mathbf{G}_{ZF} is the inverse of the shortened equivalent channel matrix given by

$$\mathbf{G}_{ZF} = \alpha \mathbf{H}_s^\dagger = \alpha (\mathbf{H}_s^H \mathbf{H}_s)^{-1} \mathbf{H}_s^H, \quad (4.22)$$

where \dagger and $(\bullet)^H$ denote the Moore-Penrose pseudo-inverse and the conjugate transpose of a matrix, respectively. The coefficient α is introduced for the power constraint of the transmit signal [61].

4.2.3 Spatial Correlation

The correlation between MU-MIMO sub-channels is modeled with an assumption that the correlation among the receive antennas of users is independent of the correlation between the transmit antennas and there is no correlation among the receive antennas of different users. We can include the correlation into the MU-MIMO UWB channel model by introducing fixed transmit and receive correlation matrices following the well-known Kronecker model, so that [68]

$$\mathbf{H} = \mathbf{R}_{\text{Rx}}^{1/2} \mathbf{H}_w \mathbf{R}_{\text{Tx}}^{1/2}, \quad (4.23)$$

where \mathbf{H}_w is the global channel matrix given by

$$\mathbf{H}_w = [\mathbf{H}_w^{(1)\text{T}}, \mathbf{H}_w^{(2)\text{T}}, \dots, \mathbf{H}_w^{(K)\text{T}}]^{\text{T}}. \quad (4.24)$$

where $\mathbf{H}_w^{(k)}$ with $k = 1, \dots, K$ is the channel matrix of $N \times M$ independent channel realizations. \mathbf{R}_{Tx} is the transmit correlation matrix with dimension $M \times M$ and \mathbf{R}_{Rx} is the block-diagonal receive correlation matrix which is defined as

$$\mathbf{R}_{\text{Rx}} = \begin{pmatrix} \mathbf{R}_{\text{Rx}}^{(1)} & 0 & \dots & 0 \\ 0 & \mathbf{R}_{\text{Rx}}^{(2)} & \dots & 0 \\ \vdots & \vdots & \ddots & \vdots \\ 0 & 0 & \dots & \mathbf{R}_{\text{Rx}}^{(K)} \end{pmatrix}, \quad (4.25)$$

where $\mathbf{R}_{\text{Rx}}^{(k)}$ with $k = 1, \dots, K$ is the receive correlation matrix with dimension $N \times N$ for the k -th user.

For the fixed correlation matrix in the Kronecker model, there are some variations in terms of whether or not the impact of inter-element distance being considered [47, 91]. In our work, the exponential decay of the correlation is deployed [47, 37]. Hence, the transmit correlation matrix is

$$\mathbf{R}_{\text{Tx}} = \begin{pmatrix} 1 & \rho_{\text{Tx}} & \rho_{\text{Tx}}^2 & \dots & \rho_{\text{Tx}}^{M-1} \\ \rho_{\text{Tx}} & 1 & \rho_{\text{Tx}} & \dots & \rho_{\text{Tx}}^{M-2} \\ \vdots & \vdots & \vdots & \ddots & \vdots \\ \rho_{\text{Tx}}^{M-1} & \rho_{\text{Tx}}^{M-2} & \rho_{\text{Tx}}^{M-3} & \dots & 1 \end{pmatrix}, \quad (4.26)$$

and the receive correlation matrix for the k -th use is

$$\mathbf{R}_{\text{Rx}}^{(k)} = \begin{pmatrix} 1 & \rho_{\text{Rx}}^{(k)} & \rho_{\text{Rx}}^{(k)2} & \dots & \rho_{\text{Rx}}^{(k)N-1} \\ \rho_{\text{Rx}}^{(k)} & 1 & \rho_{\text{Rx}}^{(k)} & \dots & \rho_{\text{Rx}}^{(k)N-2} \\ \vdots & \vdots & \vdots & \ddots & \vdots \\ \rho_{\text{Rx}}^{(k)N-1} & \rho_{\text{Rx}}^{(k)N-2} & \rho_{\text{Rx}}^{(k)N-3} & \dots & 1 \end{pmatrix}, \quad (4.27)$$

where ρ_{Tx} is the correlation coefficient of transmit antennas and $\rho_{Rx}^{(k)}$ is the correlation coefficient of receive antennas of the k -th user. In the multi-user SM-MIMO UWB system, the correlations are at both transmit and receive sides. These correlation will doubly degrade the performance of system.

From Eq. (4.20), we can learn that the maximum number of independent data streams the system can achieve is N_R , which is the number of receive antennas of all users instead of transmit antennas. This happens similarly for the case of the single user system. Several data streams of several users can be also multiplexed to transmit over one antenna only. However, like the single user case, the system with the single transmit antenna equipped AP cannot achieve the transmit diversity gain.

4.2.4 Numerical Result

Table 9: Simulation parameters

Parameters	Value	Unit
Channel	CM4 [29]	-
T	2	ns
t_c	1	ns
w	0.5	ns
s	50	ns
L_s	180	ns
ρ_{Rx}	0.3	-

The performance of the spatial multiplexing BC-MIMO UWB system using concurrently both the ZF pre-equalizer and the TR pre-filter is analyzed based on simulation results. We also verify the impact of the transmit spatial correlation on the system performance. In simulation, BPAM is always used, the monocycle waveform is the same as Equ. 3.28. The IEEE 802.15.3a CM4 channel model [29] is used for each channel in simulation. Other assumptions are that the signal is transmitted over UWB channels and perfectly synchronized at the receiver; the receiver for every data stream is a simple integrate-and-dump (I&D) receiver. Simulation parameters are presented in Table 9.

It is noted that $m \times (k \times n)$ MIMO denotes a MIMO system having m transmit antennas transmitting to k users and each user being equipped with n receive antennas.

The average BER as a function of the transmit correlation coefficient ρ_{Tx} is shown in Fig. 34, 35 and 36. Increasing the number of users while keeping the number of transmit antennas and receive antennas constant makes the number of simultaneously transmitted data streams from transmit antennas increase. This leads to degrade the system performance as shown in Fig. 34.

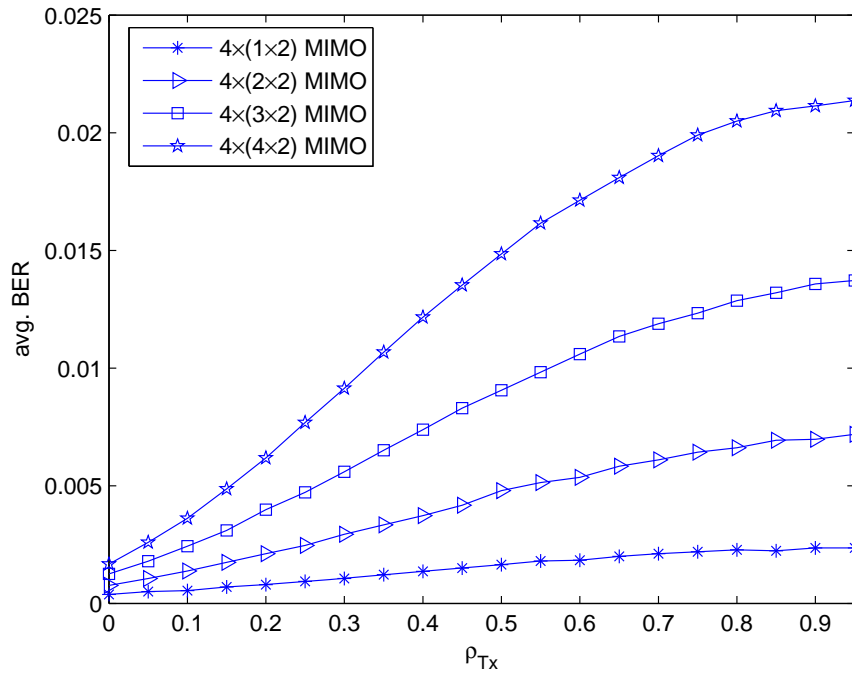


Figure 34: Average BER versus the transmit correlation coefficient with $M = 4$, $N = 2$, SNR = 12 dB for the different number of users $K = 1, 2, 3, 4$.

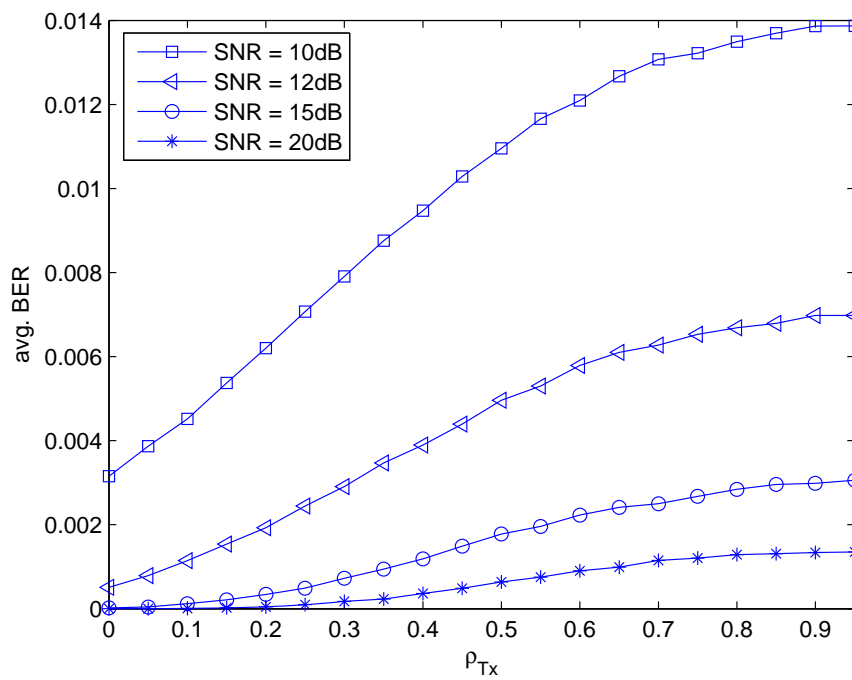


Figure 35: Average BER versus the transmit correlation coefficient with $M = 4$, $K = 2$, $N = 2$ for the different values of SNR = 10, 12, 15, 20.

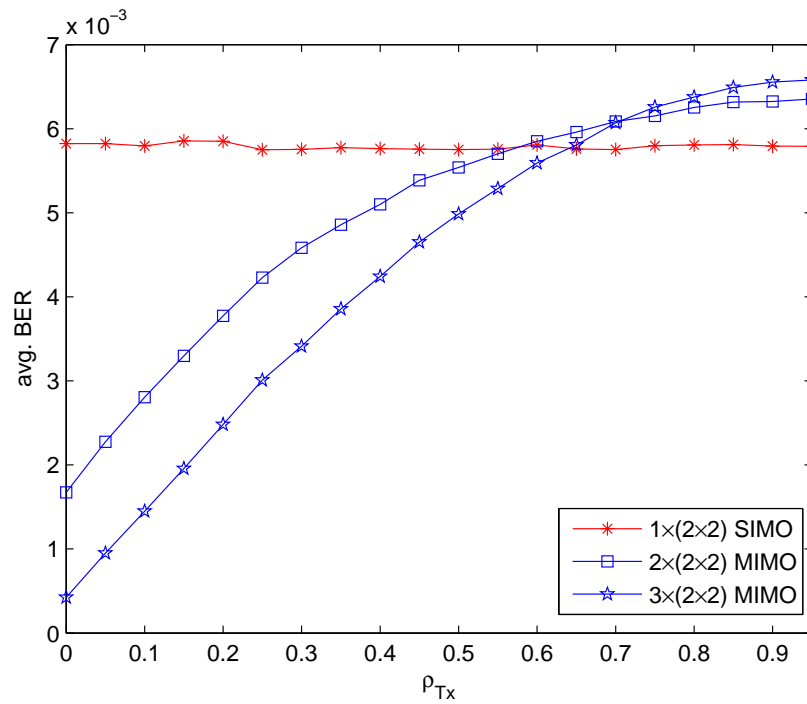


Figure 36: Average BER versus the transmit correlation coefficient with $K = 2$, $N = 2$, $\text{SNR} = 12$ dB for the different numbers of transmit antenna $M = 1, 2, 3$

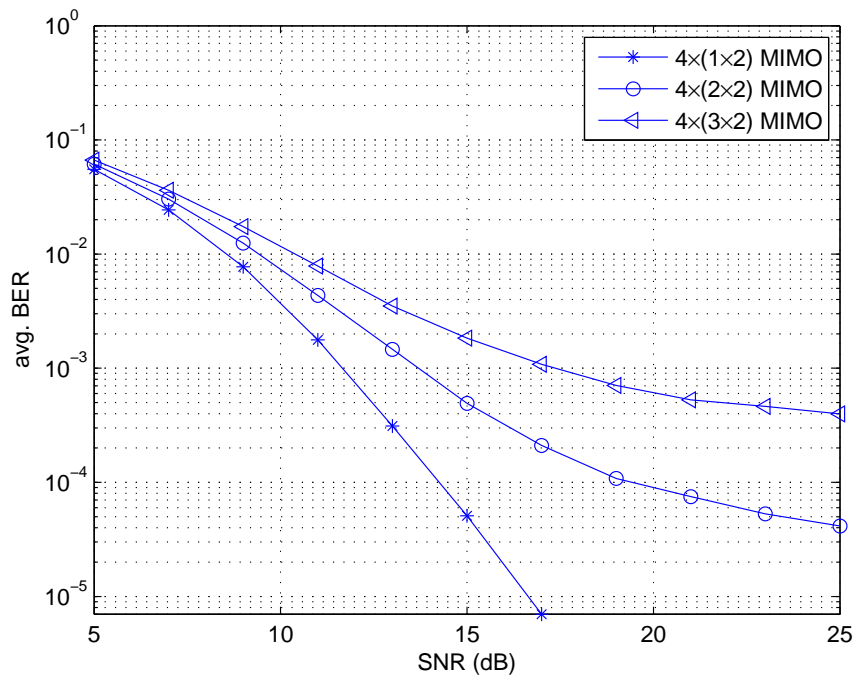


Figure 37: Average BER versus SNR with $M = 4$, $N = 2$, $\rho_{Tx} = 0.3$ for the different number of users $K = 1, 2, 3$.

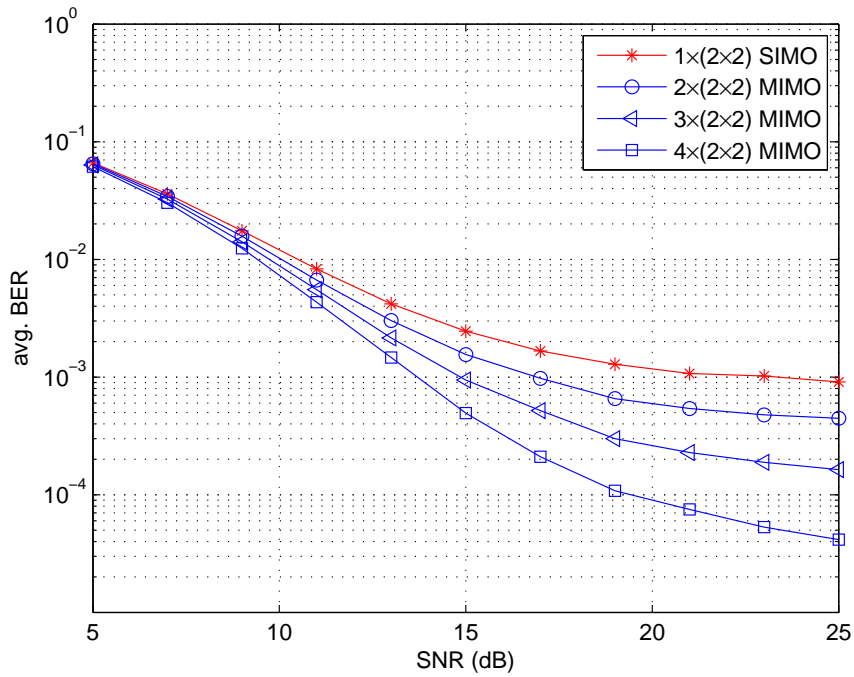


Figure 38: Average BER versus SNR with $K = 2$, $N = 2$, $\rho_{Tx} = 0.3$ for the different numbers of transmit antenna $M = 1, 2, 3, 4$.

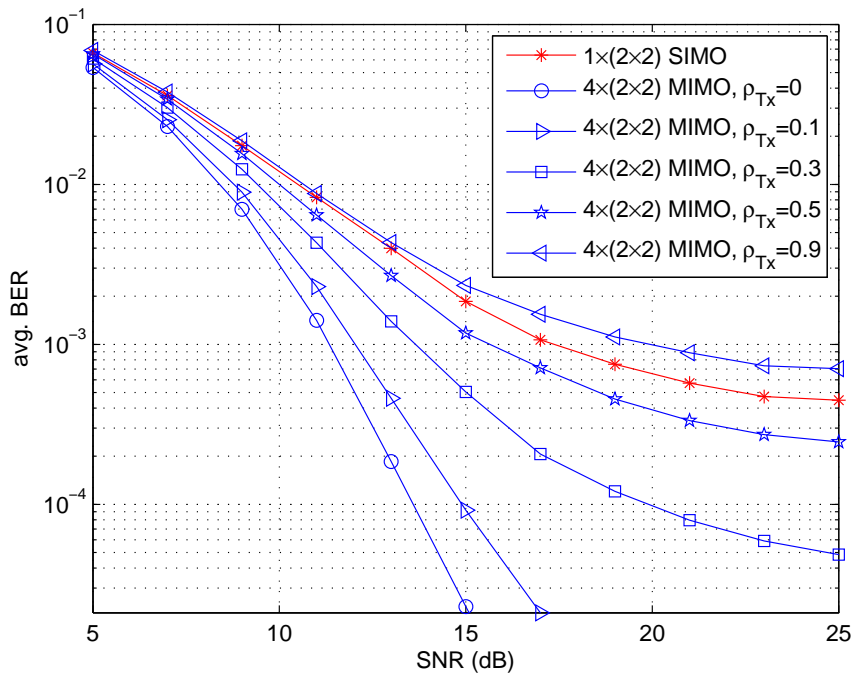


Figure 39: Average BER versus SNR with $M = 4$, $K = 2$, $N = 2$ for the different values of transmit correlation coefficient $\rho_{Tx} = 0, 0.1, 0.3, 0.5, 0.9$.

It can be observed from Fig. 35 that with the same number of transmit and receive antenna ($M = 4$, $K = 2$, $N = 2$), the lower SNR is, more severely the transmit correlation affects the system performance. In Fig. 36, we examine the effect of the transmit correlation on the performance for the two-user case with two receive antennas per user. We can see from this figure that, when ρ_{Tx} increases, the average BER of the single transmit antenna system (called as SIMO) keeps unchanged while it increases for the case of the multiple transmit antenna system (called as MIMO). At the low transmit correlation regime, the more transmit antennas the system has, the better BER performance the system can achieve. This is the advantage of the transmit diversity possessed by the MIMO-TR-UWB system. However, if the correlation is strong, more transmit antennas will rapidly degrade the performance of MIMO systems. For example, when the transmit correlation coefficient ρ_{Tx} is greater than 0.6, the performance of the $1 \times (2 \times 2)$ SIMO system outperforms the performance of the $2 \times (2 \times 2)$ MIMO system and when ρ_{Tx} is greater than 0.65 the the performance of the $2 \times (2 \times 2)$ MIMO system is better than the performance of the $3 \times (2 \times 2)$ MIMO system.

In Fig. 37, 38 and 39, we investigate the average BER of the system versus the signal-to-noise ratio (SNR). In Fig. 37, data streams are transmitted over 4 transmit antennas to $K = 1, 2, 3$ users which are equipped the same number of receive antennas $N = 2$ per user. In case of single user, i.e. $K = 1$, the good performance can be achieved. When number users are more than one, the BER performance reaches an error floor which is 5×10^{-4} for the case of 3 users and 5×10^{-5} for the case of 2 users.

As shown in Fig 38, when the transmit correlation coefficient is assumed to be constant ($\rho_{Tx} = 0.3$) and with the same number of users, the same number of receive antennas per user, increasing the number of transmit antennas will improve evidently the BER performance of the system. However this is not always true as shown in Fig. 39.

In Fig. 39, the BER performances of the SIMO and MIMO system with the same number of users as well as number of receive antennas per user are presented. Similar to results in Fig. 36, for the MIMO system with 4 transmit antennas, good performance can be obtained at the low transmit correlation regime but the performance becomes worse sharply when ρ_{Tx} increases. It can be seen in Fig. 39, the BER performance of 4 transmit antenna system reaches an error floor when $\rho_{Tx} \geq 0.3$ and the BER performance of the $4 \times (2 \times 2)$ MIMO system is even worse than the $1 \times (2 \times 2)$ SIMO system when transmit antennas are highly correlated ($\rho_{Tx} = 0.9$).

4.3 MULTIPLE ACCESS MU-MIMO UWB SYSTEM

In many UWB applications, the communication is required in both directions, uplink and downlink, but the complexity is allowed only at the AP side and the user terminal needs to be simple and low cost. In order to satisfy these requirements, we propose to deploy a TR filter combining with a ZF equalizer at the receiver to deal with the ISI, the MSI and the MUI in

the reverse link. This is a reversible mechanism of those is implemented in the forward link, represented in Section 4.2.

4.3.1 System Model

In the investigated multiple access MIMO UWB system shown in Fig. 40, K decentralized users, each being equipped with N transmit antennas, transmit the signal to M receive antennas of the AP. The total number of transmit antennas is $N_T = NK$. It can be observed from this assumption that, in both sides, users and the AP, the number of transmit antennas in the MAC channel is assumed equal to the number of receive antennas in the BC channel and the number of receive antennas in the MAC channel is assumed equal to the number of transmit antennas in the BC channel. The

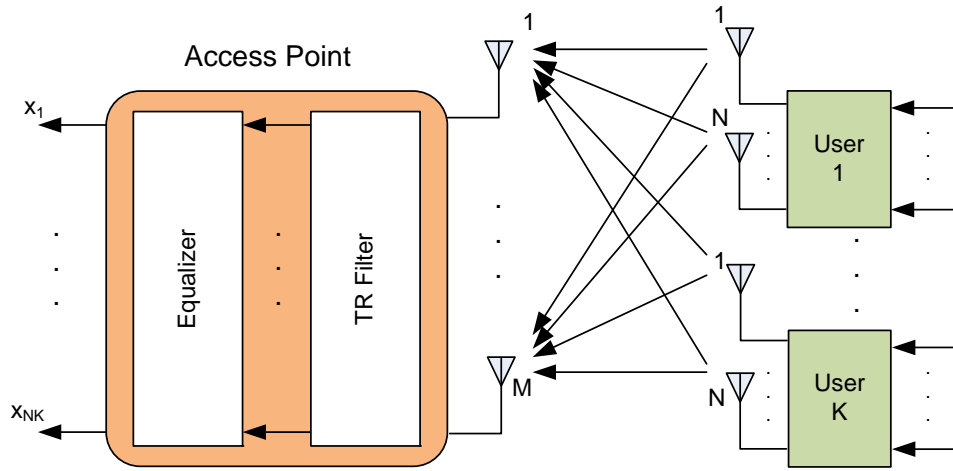


Figure 40: The multiple access MU-MIMO UWB system with a filter and equalizer.

CIR and its discrete form of the channel between the j -th transmit antenna of the k -th user and the i -th receive antenna of the AP are similar to Eq. 4.1 and 4.2, respectively. The entire channel between the k -th user and the AP is thus represented as

$$\mathbf{H}^{(k)} = \begin{pmatrix} \mathbf{h}_{11}^{(k)} & \mathbf{h}_{12}^{(k)} & \dots & \mathbf{h}_{1N}^{(k)} \\ \mathbf{h}_{21}^{(k)} & \mathbf{h}_{22}^{(k)} & \dots & \mathbf{h}_{2N}^{(k)} \\ \vdots & \vdots & \ddots & \vdots \\ \mathbf{h}_{M1}^{(k)} & \mathbf{h}_{M2}^{(k)} & \dots & \mathbf{h}_{MN}^{(k)} \end{pmatrix}, \quad (4.28)$$

with the dimension $M \times NL$.

Let us consider a block $V + L$ symbols of transmit data at the j -th antenna of the k -th user. We assume that channel does not change when sending

this block. This block of data can be represented by an $L \times V$ Hankel matrix as following

$$\mathbf{x}_j^{(k)} = \begin{pmatrix} \mathbf{x}_j^{(k)} [v-L+1] & \mathbf{x}_j^{(k)} [v-L+2] & \cdots & \mathbf{x}_j^{(k)} [v-L+V] \\ \vdots & \vdots & \ddots & \vdots \\ \mathbf{x}_j^{(k)} [v-1] & \mathbf{x}_j^{(k)} [v] & \cdots & \mathbf{x}_j^{(k)} [v+V-2] \\ \mathbf{x}_j^{(k)} [v] & \mathbf{x}_j^{(k)} [v+1] & \cdots & \mathbf{x}_j^{(k)} [v+V-1] \end{pmatrix}. \quad (4.29)$$

The entire transmit signal matrix from the k -th user is

$$\mathbf{x}^{(k)} = \frac{1}{\sqrt{N}} [\mathbf{x}_1^{(k)}, \mathbf{x}_2^{(k)}, \dots, \mathbf{x}_N^{(k)}]^T, \quad (4.30)$$

with dimension $NL \times V$. The scale factor $1/\sqrt{N}$ keeps the total transmit power of signal as the same as it in the SISO case.

The signal received at the AP is an $M \times V$ matrix, \mathbf{y} , given by

$$\begin{aligned} \mathbf{y} &= \sum_{k=1}^K \mathbf{H}^{(k)} \mathbf{x}^{(k)} + \mathbf{n} \\ &= \mathbf{H}\mathbf{x} + \mathbf{n}, \end{aligned} \quad (4.31)$$

where

$$\mathbf{x} = [\mathbf{x}^{(1)} \mathbf{x}^{(2)} \dots \mathbf{x}^{(K)}]^T, \quad (4.32)$$

\mathbf{H} is the global channel matrix of the system, represented as

$$\mathbf{H} = [\mathbf{H}^{(1)} \mathbf{H}^{(2)} \dots \mathbf{H}^{(K)}], \quad (4.33)$$

and \mathbf{n} is the entire noise matrix with dimension of $M \times V$, given by

$$\mathbf{n} = [\mathbf{n}_1, \mathbf{n}_2, \dots, \mathbf{n}_N]^T, \quad (4.34)$$

where

$$\mathbf{n}_i = [\mathbf{n}_i [v], \mathbf{n}_i [v+1], \dots, \mathbf{n}_i [v+V-1]]. \quad (4.35)$$

4.3.2 Interference Mitigation for MAC-MU-MIMO System

In the uplink MU-MIMO channel, MAC-MIMO, the MUI and the MSI appear when users simultaneously transmit several data streams to the AP. The combination of a TR filter and a ZF equalizer are proposed to implement at the AP to cancel these interferences as well as the ISI.

4.3.2.1 Time Reversal Filter

Like the TR pre-filter in the downlink channel, the TR filter is designed based on information from s strongest paths of the whole CIR. The filter matrix, \mathbf{G} , can be expressed as

$$\mathbf{G} = [\mathbf{G}^{(1)T} \mathbf{G}^{(2)T} \dots \mathbf{G}^{(K)T}]^T, \quad (4.36)$$

where $\mathbf{G}^{(k)}$ is computed from matrix $\mathbf{H}^{(k)}$ by transposing in space, time reversing their elements. Hence, $\mathbf{G}^{(k)}$ is written as

$$\mathbf{G}^{(k)} = \begin{pmatrix} \mathbf{h}_{11}^{(k)*} & \mathbf{h}_{21}^{(k)*} & \dots & \mathbf{h}_{M1}^{(k)*} \\ \mathbf{h}_{12}^{(k)*} & \mathbf{h}_{22}^{(k)*} & \dots & \mathbf{h}_{M2}^{(k)*} \\ \vdots & \vdots & \ddots & \vdots \\ \mathbf{h}_{1N}^{(k)*} & \mathbf{h}_{2N}^{(k)*} & \dots & \mathbf{h}_{MN}^{(k)*} \end{pmatrix}, \quad (4.37)$$

where $\mathbf{h}_{ij}^{(k)*}$ is the time reversal of s -strongest paths of $\mathbf{h}_{ij}^{(k)}$.

The signal that we receive after the TR filter is written as

$$\begin{aligned} \mathbf{y} &= \mathbf{G}\mathbf{H}\mathbf{x} + \mathbf{n} \\ &= \mathbb{H}\mathbf{x} + \mathbf{n}, \end{aligned} \quad (4.38)$$

where \mathbb{H} is defined as the equivalent channel matrix. \mathbb{H} is an $K \times K$ block matrix which is expressed as

$$\mathbb{H} = \begin{pmatrix} \hat{\mathbf{H}}_{11} & \hat{\mathbf{H}}_{12} & \dots & \hat{\mathbf{H}}_{1K} \\ \hat{\mathbf{H}}_{21} & \hat{\mathbf{H}}_{22} & \dots & \hat{\mathbf{H}}_{2K} \\ \vdots & \vdots & \ddots & \vdots \\ \hat{\mathbf{H}}_{K1} & \hat{\mathbf{H}}_{K2} & \dots & \hat{\mathbf{H}}_{KK} \end{pmatrix}, \quad (4.39)$$

where $\hat{\mathbf{H}}_{pq} = \mathbf{G}^{(q)}\mathbf{H}^{(p)}$, with $p, q = 1, \dots, K$, is an $N \times N$ matrix. The components of $\hat{\mathbf{H}}_{pq}$ are calculated by

$$\begin{aligned} \hat{\mathbf{h}}_{ij}^{(pq)} &= \sum_{m=1}^N \mathbf{h}_{im}^{(p)*} \mathbf{h}_{jm}^{(q)}, \quad i, j = 1, \dots, M, \\ & \quad p, q = 1, \dots, K. \end{aligned} \quad (4.40)$$

It can be observed from Equ. 4.39 that the equivalent channel is a $K \times K$ block matrix and each block is an $N \times N$ matrix. The dimensions of the (block) matrix depend on the number of users, K , and the number of transmit antennas per user, N , and are independent of the number of receive antennas of the AP, M . The maximum number of independent data streams the system can achieve is $N_T = KN$, which is total number of transmit antennas of all users. It means that the AP can receive all data streams from dispersed users with single receive antenna.

4.3.2.2 Zero Forcing Equalizer

Thanks to the TR filter, the equivalent channel is highly compressed in the time domain. Therefore, like designing the ZF pre-equalizer in the previous section, we shorten the equivalent CIR before computing the ZF equalizer. The equalizer matrix \mathbf{G}_{ZF} is the inverse of the shortened equivalent channel matrix given by

$$\mathbf{G}_{ZF} = \alpha \mathbb{H}_s^\dagger = \alpha (\mathbb{H}_s^H \mathbb{H}_s)^{-1} \mathbb{H}_s^H, \quad (4.41)$$

where \mathbb{H}_s is defined similarly to Equation 4.19 and α is a constant coefficient used for the power constraint.

4.3.3 Spatial Correlation

Users are assumed to be separately located, so there is no correlation among the transmit antennas of different users. The transmit correlation is assumed to be independent of the correlation among the receive antennas.

The transmit and receive correlation matrix is included in the MAC-MU-MIMO UWB channel model same as Equation 4.23. The differences between correlation models of the BC-MIMO and MAC-MIMO channel are in the transmit and receive correlation matrices. Since there is no correlation between transmit antennas of different users, \mathbf{R}_{Tx} is a block diagonal $K \times K$ matrix written as

$$\mathbf{R}_{\text{Tx}} = \begin{pmatrix} \mathbf{R}_{\text{Tx}}^{(1)} & 0 & \dots & 0 \\ 0 & \mathbf{R}_{\text{Tx}}^{(2)} & \dots & 0 \\ \vdots & \vdots & \ddots & \vdots \\ 0 & 0 & \dots & \mathbf{R}_{\text{Tx}}^{(K)} \end{pmatrix}, \quad (4.42)$$

where $\mathbf{R}_{\text{Tx}}^{(k)}$ with $k = 1, \dots, K$ is the transmit correlation matrix with dimension $N \times N$ for k -th user. Deploying the exponential decay of the correlation, $\mathbf{R}_{\text{Tx}}^{(k)}$ is modeled as

$$\mathbf{R}_{\text{Tx}}^{(k)} = \begin{pmatrix} 1 & \rho_{\text{Tx}}^{(k)} & \rho_{\text{Tx}}^{(k)2} & \dots & \rho_{\text{Tx}}^{(k)N-1} \\ \rho_{\text{Tx}}^{(k)} & 1 & \rho_{\text{Tx}}^{(k)} & \dots & \rho_{\text{Tx}}^{(k)N-2} \\ \vdots & \vdots & \vdots & \ddots & \vdots \\ \rho_{\text{Tx}}^{(k)N-1} & \rho_{\text{Tx}}^{(k)N-2} & \rho_{\text{Tx}}^{(k)N-3} & \dots & 1 \end{pmatrix}, \quad (4.43)$$

and the receive correlation matrix is calculated by

$$\mathbf{R}_{\text{Rx}} = \begin{pmatrix} 1 & \rho_{\text{Rx}} & \rho_{\text{Rx}}^2 & \dots & \rho_{\text{Rx}}^{M-1} \\ \rho_{\text{Rx}} & 1 & \rho_{\text{Rx}} & \dots & \rho_{\text{Rx}}^{M-2} \\ \vdots & \vdots & \vdots & \ddots & \vdots \\ \rho_{\text{Rx}}^{M-1} & \rho_{\text{Rx}}^{M-2} & \rho_{\text{Rx}}^{M-3} & \dots & 1 \end{pmatrix}, \quad (4.44)$$

where $\rho_{\text{Tx}}^{(k)}$ is the correlation coefficient among transmit antennas of the k -th user and ρ_{Rx} is the correlation coefficient of receive antennas of the AP.

As studied in section 4.3.2.1, with only one receive antenna, the AP can receive simultaneously more than one data streams from dispersed users. In this situation, the spatial correlation at the receiver is avoided, however, the receive diversity gain is not achieved as a result.

4.3.4 Numerical Result

In this section, we analyze the performance of the spatial multiplexing MAC-MIMO UWB system in which the combination of the TR filter and the ZF equalizer is used to combat the interference problems. The efficiency of the equalizer in improving the system performance is evaluated by simulation results.

In the earlier sections, the ability that ignoring the receive diversity gain, data streams from users can be received by a single antenna at the AP to dodge the receive correlation is stated. Therefore, the impact of the receive correlation on the performance is assessed by simulation in this section. The simulation parameters and assumptions in section 4.2.4 are applied. In the simulation figures, $(k \times n) \times m$ MIMO denotes a MIMO system in which k users, n transmit antennas are equipped for each user, communicate with m receive antennas of the AP.

The efficiency of the equalizer on the system performance is represented in figures 41 and 42. In these figures, the correlation coefficients are fixed at 0.3. It is shown in both figures that the performance of the MAC-MIMO UWB system is lessened severely when the ZF equalizer is not used. In other words, the proposed equalizer can significantly improve the performance of the systems. For instance, in Fig. 41, in the best situation, two users transmit one their own data stream simultaneously to the two-receive-antenna-AP, the BER performance of the system reaches an error floor at 7×10^{-4} when the equalizer is not used while the BER error floor of the system is broken up when the equalizer is used.

The greater number of data streams (in Fig. 41) or users (in Fig. 42) the worse the BER performance of the system is. This is caused by involved the MSI increasing with number of data streams or the MUI increasing with number of users. It could be said that the MUI and the MSI decrease seriously the system performance. As shown in Fig. 41, in case of the equalizer being use, with the same number of users and number of receive antennas, if users transmit one data stream, the BER performance can be achieved at SNR = 10dB is 5×10^{-3} while at this SNR value, the BER performance is much worse, 9×10^{-2} , if users transmit two data streams. Similar results can be achieved in Fig. 42 when the number of users is varied.

The importance of the receive diversity gain is shown in Fig. 43. With given correlation coefficients, $\rho_{Tx} = \rho_{Rx} = 0.3$, increasing the number of receive antennas equipped for the AP, we can get a better system performance in term of the average BER. However, on a limited-dimension equipment, increasing the number of receive antennas may lead to put up the spatial correlation due to narrowing the distance between antennas. In this case, number of antennas can not compensate for the loss caused by the spatial correlation. This can be seen in Fig. 44.

Figure 44 shows the impact of the receive coefficient on the system performance. Examining the BER performance of the $(2 \times 2) \times 4$ MIMO system we can see that if the receive correlation coefficient is ignored, a good performance is obtained. The BER performance becomes worse, however, when the receive correlation coefficient is taken into account. Namely, with $\rho_{Rx} = 0.3$, the average BER reaches an error floor at 6×10^{-5} and the error floor of the BER performance is raised to 6×10^{-4} when $\rho_{Rx} = 0.9$.

It can be also observed from Fig. 44 that in the higher SNR regime, with the same number of users and number of transmit antennas per user, the four-antenna-AP in the high spatial correlation condition may provide a

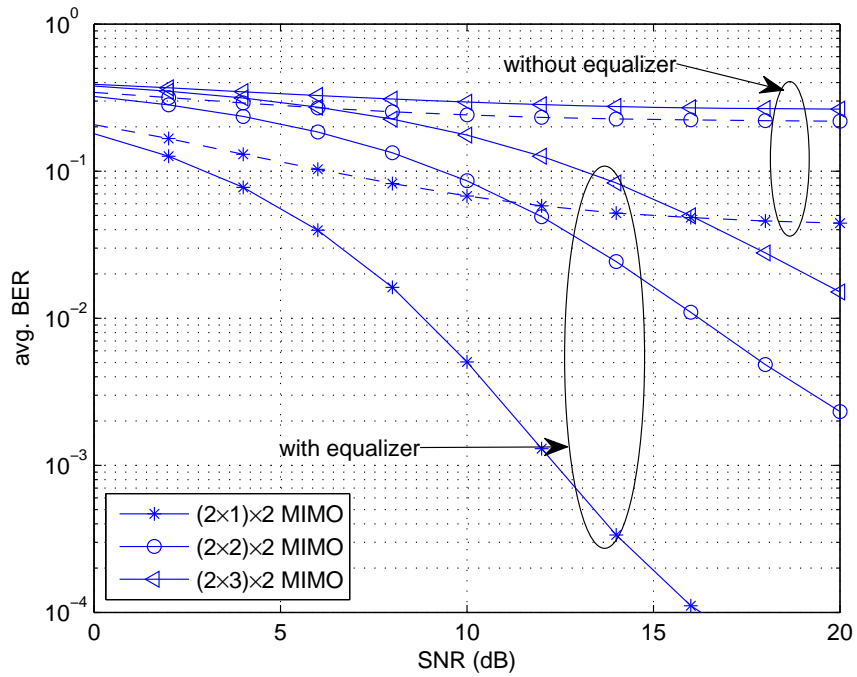


Figure 41: Average BER versus SNR with $K = 2$, $M = 2$, $\rho_{R_x} = \rho_{T_x} = 0.3$ for the different numbers of transmit antennas per user $N = 1, 2, 3$.

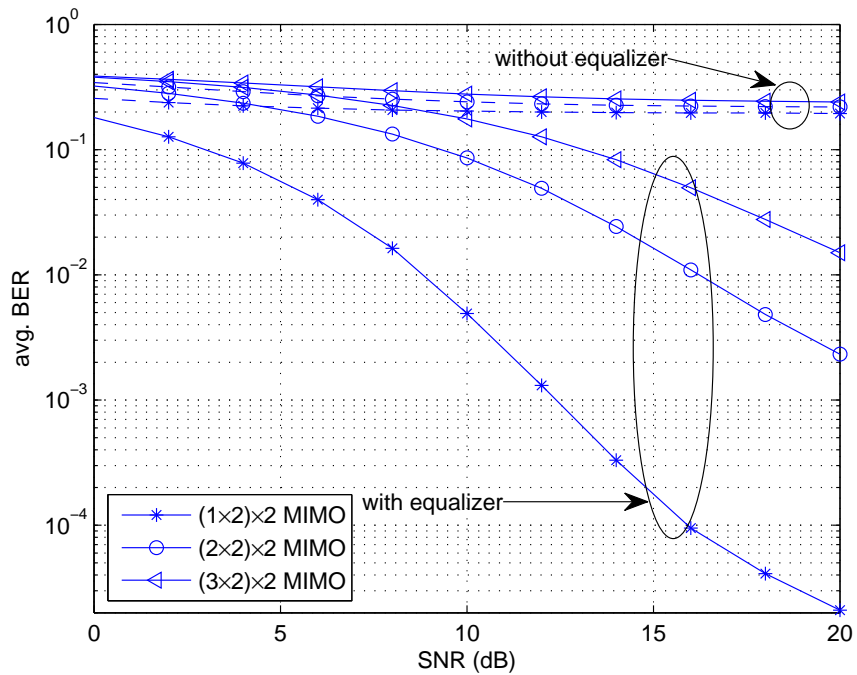


Figure 42: Average BER versus SNR with $N = 2$, $M = 2$, $\rho_{R_x} = \rho_{T_x} = 0.3$ for the different numbers of users $K = 1, 2, 3$.

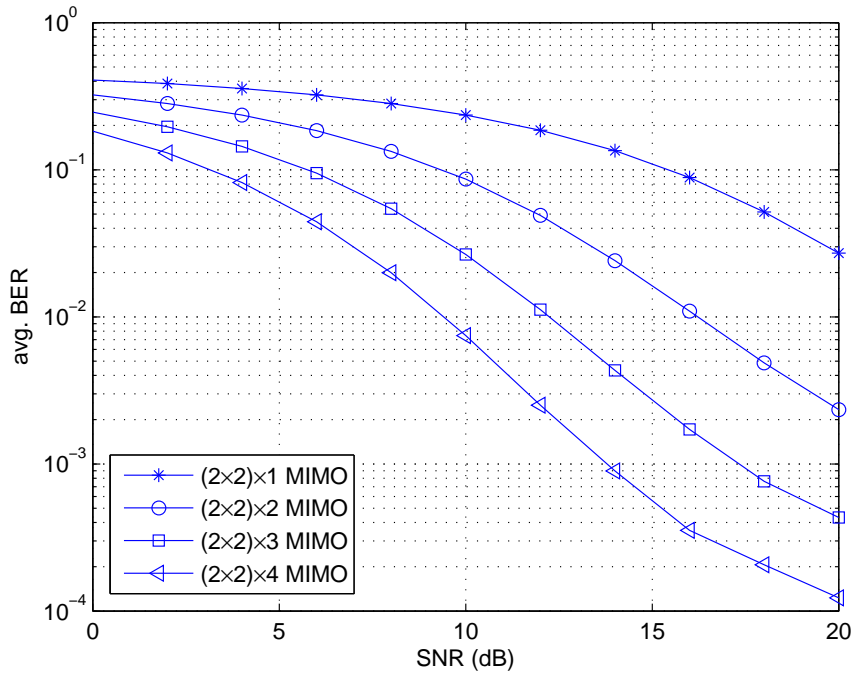


Figure 43: Average BER versus SNR with $K = 2$, $N = 2$, $\rho_{Rx} = \rho_{Tx} = 0.3$ for the different numbers of receive antennas $M = 1, 2, 3, 4$.

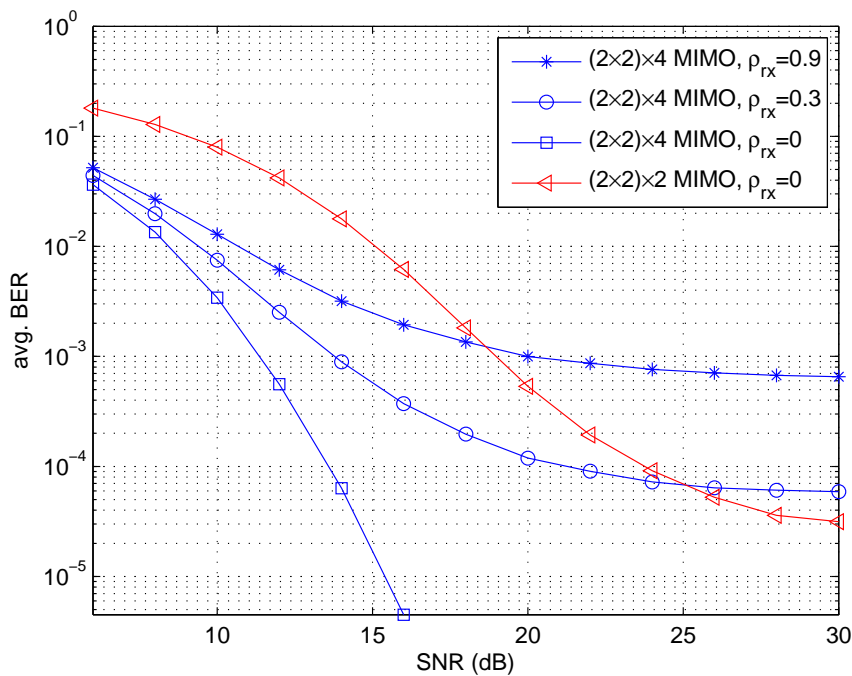


Figure 44: Average BER versus SNR with $K = 2$, $N = 2$, $M = 2$ or 4 , $\rho_{Tx} = 0.3$ for the different values of the receive correlation coefficient $\rho_{Rx} = 0, 0.3, 0.9$.

worse performance than the two-antenna-AP in the lower spatial correlation condition does. For example, the average BER of the $(2 \times 2) \times 4$ MIMO system with $\rho_{\text{Rx}} = 0.3$ and $\rho_{\text{Rx}} = 0.9$ is worse than the average BER of the $(2 \times 2) \times 2$ MIMO system without spatial correlation when $\text{SNR} \geq 25$ and $\text{SNR} \geq 18$, respectively. A remark obtained here is that the system performance can not be improved if increasing the number receive antennas at the AP causes the spatial correlation to be higher.

4.4 SUMMARY

Another approach in MIMO communications is to deploy multiple antennas at the base station (or access point) to support multiple users with one or more antennas per user terminal. The access point communicates with the multiple users simultaneously in the same frequency channel by exploiting differences in spatial signatures at the access point antenna array induced by spatially dispersed users. In UWB communications, due to very long delay spread property of the channel, however, the SM-MU-MIMO system suffers from not only the ISI but also the MSI and the MUI. In this chapter, we propose to use the TR filter combined with the ZF equalizer to suppress these interferences. The broadcast channel and multiple access channel are separately investigated. In order to simplify the user terminal, in the BC channel, we propose to implement this combination at the transmitter side, so called the pre-filter and the pre-equalizer and in the reverse link, the MAC channel, it is deployed at the receiver side. Therefore, in the whole MU-MIMO UWB system, the interference mitigation mechanism is only located at the AP.

The spatial correlation problem is studied in this chapter for the SM-MU-MIMO UWB systems. The spatial correlation models are given for such systems. The effect of the spatial correlation on the system performance is analyzed by simulation results.

MEASUREMENTS AND VALIDATIONS

UWB channel measurements that have been carried out in the IKT laboratory is introduced in this chapter. The measured data is used to validate the simulation results presented in the previous chapters. This chapter is organized as follows: in the first Section, UWB Channel Sounding techniques are introduced; Our measurement campaign is presented in Section 5.2, followed by BER Performance Evaluation Based on Measured CIRs in Section 5.3; and the final Section is Summary.

5.1 UWB CHANNEL SOUNDING

In a realistic environment, signal launched from the transmit antenna experiences not only the direct path, but also a number of distinct propagation paths before it is captured by the receive antenna. These paths undergo various effects such as reflection, transmission, diffraction, diffusion, and so on. The received signal corresponds to a combination of different paths, each of them showing a distinct attenuation, a different phase rotation and a different delay linked to the length of propagation. This multipath propagation mechanism may lead to a significant distortion of the received signal and lessen the performance of the system. On the other hand, a direct path, known as the line of sight (LOS) path, is not always available, which is particularly frequent in indoor configurations. In this case, non-line of sight (NLOS) paths are necessary to enable efficient radio communication.

Characterization of the wireless channels including finding the delays and attenuations corresponding to each path is one of the most important tasks for the optimum transmitter and receiver design. Generally, a probe signal is sent to sound the channel and the channel parameters are estimated based on the received signal. This is called channel sounding technique. Channel sounding techniques are normally categorized into two groups: time domain channel sounding and frequency domain channel sounding.

The purpose of channel sounding is to measure the impulse response $h(t, \tau)$ linking the received signal $x(t)$ to the transmitted signal $y(t)$. A convolution between the channel impulse response and the probe impulse response is shown in Fig. 45. Practically, a unique inverse convolution operation that allows for the extraction of the impulse response from arbitrary signals $x(t)$ and $y(t)$ is not available. However, a number of techniques using specific signals $x(t)$ can be used, where the channel impulse response is obtained by processing the signals $x(t)$ and $y(t)$.

Depending on the channel sounding method, different properties need to be caught the attention, some of them generally being considered as key characteristics are given as follows:

- Analyzed bandwidth: The analyzed bandwidth corresponds to the frequency band over which the impulse response is estimated. It

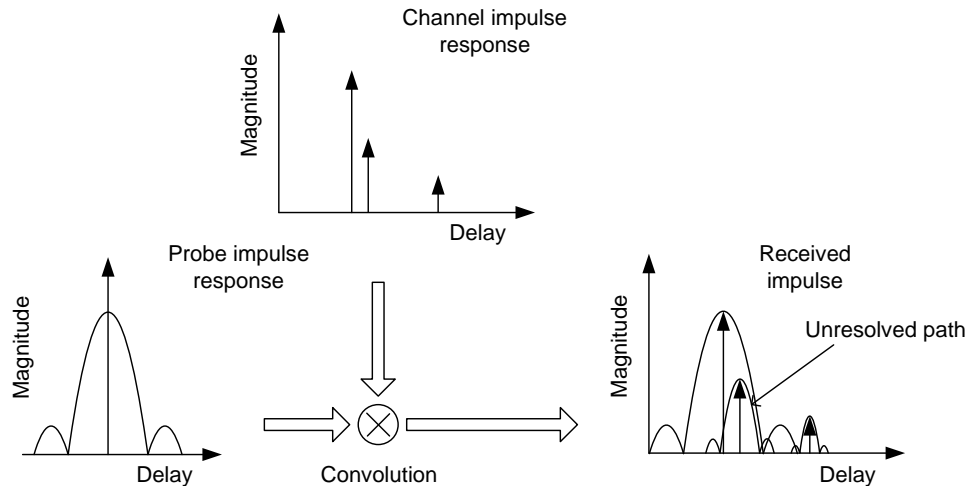


Figure 45: Time resolution in channel sounding

generally corresponds to the bandwidth of the transmitted probe signal. In the case of UWB signals, the bandwidth of several GHz may represent a challenge for channel measurements.

- **Time resolution:** The time resolution characterizes the sounder's capability to distinguish between two paths with very close delays. The impulse response estimated by the sounder corresponds to a convolution between the channel impulse response over an infinite bandwidth and the sounder's impulse response over the analyzed band. The time resolution is generally defined as half the width of the sounder impulse response peak. As an approximation, it may also be defined as the inverse of the analyzed bandwidth. Since the time resolution is generally high, due to the extremely wide bandwidth of the UWB signal, UWB channel sounding in a low measurement duration is a challenging task.
- **Maximum Doppler shift:** When the propagation channel varies with time, we can measure its frequency dispersion by studying its Doppler spectrum. For this purpose, the sounder needs to be able to quickly measure successive impulse responses. The measurement repetition duration ΔT is defined as the duration separating two successive channel measurements. It is then possible to measure a maximum absolute Doppler shift $\nu_{\max} = \frac{1}{2\Delta T}$. However, it should be noted that during the measurement of a single impulse response, the channel should be considered as static.
- **Dynamic and length of the channel impulse response:** The impulse response dynamic corresponds to the power ratio between the maximum impulse response and the noise level. A high dynamic allows the sounder to detect strongly attenuated paths. The length of the channel's impulse response corresponds to the maximum delay that can be measured.

Due to the very wide measured frequency band, behavior of the sounding equipment may vary strongly, and this needs to be accounted for in the measurement process. In particular, the antennas characteristics need to be stable across the measured frequency band. The properties of some other equipments, such as cables or amplifiers, may also vary in frequency, and these item should be accurately characterized before the measurement.

5.1.1 Time Domain Channel Sounding

In time domain channel sounding methods, the pulsed technique is mathematically the most straightforward. A pulse generator is used to enable the emission of short signals with a duration Δt in the order of picoseconds. At the receiver, a very fast acquisition of the signal is necessary. A digital sampling oscilloscope (DSO) is generally used, with sampling rates up to 20 Gsamples. A block diagram of the time domain channel sounding is shown in Fig. 46.

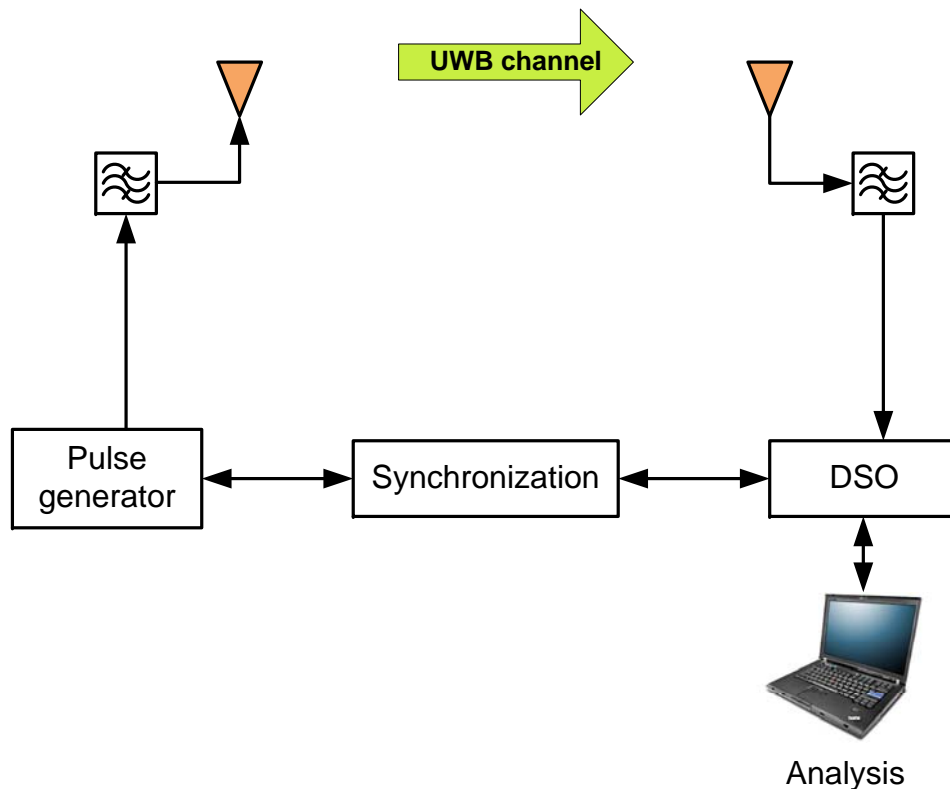


Figure 46: Time domain channel sounding

The main advantage of the pulsed sounding technique is its low acquisition duration, the channel impulse response being recorded in real time. In other words, the time domain technique can support non-stationary channels. Time domain sounding methods, however, require the generation of ultra-short pulses (ideal pulse shape should be like a Delta function), which is hard to implement. Moreover, the observed impulse response is always impaired by the use of non-ideal transmit antennas. For these

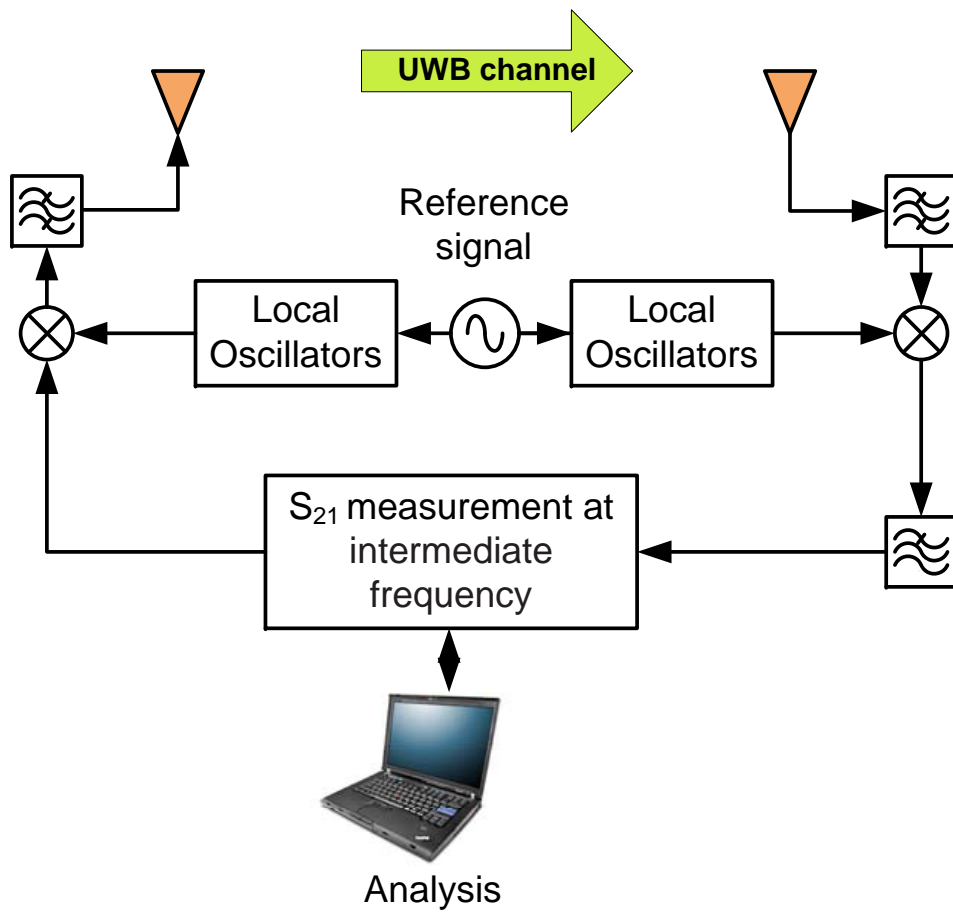


Figure 47: Frequency domain channel sounding

reasons, a deconvolution technique is required to extract the real CIR from the observed CIR.

Another time domain sounding technique is named sliding correlator, that is a possible way to increase the signal to noise ratio at the receiver, is to use the autocorrelation properties of pseudo-noise (PN) sequences. In this method, a direct sequence spread spectrum signal is transmitted into the wireless channel. At the receiver, the spread spectrum waveform is processed via sliding correlation, i.e., the received signal is correlated with slower copy of the transmitted PN sequence. The slower rate of the local PN sequence makes it slide past the received sequence so a correlation can be performed between them over all time delays. For Sliding correlator channel sounding, accurate results require the measurement to take place within the channels' coherence time.

5.1.2 Frequency Domain Channel Sounding

In the frequency domain methods, the analyzed bandwidth is divided into N samples separated by a frequency step Δf . Narrowband signals are transmitted at fixed frequencies, the attenuation and the relative phase of the received signals are measured. The impulse response is obtained using an inverse Fourier transform along the frequency axis.

In practice, the vector network analyzer (VNA) is used to characterize the channel using a frequency sweeping method (see Fig. 47). This device is generally used to characterize high frequency quadripoles through the measurement of S-parameters. For the purpose of channel sounding, port 1 is connected to the transmitting antenna and port 2 is connected to the receiving antenna. The channel transfer function is derived from parameter $S_{21}(f)$. Frequency domain channel sounding technique offers many advantages such as large dynamic range and high multipath resolution. However, the measurement duration is proportional to the number of measured frequency tones. Hence, this technique cannot be used for time varying channels. In addition, since both the transmit and the receive antennas are connected to the same device by cables, the range of the measurement channel is limited due to power attenuation in the feeding cables. These features restrict its use only to the characterization of the short radio links where the channel is relatively stationary.

5.2 UWB CHANNEL MEASUREMENT IN IKT

In our Institut für Kommunikationstechnik (IKT) Lab, we have already performed a series of experiments with the UWB signal including DSO-based time domain channel sounding.

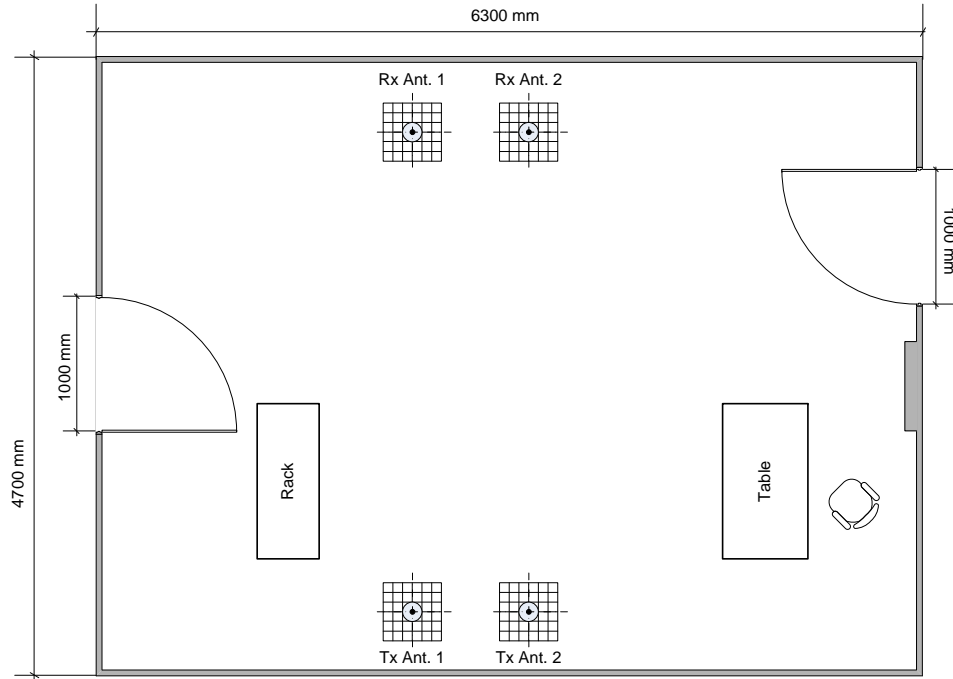


Figure 48: Floor plan and measurement configuration

5.2.1 Setup

Channel measurements are conducted for both LOS and NLOS scenarios within a $4.7 \text{ m} \times 6.3 \text{ m}$ room with a table, a chair, a wooden rack and different kinds of smaller scattering objects as shown in Fig. 48. The floor and walls of this room are constructed from concrete materials. The ceiling (3.2 m above the floor) is composed of iron sheets and metallic beams.

Fig. 49 illustrates a sketch of the whole system and setups of UWB channel measurement for the LOS and NLOS environments are shown in Fig. 50. The major components used in the measurements are a Tektronix AWG7102 arbitrary waveform generator (AWG) and a Tektronix DPO71604 digital phosphor oscilloscope (DPO). AWG supports two channels with up to 10 GSamples/s (GS/s) sampling rate and 3.5 GHz bandwidth or one channel with up to 20 GS/s sampling rate and 5.8 GHz analog bandwidth using interleaving, as well as 32 Msample memory size. The DPO provides four channels with up to 50 GS/s sampling rate and 16 GHz frequency span.

As shown in Fig. 49, an output of AWG is connected to a UWB antenna which is a small-size omni-directional UWB patch antenna. At the receiver side, a UWB antenna is connected to the DPO through a bank of bandpass filters (1.5 GHz bandwidth) and +55 dB low-noise amplifiers for reliable signal acquisition under harsh SNR conditions. The transmit and receive antennas are placed at a same height of 1.1 m. AWG and DPO are synchronized by the reference clock signal and connected to the processing computer via Ethernet.

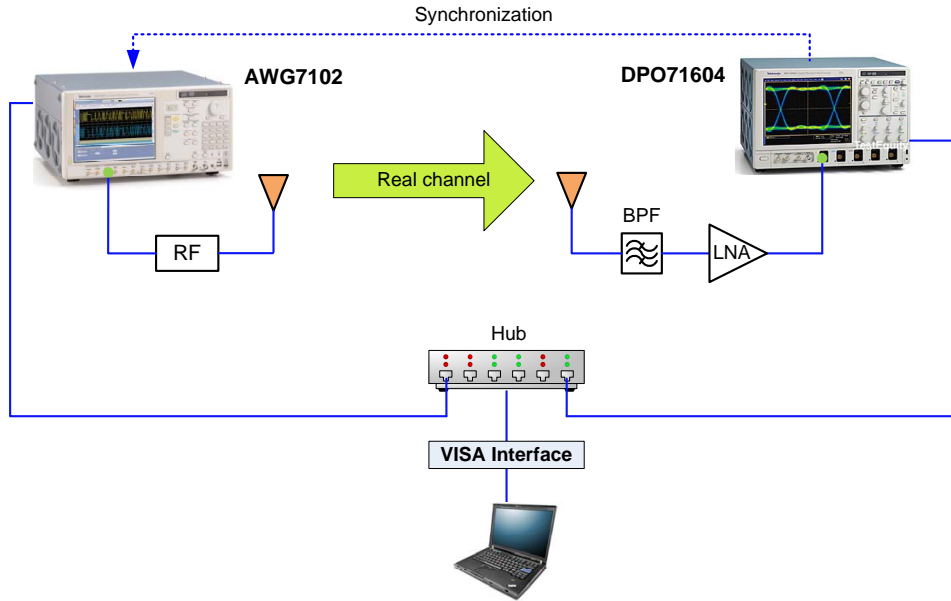


Figure 49: A sketch of measurement system

In all measurements, the probe UWB pulse used is a second order derivative Gaussian pulse, which is defined as

$$p(t) = \left[1 - 4\pi \left(\frac{t - t_c}{w} \right)^2 \right] e^{-2\pi \left(\frac{t - t_c}{w} \right)^2}, \quad (5.1)$$

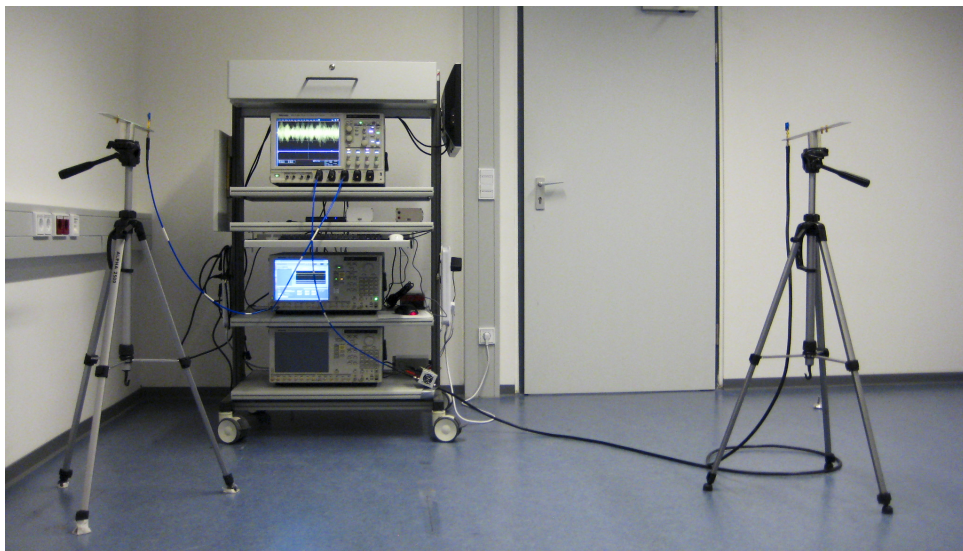
where w is a parameter corresponding to the pulse width, set to be 0.2 ns, and t_c is a time shifting of the pulse, set to be zero. The probe pulse waveform is shown in Fig. 51. Theoretically, in order to avoid the ISI, the symbol duration should be equal or greater than the channel delay. With several trial measurements, we found that if the symbol duration $T = 250$ ns, the ISI can be ignored.

The summary of setup parameters of the probe pulse sequences, AWG and DPO are described in Table 10

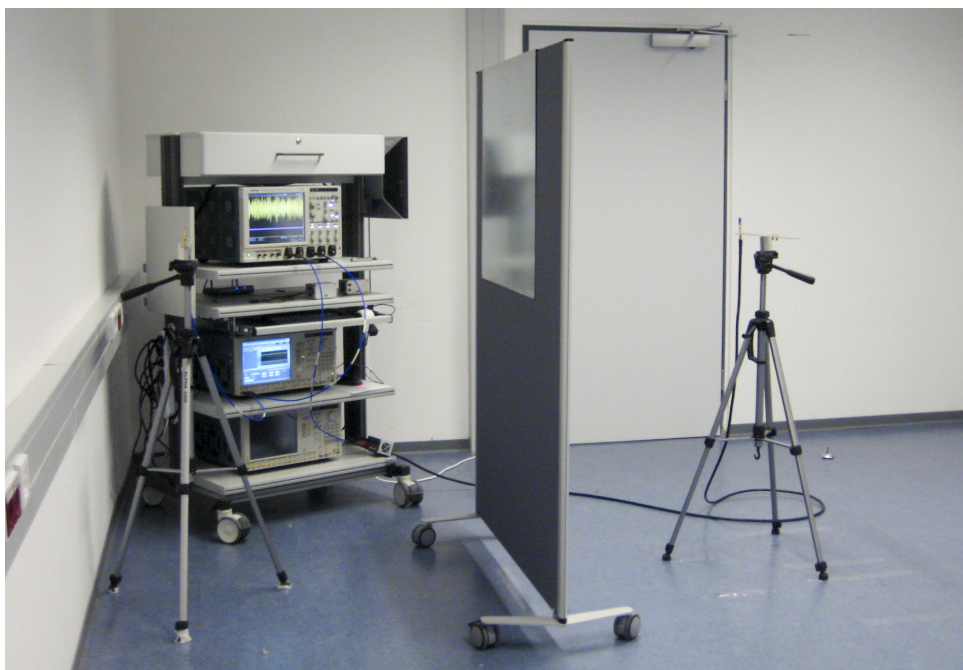
5.2.2 Measurement

Measurements of both unobstructed LOS and NLOS indoor propagation scenarios are conducted where the blockage for the NLOS scenario is created by vertically placing a large iron sheet in the direct propagation path at a distance of 1 m from the transmitter (see Fig. 50b), while the other aspects of the measurement environment are kept identical to those in the LOS scenario. The temporal stationarity of the environment is ensured by the absence of mobile objects/persons, thus allowing us to assume that the channels for the links are quasi-static over the duration of data transmissions.

For each SISO channel measurement, in order to get statically reliable data sets, the location of the transmit antenna is fixed while a planar positioning



(a) LOS environment



(b) NLOS environment

Figure 50: Photos of the implementation

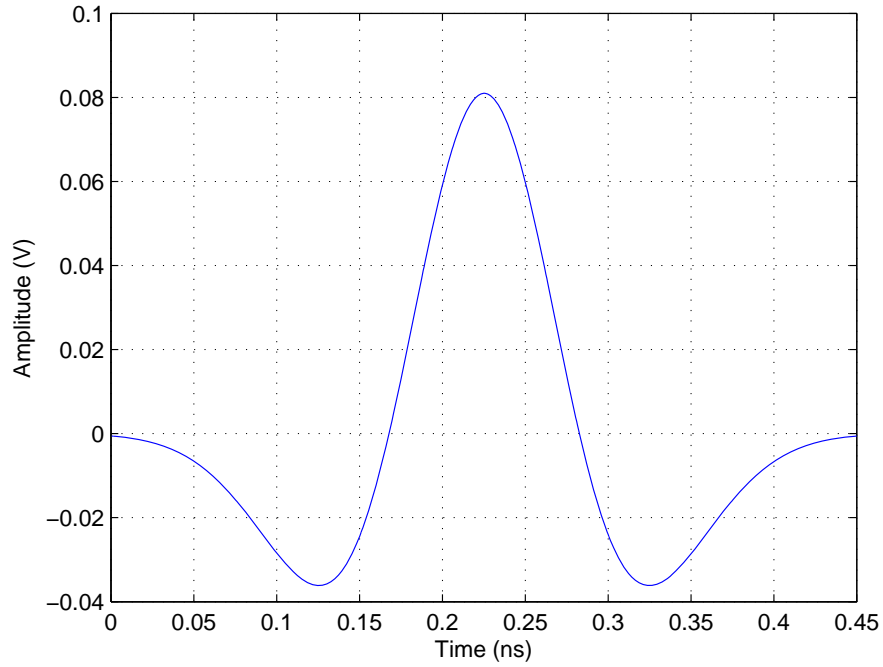


Figure 51: The probe UWB pulse

Table 10: AWG, DPO and probe pulse sequences setting

Parameters	Value	Unit
AWG interleaving	on	-
AWG sampling rate	20	GS/s
DPO sampling rate	50	GS/s
Pulse shape Gaus.	2 nd der.	-
Pulse width	0.2	ns
Pulse duration	0.45	ns
Time shifting of the pulse	0	ns
Symbol duration	250	ns

grid is used to position the receive antenna at 49 individual points within an area of $0.21 \text{ m} \times 0.21 \text{ m}$, with 0.03 m spacing. Consequently, 49 individual realizations are obtained.

For the MIMO channels, the spatial antenna arrays at both transmitter and receiver are synthesized by sequential measurements exploiting such temporal stationarity. Due to this array synthesis, our measurement results do not include the effects of antenna coupling. A (2×2) virtual MIMO channel, corresponding to 16 SISO channels (49 realizations for each), are measured in our campaign. In [96, 48], it was suggested that low spatial correlation can be achieved by setting the inter-element spacing greater than the half wavelength of the lowest UWB signal frequency. Therefore, the inter-element spacing is chosen to be 0.2 m here.

5.2.3 CIR Extract

A deconvolution technique is required to extract the real CIR from the observed CIR. A common technique used is Clean Algorithm whose accuracy applied to UWB channel extraction has been investigated in [13]. Clean Algorithm is also used to extract the channel impulse response from the received waveforms in [95].

In Clean Algorithm, the channel is assumed to be a series of impulses, represented by a group of Delta functions, with different delays and amplitudes. Mathematically, the channel is modeled as

$$h(t) = \sum_{l=0}^{L-1} \alpha_l \delta(t - \tau_l), \quad (5.2)$$

where L is number of taps of the channel, α_l and τ_l are the corresponding gain and the delay of the l -th tap. The received signal, which will be measured by DPO, is expressed as

$$r(t) = h(t) * p_{\text{LOS}}(t), \quad (5.3)$$

where $p_{\text{LOS}}(t)$ is the pulse waveform template for only LOS propagation. The template includes the effects of both the transmit and the receive antennas, as well as probe pulse ($p(t)$), is expressed as

$$p_{\text{LOS}}(t) = h_{\text{rx}}(t) * h_{\text{tx}}(t) * p(t), \quad (5.4)$$

where $h_{\text{tx}}(t)$ and $h_{\text{rx}}(t)$ are the response of the transmit and receive antenna respectively.

In our work, the template is obtained by performing a LOS measurement where the distance between the transmitter and receiver is 1 m . For the template measurement, we use the same antennas in other measurements, so antenna aspects are not separately studied in our experiment. The template measured for Clean Algorithm is shown in Fig. 52

The measured template is correlated with the received waveform iteratively to find the maximum peak. The steps for Clean Algorithm are as follows [13]:

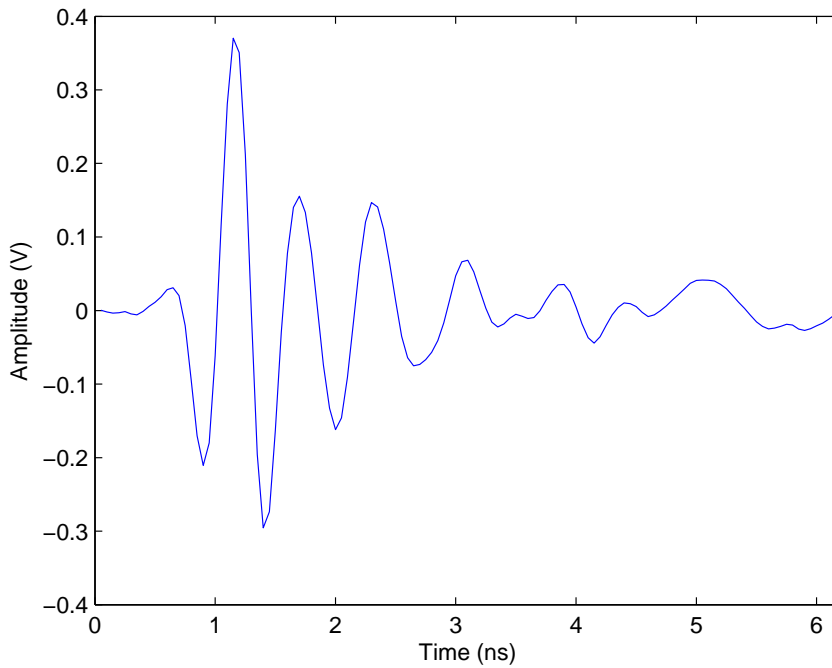


Figure 52: The measured template used for Clean Algorithm

1. Calculate the autocorrelation of the template $R_{pp}(t) = p_{LOS}(t) * p_{LOS}(-t)$.
2. Calculate the cross correlation of the template with the received signal $r(t)$, $R_{pr}(t) = p_{LOS}(t) * r(t)$.
3. Find the largest correlation peak in $R_{pr}(t)$, record the normalized amplitude α_1 , and the relative time delay τ_1 of the correlation peak.
4. Subtract $R_{pp}(t)$ scaled by α_1 from $R_{pr}(t)$ at the time delay τ_1 .
5. Compare α_1 to a minimum threshold γ_0 , (e.g., set $\gamma_0 = \alpha_0/10$, where α_0 is the normalized amplitude of the first correlation peak in Step 2). If $\alpha_1 < \gamma_0$, program stops. Otherwise go to step 2 for another iteration, until the condition $\alpha_1 < \gamma_0$ is met.

One realization of the SISO channel which is extracted from the received signal by using Clean Algorithm corresponding to the threshold $\gamma_0 = 22$ dB is shown in Fig. 53 as an example. Figures 54, 55, 56 and 57 show the realizations of the SISO CIR extracted from measured data of measurements in LOS and NLOS environments with 2 m and 4 m distance between transmitter and receiver, respectively.

Realizations of the MIMO channel are also extracted from the received signal by using Clean Algorithm similarly. An example of measured (2×2) MIMO channel is shown in Fig. 58.

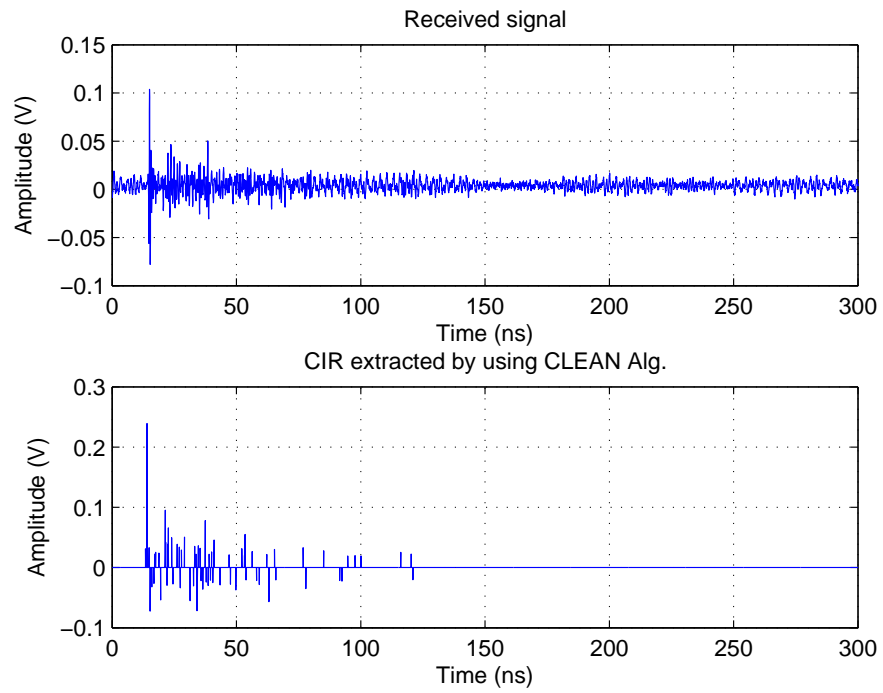


Figure 53: An example of the received signal and the extracted CIR

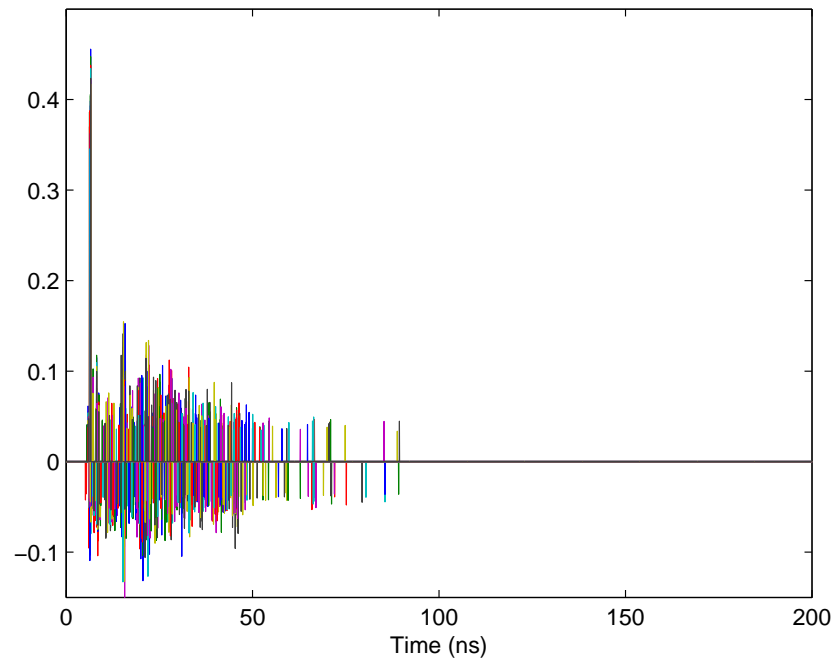


Figure 54: Realizations of CIR measured in LOS environment, 2m of the distance between transmitter and receiver

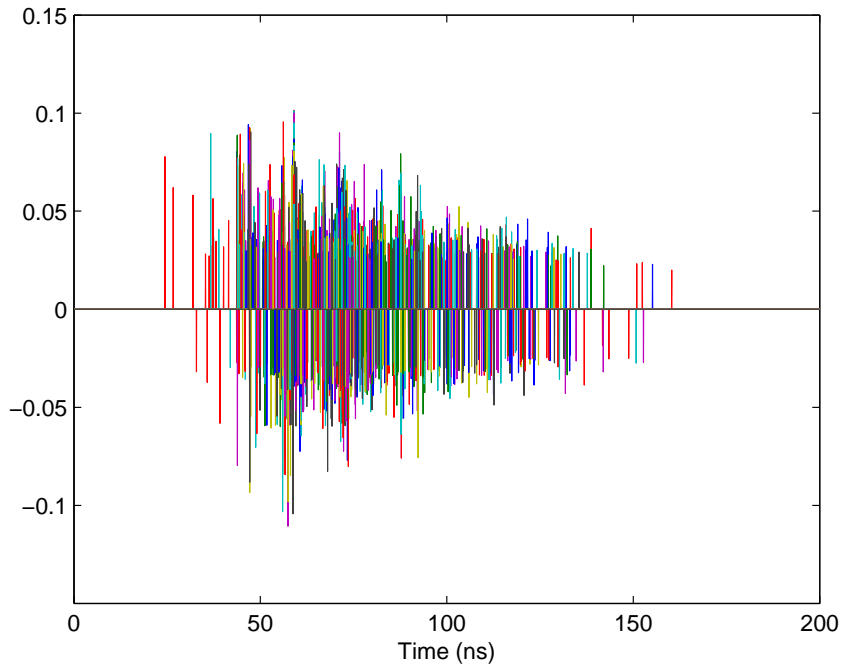


Figure 55: Realizations of CIR measured in NLOS environment, 2m of the distance between transmitter and receiver

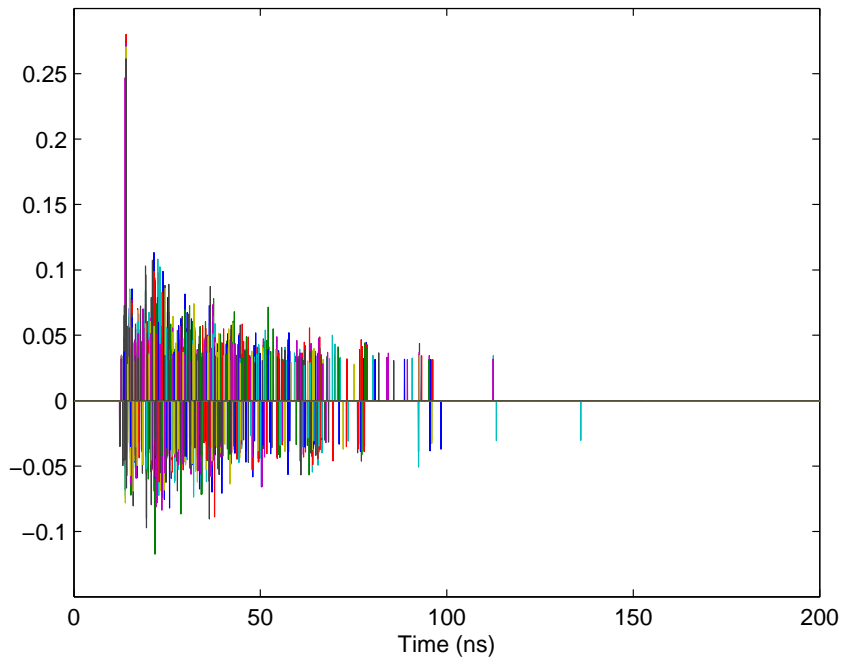


Figure 56: Realizations of CIR measured in LOS environment, 4m of the distance between transmitter and receiver

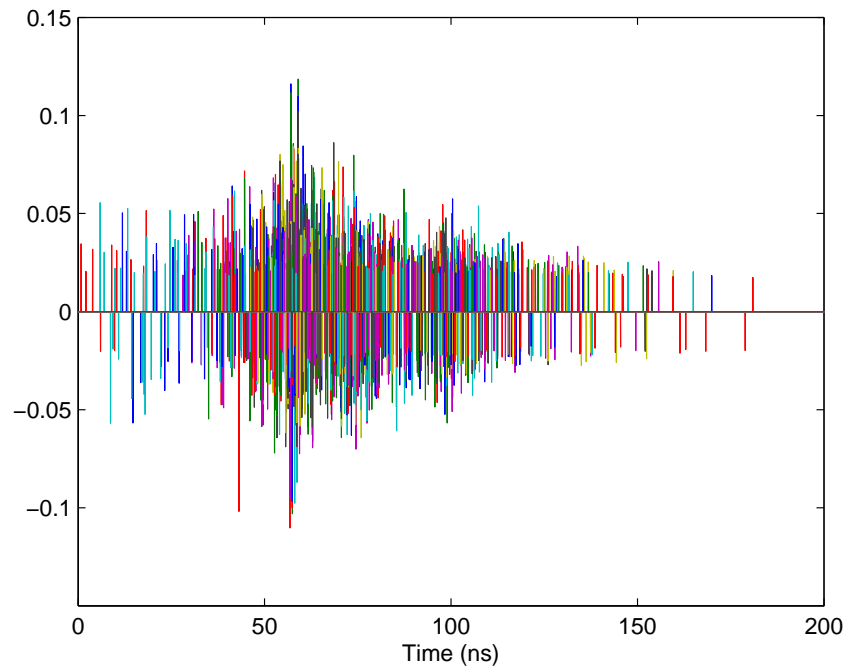


Figure 57: Realizations of CIR measured in NLOS environment, 4m of the distance between transmitter and receiver

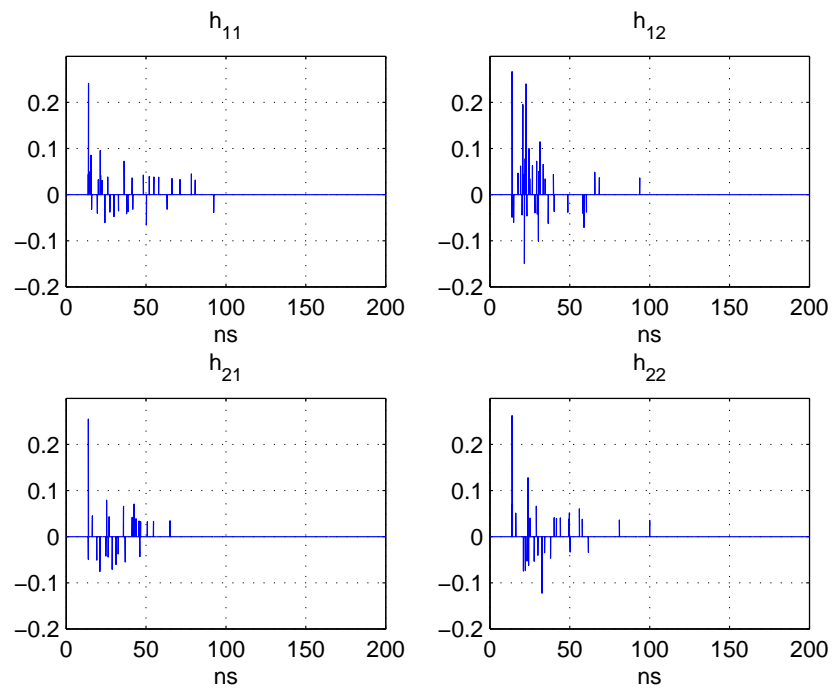


Figure 58: An example of the measured (2×2) MIMO channel

5.3 BER PERFORMANCE EVALUATION BASED ON MEASURED CHANNELS

Some of analyses, which are executed with the standard channel models in previous chapters, are verified with the measured channels. Generally, in this section, the results are obtained based on the average of 49 realizations of the measured channels.

Let's start with the SISO channels. In figures 59 and 60, we evaluate the BER performance of SISO-UWB systems with different TR schemes for the measured CIRs. BER performances are calculated for A-, S- and P-TR pre-filters where number of used taps for S- and P-TR is $s = 100, 30, 10$, respectively. It can be seen from both figures that with the same number of used taps, the S-TR scheme performs significantly better than the P-TR one. Moreover, the difference in the performance of the systems using two kinds of those TR pre-filter in the NLOS environment is larger than in the LOS environment. For example, with $s = 30$, at $\text{BER} = 3 \times 10^{-3}$, in the LOS environment, the system using the S-TR pre-filter can achieve the performance with 3dB better than the system using the P-TR pre-filter. Meanwhile, in the NLOS environment, the benefit is approximately 7dB. This is due to the fact that in the received signal after passing the NLOS environment, the direct path component is not available. In order to catch the most of channel power, selecting the strongest non-direct paths is more important and this property is only belong to the S-TR pre-filter. Obviously, increasing number of taps used for the S- or P-TR pre-fiter leads to improving the system performance. However, the performance of the system using the S-TR pre-filter with $s = 100$ is nearly same as the performance of the system using the A-TR pre-filter in both LOS and NLOS environments.

As stated in Chapter 3 and 4 that, we use the shorten equivalent CIRs when designing the pre-equalizer. In Fig. 61, we investigate the shorten rate of equivalent measured CIRs by plotting the BER performance as a function of the ratio between the length of shortened equivalent channel L_s and the full equivalent channel length L_e . In this figure, an 2×2 SM-MIMO system is considered and number of used taps is 30 for both S- and P-TR pre-filter. It can be observed that the BER seems to reach a saturation value when $L_s/L_e \geq 0.4$ for the S-TR pre-filter. In other word, we can shorten 2/5 the length of the measured equivalent channel to design the pre-equalizer for the SM-MIMO UWB system.

The efficiency of the pre-equalizer is once more presented in Fig. 62 for the measured channels. The results are simulated for the 2×2 MIMO system and the solid curves are the performances of the system using the ZF pre-equalizer. It can be seen that without pre-equalizer the BER performance reaches an error floor while for the system using the pre-equalizer, no error floor is observed, in both LOS and NLOS environment. Thus, the same conclusion that the pre-equalizer can also significantly improve the performance of the systems is again drawn with measured channels.

The performances of SISO and MISO UWB systems simulated with measured channels are shown in Fig 63. In this figure, it is assumed that the

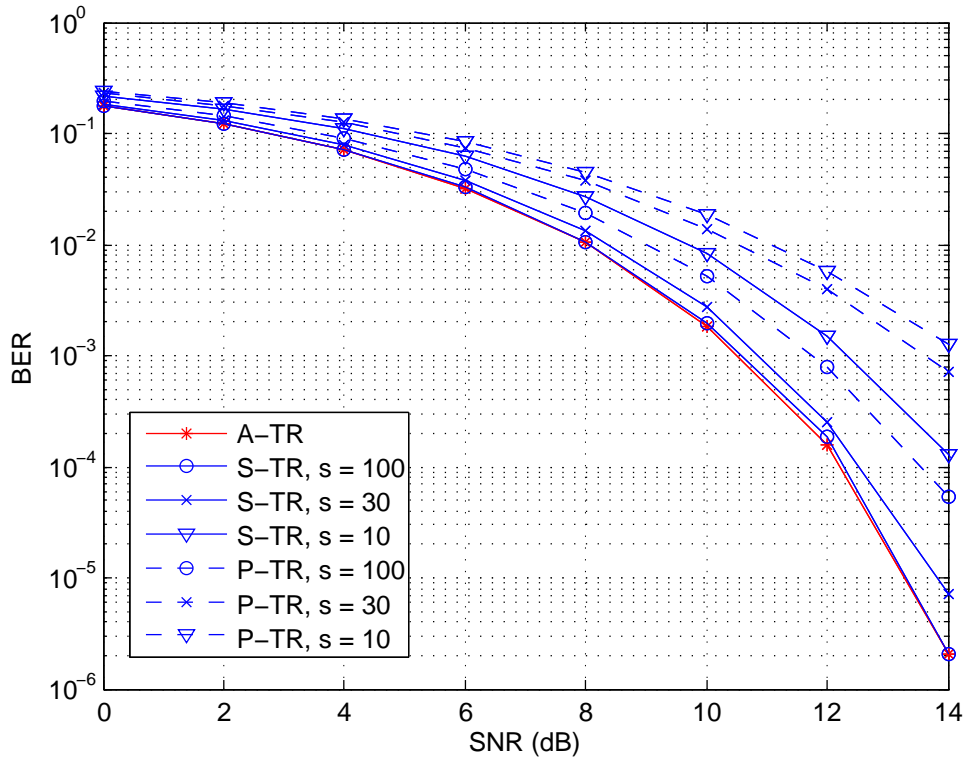


Figure 59: BER vs. SNR for different TR schemes, measured CIRs in LOS environment

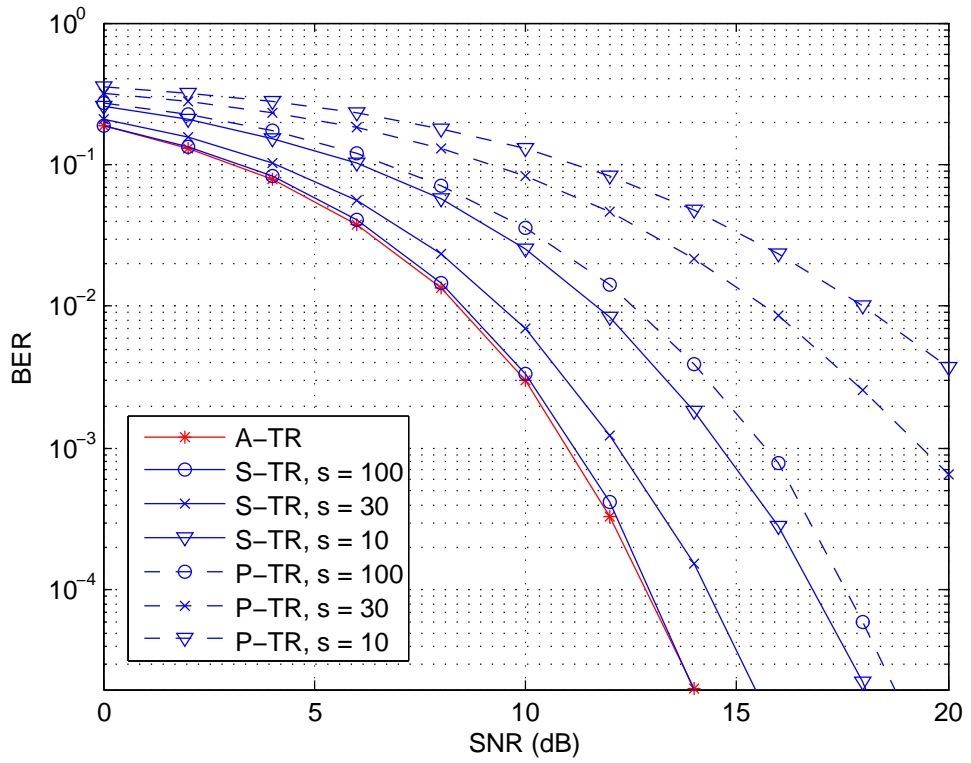
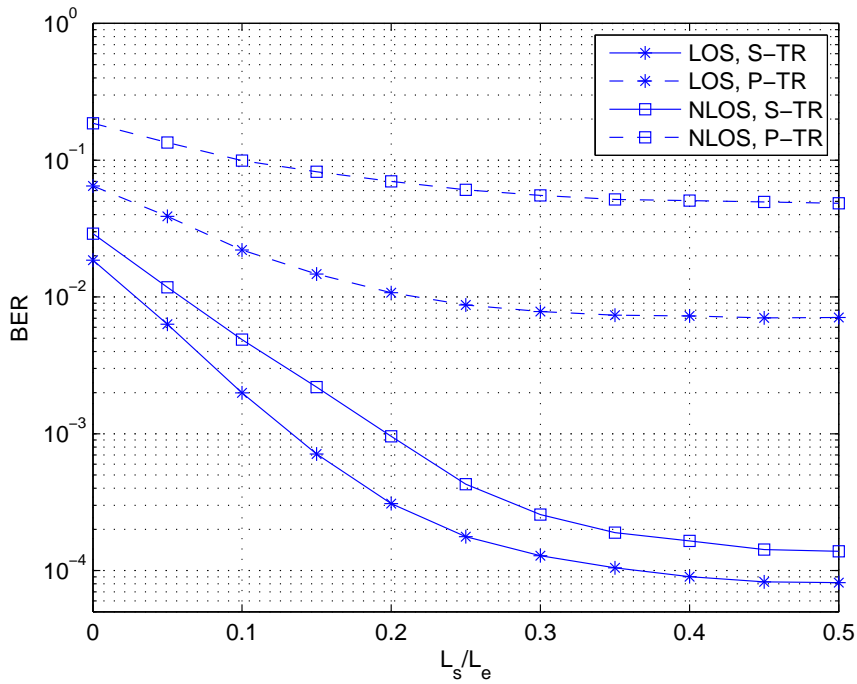
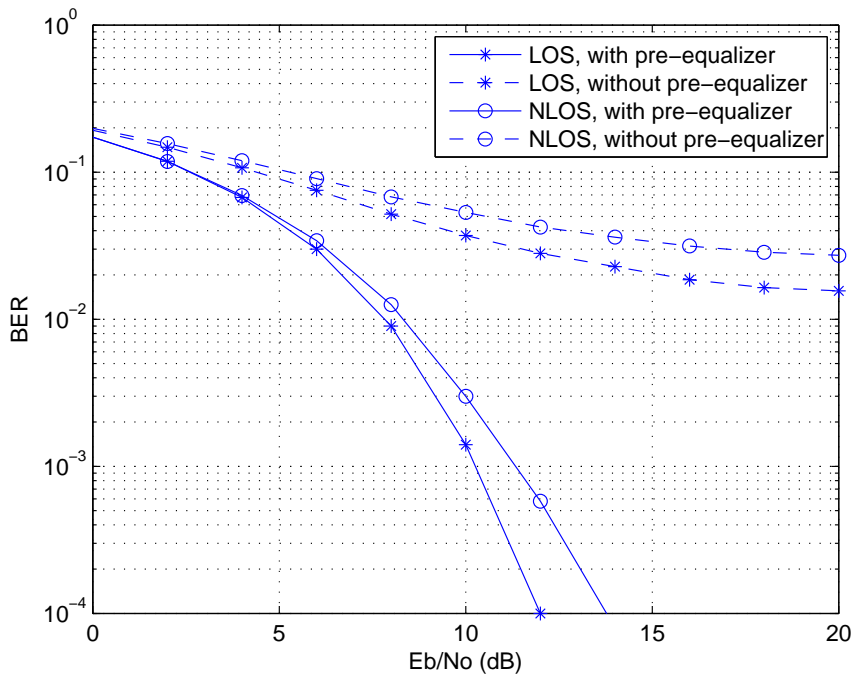


Figure 60: BER vs. SNR for different TR schemes, measured CIRs in NLOS environment

Figure 61: BER versus the shorten channel ratio (L_s/L_e) for measured channelsFigure 62: The BER performance of the 2×2 MIMO-UWB system simulated with measured channels

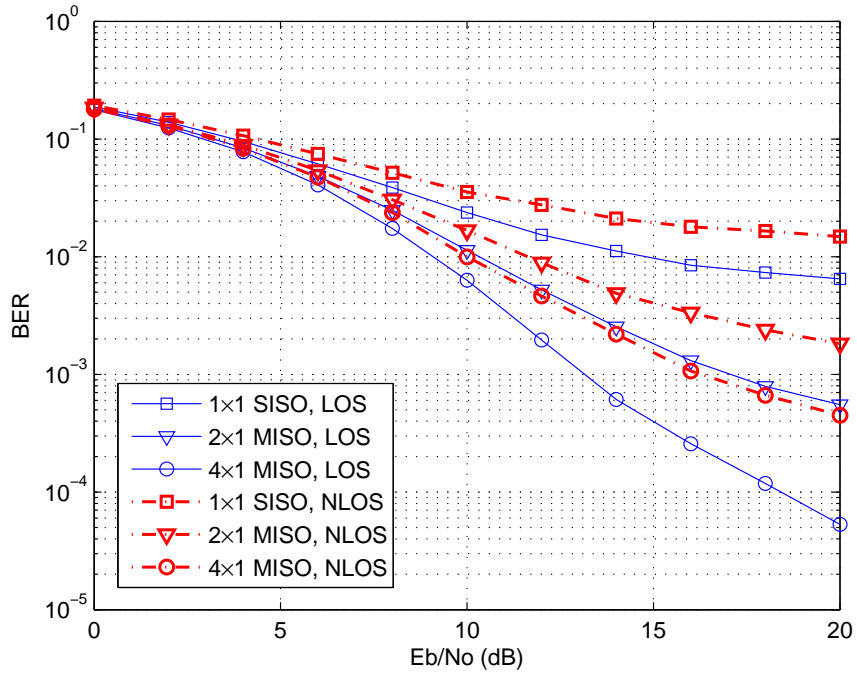


Figure 63: The BER performances of the SISO- and MISO-UWB systems simulated with measured channels

S-TR pre-filter with 100 taps is used and no pre-equalizer is used. With only one receive antenna, implementing more transmit antennas can improved significantly the system performance due to the benefit of the transmit diversity.

As discussed in previous Chapter, however, the benefit of the transmit diversity is remarkably reduced if the spatial correlation is high. In order to quantify the correlation among measured channels, we search an appropriate value of correlation coefficient so that the BER results on adopted correlated channel model (see Section 3.4) are closely matched with those on the measured indoor channel. With our measurement setups described in Section 5.2.1, the measured channels are referred to as CM1 (for LOS environment) and CM2 (for NLOS environment) in the IEEE 802.15.3a channel models. These scenarios are common in applications of UWB systems, which are short-range communications in a small office or home environment.

Figure 64 shows the BER performance of a 2×2 MIMO system operating in the modified CM1, CM2 channels with the matched transmit correlation coefficient and in the measured LOS and NLOS channels. In this simulation, for the fair comparison, we use the A-TR pre-filter and shorten the equivalent channel when designing the ZF pre-equalizer with the same ratio $L_s/L_e = 0.2$ for standard channels and measured channels. The receive correlation coefficient is fixed at $\rho_{R_x} = 0.2$. The value of the transmit correlation coefficient matched with the measurement result is found by exhaustive search and is then rounded to one decimal place. It can be seen

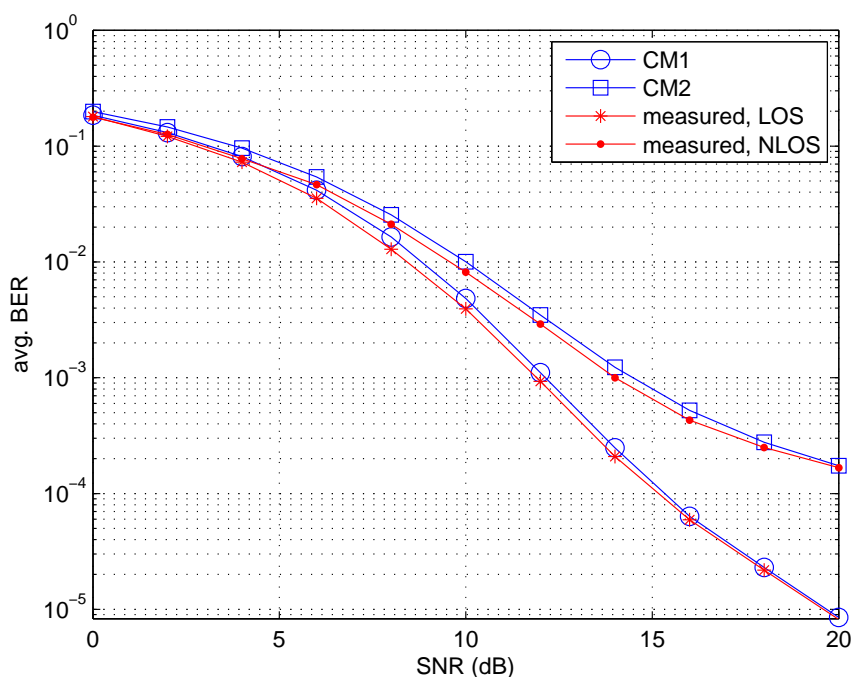


Figure 64: BER performance comparison, for standard channels with $\rho_{Tx} = 0.2$ and for measured indoor channels

that the average BERs based on realizations of CM1 and CM2 with the selected value of $\rho_{Tx} = 0.2$ are closely matched with those based on the corresponding measured channels. It is noted that this value of the correlation coefficient is specific to our measurement setting.

5.4 SUMMARY

Understanding the characteristic of the propagation channel is one of the most important tasks when studying wireless networks. For this reason, one of our experiments with UWB signals is sounding the UWB channels. In this chapter, we detail the UWB channel measurements that we have carried out in the time domain in the laboratory of IKT.

In order to verify conclusions gained with standard channel models in previous chapters, we execute some analyses with measured channels, such as the BER performance varying with the number of taps used for the TR pre-filter, the shortened rate of the measured equivalent channel for designing the pre-equalizer, the BER performance of the MISO systems with different number of transmit antennas. In addition, the BER performance based on the fixed correlation model generated from the standard UWB channel models is compared with those based on the MIMO UWB channels measured in indoor environment and the matched value of the spatial correlation coefficient is found.

CONCLUSIONS AND RECOMMENDATIONS

This chapter summarizes conclusions that are drawn and discussed in previous chapters and guidelines for future work are given.

6.1 CONCLUSIONS

The objective of our work is to apply the time reversal technique to the UWB communications systems as a low-complexity-receiver solution to mitigate the interferences and enhance the system performance. Various models and configurations of UWB systems such as SISO, SU-MIMO, MU-MIMO (BC and MAC channels) are investigated.

Due to commonly adoption of the TH-PPM modulation scheme in the UWB communications, the interferences relevant to this modulation scheme such as the CMI and the IFI in the TH-PPM-UWB system attract our investigation. With the unique feature of space-time domain focusing, the TR pre-filtering has been considered as a solution to deal with the ISI in the UWB systems while keeping the receiver in simple. In the same way, here, the TR pre-filter is proposed to suppress both the CMI and the IFI. Three TR schemes, namely the A-, P-, and S-TR, are investigated. In comparison with the A-TR pre-filter, with a limited number of taps being used, the S-TR pre-filter can reduce significantly the complexity of the transmitter while the system performance degrade is negligible. This is verified by BER performance analyses based on simulation results with IEEE 802.15.3a channel models (CM1-CM4) in Chapter 2 and with measured channels in Chapter 5 for the SISO configuration. The efficiency of the S-TR pre-filter is again proved in Chapter 3 for the MIMO configurations. Truncating the length of the TR pre-filter is very useful in practically implementing when UWB channels have very long delay spread due to extremely wide frequency bands.

The SM-MIMO system where several data streams are transmitted simultaneously from several antennas to a multiple antenna receiver is another objective of our study as represented in Chapter 3. In such a system, not only the ISI but also the MSI exists, so the TR pre-filter is not enough to deal with these interferences. Combining the TR pre-filter and a pre-equalizer is a good solution. The combination the TR pre-filter and the ZF pre-equalizer is adopted in our work is to mediate the effect of the interferences while guaranteeing the simplicity in the receiver side. The appearance of the TR pre-filter is not only to lessen the ISI but also to shorten the overall CIR, which is used in designing the pre-equalizer. Therefore, the complexity of the transmitter is also significantly reduced.

Additionally, thank to implementing the TR pre-filter, the maximum number of data streams simultaneously transmitted depends on the number

of receive antennas instead of transmit antennas. Therefore, it is possible to transmit several data streams at the same time with only one transmit antenna, then the system is named as the virtual MIMO system. Obviously, in the virtual MIMO system the transmit diversity gain is not achieved as in the real MIMO system. Nevertheless, the analyses in Chapter 3 show that the virtual MIMO system or the real one with fewer transmit antennas can perform better than the MIMO system having more transmit antennas in the high correlation conditions. This is because the spatial correlation among transmit antenna elements degrades severely the system performance. This remark should be taken into account when one designs the system, since integrating too many antennas in a narrow space on a limited-dimension device may cause high spatial correlation.

The investigation for the SU-SM-MIMO UWB system is extended to the MU-SM-MIMO UWB system as presented in Chapter 4. We consider the two-direction-communication MU-MIMO-UWB system including the BC channels and MAC channels. In investigated systems, since several data streams are simultaneously transmitted from/to distinct users, the ISI, the MSI and the MUI exist together. Focusing on applications where a powerful access point communicates with a number of non-complexity user terminals, we propose to implement the combination of the TR pre-filter and the ZF pre-equalizer at the transmitter side on the BC channels and the combination of the TR filter and the ZF equalizer at the receiver side on the MAC channels to deal with above mentioned interferences for the such system. The spatial correlation problem is also investigated in Chapter 3 for the such systems and similar conclusions are withdrawn.

In our work, series of measurements with UWB signals including UWB channel measurements are conducted. The measurements are performed in the time domain in the UWB laboratory of IKT equipped with powerful equipments such as the waveform generator Tektronix AWG7102, the digital phosphor oscilloscope Tektronix DPO71604. We performed both SISO channel and MIMO channel measurements in the LOS and NLOS environments, where MIMO channels are synthesized by sequential measurements of SISO channels. From the measured data, CIRs are extracted by applying CLEAN algorithm. BER performance analysis for several cases with measured CIRs is presented to confirm again the conclusions and remarks which are obtained by theoretical study.

6.2 RECOMMENDATIONS FOR FUTURE WORK

As illustrated, several problems in applying the TR technique into the UWB communications systems have been identified, made clear and solved. This research work, however, has opened numerous areas for future work which need to be further explored, studied and improved. Some of them can be summarized as follow:

- UWB-MIMO channel model: In our simulation, UWB-MIMO channels are generated by modifying the channel models in the IEEE 802.15.3a or IEEE 802.15.4a standards, which are formulated for the UWB-SISO

system. This method is usually adopted in many researches. In our experiment, due to limitation of the equipment and performing time, measurements of "real" MIMO-UWB channels have been missing. Some effects as antenna coupling, correlation are ignored for the such model. Though UWB-MIMO channels have been well investigated in the UWB literature (see, e.g., [39] and references therein), standard MIMO channels for UWB communications in different propagation environments have been waiting for releasing.

- Spatial correlation model for UWB: Practically, in the systems using multiple antennas, spatial correlation among antenna elements (transmit or receive antennas) normally exists. The fixed transmit and receive correlation matrices following the well-known Kronecker model that proposed for the fixed broadband wireless channel are adopted in our study with some variations. In order to verify the adopted correlation model, as shown in Chapter 5, we search an appropriate value of correlation coefficient so that the BER results on adopted correlated channel model are closely matched with those on our measured indoor channels. This value is specific to our measurement setting. Different appropriate correlation coefficients for different scenarios or propagation environments are also encouraged to generate and further study on the spatial correlation in MIMO-UWB systems is worthwhile.
- Channel capacity of the TR-UWB system: The performance in term of bit error rate of the TR-UWB system is investigated in our work and normally in literature as well. However, how improvement in channel capacity that the TR technique can provide also needs to be studied. Additionally, it has been revealed that the channel capacity of the SM-MIMO normally increases with number of antennas. As shown in previous chapters, the spatial correlation has bad effect on the BER performance of the system using multiple antennas, so it may impact similarly on the capacity of the system. It is also interesting to determine this influence.
- Optimum value of effective multipath components using for the TR pre-filter and the pre-equalizer: For the channel with the length on the order of thousand taps as UWB channels, selecting effective taps to use is very important since this helps to reduce significantly the complexity of the transceiver. This issue is considered in this dissertation where the S-TR scheme is used for filtering, and equivalent channel using for the pre-equalizing is also shorten. However, the optimal shorten rate for a target system performance still needs to be investigated.
- Other types of the pre-equalizer: because of the simplicity, the ZF pre-equalizer is adopted in our work combined with the TR pre-filter to deal with interferences for UWB systems. However, further study

on other equalizing methods may be conducted to improve the system performance.

BIBLIOGRAPHY

- [1] Revision of Part 15 of the Commission's Rules Regarding Ultra-Wideband Transmission Systems. Technical report, Federal Communications Commission, ET-Docket 98–153, 2002. URL <http://www.fcc.gov/Bureaus/EngineeringTechnology/Orders/2002/fcc02048.pdf>. Adopted February 14, 2002, released April 22, 2002. (Cited on pages 1 and 2.)
- [2] C. Abou-Rjeily, N. Daniele, and J.-C. Belfiore. Space-time coding for multiuser ultra-wideband communications. *IEEE Transactions on Communications*, 54 Issue:11:1960 – 1972, Nov. 2006. (Cited on page 55.)
- [3] J. Adeane, W. Q. Malik, I. J. Wassell, and D. J. Edwards. A simple correlated channel model for ultrawideband MIMO systems. *IET Microw. Antennas Propagat*, 1(6):1177–1181, Dec. 2007. (Cited on pages 37 and 45.)
- [4] S. Ahmed and H. Arslan. Inter-Frame Interference in Time Hopping Impulse Radio Based UWB Systems for Coherent Receivers. In *IEEE Vehic. Technol. Conf. (VTC Fall), Montreal, Canada*, Sept 2006. (Cited on page 10.)
- [5] S. M. Alamouti. A simple transmit diversity technique for wireless communications. *IEEE J. Sel. Areas Commun.*, 16(8):1451–1458, October 1998. URL <http://ieeexplore.ieee.org/stampPDF/getPDF.jsp?tp=&arnumber=730453>. (Cited on page 35.)
- [6] Emre Telat Ar and I. Emre Telatar. Capacity of Multi-antenna Gaussian Channels. *European Transactions on Telecommunications*, 10:585–595, 1999. URL <http://mars.bell-labs.com/cm/ms/what/mars/papers/proof/proof.ps.gz>. (Cited on page 35.)
- [7] F. E. Aranda, N. Brown, and H. Arslan. Rake receiver finger assignment for Ultra-wideband radio. In *Proc. IEEE Workshop Sig. Processing Advances Wireless Commun. (SPAWC)*, page 239–243, June 2003. (Cited on page 4.)
- [8] H. Arslan. Cross-modulation interference reduction for pulse-position modulated UWB signals. In *Proc. IEEE Veh. Technol. Conf. Montreal, QC, Canada*, pages 1–5, September 2006. (Cited on page 10.)
- [9] H. Arslan, Z. N. Chen, and M. G. D. Benedetto. *Ultra Wideband Wireless Communication*. John Wiley & Sons, 2006. (Cited on pages 9 and 20.)
- [10] Maria-Gabriella Di Benedetto and Guerino Giancola. *Understanding Ultra Wide Band Radio Fundamentals*. Prentice Hall, 2004. (Cited on page 22.)

- [11] Itsik Bergel, Eran Fishler, and Hagit Messer. Narrow-Band Interference Suppression in Time-Hopping Impulse-Radio Systems. In *Proceedings of the Conference on Ultra Wideband Systems and Technologies*, pages 303–307, 2002. (Cited on page 21.)
- [12] G.S. Biradar, S.N. Merchant, and U.B.Desai. Frequency and Time Hopping PPM UWB Multiple Access Communication Scheme. *Journal of Communications*, 4 No. 1, Feb. 2009. (Cited on page 55.)
- [13] R. Michael Buehrer, A. Safaai-Jazi, W. Davis, and D. Sweeney. Ultra-wideband Propagation Measurements and Modeling, Final Report. In *DARPA NETEX Program*. Virginia Tech, 2004. (Cited on page 84.)
- [14] Giuseppe Caire and Shlomo Shamai (Shitz). On the Achievable Throughput of a Multiantenna Gaussian Broadcast Channel. *IEEE Trans. Inform. Theory*, 49(7), July 2003. (Cited on page 53.)
- [15] D. Cassioli, M. Z. Win, F. Vatalaro, and A. F. Molisch. Performance of low-complexity RAKE reception in a realistic UWB channel. In *Proc. IEEE Int. Conf. Commun. (ICC)*, volume 2, page 763–767, April 2002. (Cited on page 4.)
- [16] D. Cassioli, M. Z. Win, and A. F. Molisch. Effects of Spreading Bandwidth on the Performance of UWB Rake Receivers. In *Proc. IEEE Int. Conf. Communications (ICC)*, volume 5, page 3545–3549, May 2003. (Cited on page 4.)
- [17] H. Celebi and H. Arslan. Cross-modulation interference for pulse position modulated UWB signals. In *Proc. IEEE Mil. Commun. Conf. Atlantic City, NJ, USA*, pages 1–7, October 2005. (Cited on page 10.)
- [18] H. Celebi and H. Arslan. Cross-Modulation Interference and Mitigation Technique for Ultrawideband PPM Signaling. In *Proc. IEEE Transactions on Vehicular Technology*, volume 57, pages 847–858, March 2008. (Cited on page 10.)
- [19] Yunfei Chen, N.C. Beaulieu, and Hua Shao. SNR and SIR Estimation for Multiuser UWB IR Systems With TH-BPSK. *IEEE Signal Processing Letters*, 17 Issue:5:465 – 468, May 2010. (Cited on page 55.)
- [20] T. M. Cover. Comments on broadcast channels. *Information Theory, IEEE Transactions on*, 44 Issue:6:2524 – 2530, Oct. 1998. (Cited on page 54.)
- [21] Thomas M. Cover and Joy A. Thomas. *Elements of Information Theory*. John Wiley & Sons, second edition, July 2006. (Cited on page 54.)
- [22] Q. H. Dang and A. van der Veen. Resolving inter-frame interference in a transmit-reference ultra-wideband communication system. In *IEEE International Conference on Acoustics, Speech, and Signal Processing, ICASSP. Toulouse, France*, pages 481–484, May 2006. (Cited on page 10.)

- [23] A. L. Deleuze, P. Ciblat, and C. Le Martret. Inter-symbol/inter-frame interference in time-hopping ultra wideband impulse radio system. In *Proc. IEEE International Conference on UltraWideBand (ICU2005), Zurich, Switzerland*, Sep. 2005. (Cited on page 10.)
- [24] A. Derode, P. Roux, and M. Fink. Robust acoustic time reversal with high-order multiple scattering. *Phys. Rev. Lett.*, 75(23):4206–4209, Dec. 1995. (Cited on page 5.)
- [25] G. F. Edelmann, H. C. Song, S. Kim, W. S. Hodgkiss, W. A. Kuperman, and T. Akal. Underwater Acoustic Communications Using Time Reversal. *IEEE Journal of Oceanic Engineering*, 30(4):852 – 864, 2005. (Cited on page 9.)
- [26] M. Emami, M. Vu, J. Hansen, A.J. Paulraj, and G. Papanicolaou. Matched filtering with rate back-off for low complexity communications in very large delay spread channels. In *Conf. Rec. 38th Asilomar Conf. Signals, Syst., Comput.*, volume 1, pages 218 – 222, Nov. 2004. (Cited on pages 5 and 9.)
- [27] M. Fink. Time reversal of ultrasonic fields—Part I: Basic principles. *IEEE Trans. Ultrason., Ferroelectr., Freq. Control*, 39(5):555–566, Sep. 1992. (Cited on pages 5 and 9.)
- [28] M. Fink, G. Montaldo, and M. Tanter. Time-reversal acoustics in biomedical engineering. *Annu. Rev. Biomed. Eng.*, 5:465, 2003. (Cited on page 9.)
- [29] J. R. Foerster. Channel modeling sub-committee report final. Document ieeep802.15-02/490r1-sg3a, IEEE, 2003. URL http://www.ieee802.org/15/pub/2003/Mar03/02490r1P802-15_SG3a-Channel-Modeling-Subcommittee-Report-Final.zip. (Cited on pages 6, 10, 18, 29, 41, 46, and 62.)
- [30] G. J. Foschini and M. J. Gans. On limits of wireless communications in a fading environment when using multiple antennas. *Wireless Personal Communications*, 6:311–335, 1998. URL http://www.ece.utexas.edu/~rheath/courses/mimo/suggested_readings/ref/3-1.pdf. (Cited on page 35.)
- [31] Gerard J. Foschini. Layered space-time architecture for wireless communication in a fading environment when using multi-element antennas. *Bell Labs Technical Journal*, 1:41–59, 1996. URL <http://www3.interscience.wiley.com/cgi-bin/fulltext/97518800/PDFSTART>. (Cited on page 35.)
- [32] David Gesbert, Marios Kountouris, Robert W. Heath, Chan byoung Chae, and Thomas Sälzer. From Single User to Multiuser Communications: Shifting the MIMO paradigm. In *IEEE Sig. Proc. Magazine*, 2007. (Cited on page 54.)

- [33] M. Ghavamin, L. B. Michael, and R. Kohno. *Ultra Wideband Signals and Systems in Communication Engineering*. John Wiley & Sons, 2004. (Cited on pages 5 and 9.)
- [34] C. Holland. Europe approves UWB regulations. Technical report, EE Times Europe, 3 May 2007. URL http://eetimes.eu/en/europe-approves-uw- regulations?cmp_id=7&news_id=197800214. (Cited on page 2.)
- [35] S. Imada and T. Ohtsuki. Pre-RAKE diversity combining for UWB systems in IEEE 802.15 UWB multipath channel. In *Proc. Joint Ultra Wideband Systems and Technology and Intern. Workshop for Ultra Wideband Systems*, pages 236–240, May 2004. doi: 10.1109/UWBST.2004.1320971. (Cited on page 18.)
- [36] Yuanwei Jin, Yi Jiang, and José M. F. Moura. Multiple Antenna Time Reversal Transmission in Ultra-wideband Communications. In *Proc. of IEEE Globecom. IEEE*, 2007. (Cited on page 55.)
- [37] T. Kaiser, Feng Zheng, and E. Dimitrov. An Overview of Ultra-Wide-Band Systems With MIMO. *Proc. IEEE*, 97(2):285–312, Feb. 2009. doi: 10.1109/JPROC.2008.2008784. (Cited on pages 44 and 61.)
- [38] Thomas Kaiser and Feng Zheng. *Ultra Wideband Systems with MIMO*. John Wiley & Sons, March 2010. Chapter 6. (Cited on pages 2, 6, and 39.)
- [39] Thomas Kaiser and Feng Zheng. *Ultra Wideband Systems with MIMO*, chapter Chapter 2. UWB-MIMO Channel Measurement and Models, pages 17–43. John Wiley & Sons, 2010. (Cited on pages 5, 37, and 97.)
- [40] J. Keignart, C. Abou-Rjeily, C. Delaveaud, and N. Daniele. UWB SIMO channel measurements and simulations. *IEEE Transactions on Microwave Theory and Techniques*, 54, Issue:4:1812, June 2006. (Cited on page 55.)
- [41] J.P. Kermoal, L. Schumacher, K.I. Pedersen, P.E. Mogensen, and F. Frederiksen. A Stochastic MIMO Radio Channel Model with Experimental Validation. *IEEE Journal on Selected Areas in Communications*, 20(6): 1211–1226, August 2002. (Cited on page 37.)
- [42] Hassan Khani and Paeiz Azmi. A novel multi-access scheme for UWB-PPM communication systems. *European Transactions on Telecommunications*, 18 Issue 4:389–401, June 2007. (Cited on page 55.)
- [43] W.A. Kuperman, W.S. Hodgkiss, H.C. Song, P. Gerstoft, P. Roux, T. Akal, C. Ferla, and D.R. Jackson. Ocean acoustic time-reversal mirror. In *4th European Conference on Underwater Acoustics*, Rome, Italia, 1998. (Cited on page 9.)
- [44] P. Kyritsi, G. Papanicolaou, and C. Tsogka. Optimally designed time reversal and zero forcing schemes. In *Proc. Int. Symp. WPMC*, page 105–109., Sep., 18–22 2005. (Cited on pages 5 and 9.)

- [45] P. Kyritsi, P. Stoica, G. Papanicolaou, P. Eggers, and A. Oprea. Time reversal and zero-forcing equalization for fixed wireless access channels. In *Conf. Rec. 39th Asilomar Conf. Signals, Syst., Comput.*, page 1297–1301, Oct. 28 – Nov. 1 2005. (Cited on pages 5 and 9.)
- [46] Richard O. LaMaire and Michele Zorzi. Effect of Correlation in Diversity Systems with Rayleigh Fading, Shadowing, and Power Capture. *IEEE JOURNAL ON SELECTED AREAS IN COMMUNICATIONS*, 14 (3), April 1996. (Cited on page 37.)
- [47] S.L. Loyka. Channel capacity of MIMO architecture using the exponential correlation matrix. *IEEE Commun. Lett.*, 5(9):369–371, 2001. ISSN 1089-7798. doi: 10.1109/4234.951380. (Cited on page 61.)
- [48] W. Q. Malik and D. J. Edwards. Measured MIMO capacity and diversity gain with spatial and polar arrays in ultrawideband channels. *IEEE Trans. Commun.*, 55(12):2361–2370, Dec. 2007. (Cited on page 84.)
- [49] W.Q. Malik. Spatial correlation in ultrawideband channels. *IEEE Trans. Wireless Commun.*, 7(2):604–610, February 2008. doi: 10.1109/TWC.2008.060547. (Cited on pages 37, 44, and 55.)
- [50] W.Q. Malik and D.J. Edwards. UWB Impulse Radio with Triple-Polarization SIMO. In *IEEE Global Telecommunications Conference, 2007. GLOBECOM '07*, page 4124, Washington, DC, 26-30 Nov. 2007. (Cited on page 55.)
- [51] A. Martini, M. Franceschetti, and A. Massa. Capacity of wide-band MIMO channels via space-time diversity of scattered fields. In *Conference Record of the Forty-First Asilomar Conference on Signals, Systems and Computers*, pages 138 – 142, Pacific Grove, CA, Nov. 2007. (Cited on page 55.)
- [52] D. P. McNamara, M. A. Beach, and P. N. Fletcher. Spatial correlation in indoor MIMO channels. In *Proc. IEEE Int. Symp. on Personal, Indoor and Mobile Radio Communications*, September 2002. (Cited on page 37.)
- [53] Shaomin S. Mo, Nan Guo, John Q. Zhang, and Robert C. Qiu. UWB MISO Time Reversal With Energy Detector Receiver Over ISI Channels. In *Proc. of the 4th IEEE Consumer Communications and Networking Conference, (CCNC2007)*, pages 629 – 633, Jan. 2007. (Cited on page 6.)
- [54] A. F. Molisch, K. Balakrishnan, D. Cassioli, C. Chong, S. Emami, A. Fort, J. Karedal, J. Kunisch, H. Schantz, U. Schuster, and K. Siwiak. IEEE 802.15.4a Channel model final report. Technical report, 2004. URL <http://www.ieee802.org/15/pub/04/15-04-0662-02-004a-channel-model-final-report-r1.pdf>. (Cited on page 10.)
- [55] Andreas F. Molisch, Jinyun Zhang, and Makoto Miyake. Time Hopping And Frequency Hopping In Ultrawideband Systems. In *Proc.*

- IEEE Pacific Rim Conference on Communications, Computers and Signal Processing (PACRIM 2003)*, pages 28–30. IEEE, 2003. (Cited on page 55.)
- [56] Andreas F. Molisch, Ye Geoffrey Li, , Yves-Paul Nakache, Philip Orlik, Makoto Miyake, Yunnan Wu, Sinan Gezici, Harry Sheng, S. Y. Kung, H. Kobayashi, H. Vincent Poor, Alexander Haimovich, and Jinyun Zhang. A Low-Cost Time-Hopping Impulse Radio System for High Data Rate Transmission. *EURASIP Journal on Applied Signal Processing*, page 397–412, January 2005. (Cited on page 55.)
- [57] C. Muller, S. Zeisberg, H. Seidel, and A. Finger. Spreading properties of time hopping codes in ultra wideband systems. In *IEEE 10th International Symposium on Spread Spectrum Techniques and Applications, 2002 (ISSSTA '08)*, volume 1, pages 64 – 67, 2002. URL <http://ieeexplore.ieee.org/stamp/stamp.jsp?tp=&arnumber=1049287>. (Cited on pages 5 and 9.)
- [58] H. Nguyen, Z. Zhao, F. Zheng, and T. Kaiser. On the MSI Mitigation for MIMO UWB Time Reversal Systems. In *Proc. 2009 IEEE Intern. Conf. on Ultra-Wideband*, 2009. (Cited on pages 37, 38, and 39.)
- [59] H. Nguyen, F. Zheng, and T. Kaiser. Antenna Selection for Time Reversal MIMO UWB Systems. In *Proc. IEEE 69th Vehicular Technology Conference VTC '09*, 2009. (Cited on pages 37, 39, and 40.)
- [60] H. T. Nguyen, J. B. Andersen, and G. F. Pedersen. The potential use of time reversal technique in multiple elements antenna systems. *IEEE Commun. Lett.*, 9(1):40–42, 2005. (Cited on page 17.)
- [61] Hieu Nguyen, Zhao Zhao, Feng Zheng, and Thomas Kaiser. Pre-equalizer Design for Spatial Multiplexing SIMO-UWB TR Systems. *IEEE Transactions on Vehicular Technology*, 59:3798 – 3805, 2010. (Cited on pages 9, 40, 43, and 60.)
- [62] Hung Tuan Nguyen, J.B. Andersen, G.F. Pedersen, P. Kyritsi, and P.C.F. Eggers. Time reversal in wireless communications: a measurement-based investigation. *IEEE Trans. Wireless Commun.*, 5(8):2242–2252, 2006. ISSN 1536-1276. doi: 10.1109/TWC.2006.1687740. (Cited on pages 6 and 39.)
- [63] Hung Tuan Nguyen, I. Z. Kovcs, and P. C. F. Eggers. A time reversal transmission approach for multiuser UWB communications. *IEEE Trans. Antennas Propagat.*, 54(11):3216–3224, Nov. 2006. doi: 10.1109/TAP.2006.883959. (Cited on page 55.)
- [64] Trung Kien Nguyen, Thanh Hieu Nguyen, and Thomas Kaiser. CMI and IFI Mitigation for TH-PPM Ultra Wideband Systems with a Low Complexity Receiver. In *The 2009 International Conference on Advanced Technologies for Communications (ATC'09)*, Oct. 2009. URL <http://ieeexplore.ieee.org/stamp/stamp.jsp?tp=&arnumber=5349487>. Copyright © 2009, IEEE. (Cited on pages 6, 10, 22, 38, and 56.)

- [65] Trung Kien Nguyen, Hieu Nguyen, Feng Zheng, and Thomas Kaiser. Spatial Correlation in the Broadcast MU-MIMO-UWB System Using a Pre-Equalizer and Time Reversal Pre-Filter. In *The 4th International Conference on Signal Processing and Communication Systems, ICSPCS'2010*, 13 - 15 December 2010. URL <http://ieeexplore.ieee.org/stamp/stamp.jsp?tp=&arnumber=5709711>. Copyright © 2010, IEEE. (Cited on pages 7 and 60.)
- [66] Trung Kien Nguyen, Hieu Nguyen, Feng Zheng, and Thomas Kaiser. Spatial correlation in SM-MIMO-UWB systems using a pre-equalizer and pre-rake Filter. In *2010 IEEE International Conference on Ultra-Wideband (ICUWB2010)*, September 20-23 2010. URL <http://ieeexplore.ieee.org/stamp/stamp.jsp?tp=&arnumber=5616816>. Copyright © 2010, IEEE. (Cited on pages 7, 18, 38, 39, 56, and 59.)
- [67] I. Oppermann, M. Hmlinen, and J. Iinatti. *UWB Theory and Applications*. John Wiley & Sons, September 2004. (Cited on pages 5 and 9.)
- [68] A. Paulraj, R. Nabar, and D. Gore. *Introduction to Space-Time Wireless Communications*. Cambridge University Press, 2003. (Cited on pages 44, 45, and 61.)
- [69] R.C. Qiu, C. Zhou, N. Guo, and J.Q. Zhang. Time reversal with MISO for ultrawideband communications: Experimental results. *IEEE Antennas Wireless Propagat. Lett.*, 5(1):269–273, 2006. ISSN 1536-1225. doi: 10.1109/LAWP.2006.875888. (Cited on pages 9, 18, and 39.)
- [70] R. Qui. A theory of time-reversed impulse multiple-input multiple-output (MIMO) for ultra-wideband (UWB) communications. In *Proc. of the IEEE International Conference on Ultra-Wideband (ICUWB '06)*, pages 587–592, September 2006. (Cited on page 37.)
- [71] A. Rajagopalan, G. Gupta, A.S. Konanur, B. Hughes, and G. Lazzi. Increasing Channel Capacity of an Ultrawideband MIMO System Using Vector Antennas. *IEEE Transactions on Antennas and Propagation*, 55:2880 – 2887, Oct. 2007. (Cited on page 55.)
- [72] Gaur S. and Annamalai A. Improving the range of ultrawideband transmission using RAKE receivers. In *Proc. IEEE Vehicular Technology Conference, VTC Fall*, volume 1, page 597–601, Oct. 2003. (Cited on page 4.)
- [73] Zafer Sahinoglu and Ismail Guvenc. Multiuser interference mitigation in noncoherent UWB ranging via nonlinear filtering. *EURASIP Journal on Wireless Communications and Networking*, 2006 Issue 2, April 2006. (Cited on page 55.)
- [74] A. Saleh and R. Valenzuela. A Statistical Model for Indoor Multipath Propagation. *IEEE Journal on Selected Areas in Communications*, 5(2):128 – 137, Feb. 1987. (Cited on page 10.)

- [75] R.A. Scholtz, D.M. Pozar, and W. Namgoong. Ultra-Wideband Radio. *EURASIP Journal of Applied Signal Processing*, 3:252–272, 2005. (Cited on page 1.)
- [76] Xuemin (Sherman) Shen, Mohsen Guizani, Robert Caiming Qiu, and Tho Le-Ngoc, editors. *Ultra-wideband Wireless Communications and Networks*. John Wiley & Sons, 2006. (Cited on pages 4 and 10.)
- [77] C. Steiner and K. Witrissal. Multiuser interference modeling and suppression for a multichannel differential IR-UWB system. In *2005 IEEE International Conference on Ultra-Wideband*, Sept. 2005. (Cited on page 55.)
- [78] T. Strohmer, M. Emami, J. Hansen, G. Papanicolaou, and A. Paulraj. Application of time reversal with MMSE equalizer to UWB communications. In *Proc. IEEE Global Telecommunications Conference, Dallas TX*, pages 3123–3127, 2004. (Cited on pages 5, 6, 9, and 18.)
- [79] A. Taha and K. M. Chugg. A Theoretical Study on the Effects of Interference on UWB Multiple Access Impulse Radio. In *Proc. Asilomar Conf.*, 2002. (Cited on page 55.)
- [80] S. S. Tan, B. Kannan, and A. Nallanathan. Performance of UWB multiple-access impulse radio systems with antenna array in dense multipath environments. *IEEE Transactions on Communications*, 54, Issue:6:966, June 2006. (Cited on page 55.)
- [81] S.S. Tan, B. Kannan, and A. Nallanathan. Multiple access capacity of UWB m-ary impulse radio systems with antenna array. *IEEE Transactions on Wireless Communications*, 5, Issue:1:61, Jan. 2006. (Cited on page 55.)
- [82] Vahid Tarokh, Nambi Seshadri, Senior Member, and A. R. Calderbank. Space-time codes for high data rate wireless communication: Performance criterion and code construction. *IEEE Trans. Inform. Theory*, 44:744–765, 1998. URL <http://citeseerx.ist.psu.edu/viewdoc/download?doi=10.1.1.112.4293&rep=rep1&type=pdf>. (Cited on page 35.)
- [83] E. Telatar. Capacity of Multiantenna Gaussian Channels. *European Transactions on Telecommunications*, 10(6):585–595, November/December 1999. (Cited on page 35.)
- [84] M. Weisenhorn and W. Hirt. Performance of Binary Antipodal Signaling over the Indoor UWB MIMO Channel. In *Proc. IEEE ICC '03*, page 2872–2878, 2003. (Cited on page 37.)
- [85] M.Z. Win and R.A. Scholtz. Ultra-Wide Bandwidth Time-Hopping Spread-Spectrum Impulse Radio for Wireless Multiple-Access Communications. *IEEE Transactions on Communications*, 48 - Issue: 4:679 – 689, April 2000. (Cited on page 55.)

- [86] Stephen Wood and Roberto Aiello. *Essentials of UWB*. Cambridge University Press, 2008. (Cited on page 4.)
- [87] Wei-Chiang Wu. Prefiltering-Based Interference Suppression for Time-Hopping Multiuser UWB Communications over MISO Channel. *EURASIP Journal on Advances in Signal Processing*, 2009, 2009. (Cited on page 55.)
- [88] Lie-Liang Yang and L. Hanzo. Residue number system assisted fast frequency hopped synchronous ultra-wideband spread-spectrum multiple access: a design alternative to impulse radio. *IEEE Journal on Selected Areas in Communications*, 20 Issue: 9:1652, Dec. 2002. (Cited on page 55.)
- [89] Liuqing Yang and G.B. Giannakis. Analog space-time coding for multiantenna ultra-wideband transmissions. *IEEE Transactions on Communications*, 52, Issue:3:507, Mar. 2004. (Cited on page 55.)
- [90] T. C. Yang. Temporal resolutions of time-reversed and passive-phase conjugation for underwater acoustic communications. *IEEE Journal of Oceanic Engineering*, 28:229–245, 2003. (Cited on page 9.)
- [91] A. van Zelst and J.S. Hammerschmidt. A single coefficient spatial correlation model for Multiple-input Multiple-output radio channels. In *XXVIIth General Assembly of the International Union of Radio Science*, 2002. (Cited on page 61.)
- [92] F. Zheng and T. Kaiser. *UWB Communication Systems - A Comprehensive Overview*, chapter Channel capacity of MIMO UWB indoor wireless systems, pages 376–409. Hindawi Publishing Corporation, 2006. (Cited on page 55.)
- [93] Feng Zheng and Thomas Kaiser. On the evaluation of channel capacity of multi-antenna UWB indoor wireless systems. In *2004 IEEE Eighth International Symposium on Spread Spectrum Techniques and Applications*, page 525, 30 Aug.-2 Sept. 2004 2004. (Cited on page 55.)
- [94] Feng Zheng and Thomas Kaiser. On the evaluation of channel capacity of UWB indoor wireless systems. *IEEE Transactions on Signal Processing*, 56 Issue:12:6106 – 6113, Dec. 2008. (Cited on page 55.)
- [95] C. Zhou, N. Guo, and R. C. Qiu. Experimental results on multiple-input single-output (MISO) time reversal for UWB systems in an office environment. In *Proc. MILCOM 2006. IEEE*, pages 1–6, Oct. 2006. (Cited on pages 9, 17, 18, and 84.)
- [96] C. Zhou, N. Guo, and R. C. Qiu. Time-reversed ultra-wideband (UWB) multiple input multiple output (MIMO) based on measured spatial channels. *IEEE Transactions on Vehicular Technology*, 59(6):2884–2898, July 2009. (Cited on pages 37 and 84.)

- [97] Chenming Zhou, Nan Guo, Brian M. Sadler, and Robert C. Qiu. Performance Study on Time Reversed Impulse MIMO for UWB Communications Based on Measured Spatial UWB Channels. In *Proc. of IEEE Military Communications Conference, 2007. MILCOM 2007*, pages 1–6, Oct. 2007. (Cited on page 6.)

Trung Kien Nguyen

Personal Data

Place and Date of Birth Namdinh, Vietnam | 09 September 1980
Address Leibniz Universität Hannover
 Institut für Kommunikationstechnik (IKT)
 Appelstraße 9A
 30167 Hannover
Phone + 49 511 762 – 2815
Email trung.kien.nguyen@ikt.uni-hannover.de

Education

Oct. 2007 – current PhD. Student at Institute of Communications Technology,
 Wilhelm Leibniz University Hannover, Hannover
 Germany
 Topic of research: Time Reversal Transmission Approach for Ultra
 Wideband Communications

Oct. 2003 – Oct. 2005 Master of Science in Electronics and Telecommunications,
 Hanoi University of Technology, Hanoi,
 Vietnam
 Thesis: Dynamic Channel Allocation (DCA) for OFDM-based
 cellular systems

Oct. 1998 – Jul. 2003 Bachelor of Engineering in Electronics and Telecommunications,
 Hanoi University of Technology, Hanoi,
 Vietnam.
 Thesis: Analysis and Optimize CATV Networks

Work Experience

Oct. 2007 – current Research Assistant at Institute of Communications Technology,
 Wilhelm Leibniz University Hannover, Hannover
 Germany

Oct. 2003 – Oct. 2007 Researcher at Research Institute of Posts and Telecommunications,
 Vietnam Posts and Telecommunications Corporation (VNPT)
 Vietnam

Jan. 2005 – Feb. 2006 Member of “NGN-Mobile Team” of VNPT, make plan to deploy the
 NGN mobile network for VNPT.

Jan. – Dec. 2004 Member of “CDMA group” of VNPT, research on the ability to
 launch CDMA-based mobile network.

Dec. 2003 – Dec. 2005 Collaborator, “Research on the structure of terrestrial
 telecommunication system to use VINASAT efficiently”, National
 Project KC.01.19, Ministry of Science and Technology, Vietnam.

Oct. – Dec. 2003 Collaborator, “Develop the satellite link calculation software for
 VINASAT system”, VNPT